DEVELOPMENT OF MULTIPLY SENSITIZED Ho:YLF AS A LASER MATERIAL

Evan P. Chicklis, et al

Sanders Associates, Incorporated

Prepared for:

Advanced Research Projects Agency
Army Electronics Command

October 1974

UNCLASSIFIED

SECURITY CLASSIFICATION OF THIS PAGE *(When Data Entered)*

REPORT DOCUMENTATION PAGE		READ INSTRUCTIONS BEFORE COMPLETING FORM
1. REPORT NUMBER ECOM-73-0066-F	2. GOVT ACCESSION NO.	3. RECIPIENT'S CATALOG NUMBER AD/A-005623
4. TITLE *(and Subtitle)* DEVELOPMENT OF MULTIPLY SENSITIZED HO:YLF AS A LASER MATERIAL		5. TYPE OF REPORT & PERIOD COVERED Final Report 15 Dec 72 - 15 Jan 1974
		6. PERFORMING ORG. REPORT NUMBER YWN (5126) - REV 1
7. AUTHOR(s) E. P. Chicklis, R. C. Folweiler, C. S. Naiman, D. R. Gabbe, A. Linz, H. P. Jenssen		8. CONTRACT OR GRANT NUMBER(s) DAAB07-73-C-0066
9. PERFORMING ORGANIZATION NAME AND ADDRESS Sanders Associates, Inc. Electro-Optics Division 95 Canal Street, Nashua, NH 03060		10. PROGRAM ELEMENT, PROJECT, TASK AREA & WORK UNIT NUMBERS 611201D ARPA OA 1868 (Amend 1) 9210 002
11. CONTROLLING OFFICE NAME AND ADDRESS Advanced Research Projects Agency		12. REPORT DATE October 1974
		13. NUMBER OF PAGES 117
14. MONITORING AGENCY NAME & ADDRESS*(if different from Controlling Office)* US Army Electronics Command Combat Surveillance & Target Acquisition Lab ATTN: AMSEL-CT-L-E Fort Monmouth, New Jersey 07703		15. SECURITY CLASS. *(of this report)* Unclassified
		15a. DECLASSIFICATION/DOWNGRADING SCHEDULE

16. DISTRIBUTION STATEMENT *(of this Report)*

Approved for Public Release; Distribution Unlimited.

17. DISTRIBUTION STATEMENT *(of the abstract entered in Block 20, if different from Report)*

18. SUPPLEMENTARY NOTES

19. KEY WORDS *(Continue on reverse side if necessary and identify by block number)*

Infrared laser, single crystal, phase diagrams, top-seeded-solution, yttrium lithium fluoride, laser sensitization, Ho^{3+} laser, Q-switch laser, energy transfer.

20. ABSTRACT *(Continue on reverse side if necessary and identify by block number)*

The results of a 12 month program to develop multiply sensitized Ho:YLF as a Q-switched laser material are presented. The program goals were the investigation of: repetitively pulsed operation, up to 20 PPS, at and near room temperature; Q-switched performance and the susceptibility of the material to damage during Q-switch operation; effects of compositional variations on laser performance; and the effects of crystal growth parameters on damage susceptibility and crystal quality. The performance goal of the

DD FORM 1 JAN 73 1473 EDITION OF 1 NOV 65 IS OBSOLETE

Unclassified

SECURITY CLASSIFICATION OF THIS PAGE *(When Data Entered)*

Ho:YLF material was 50 millijoules Q-switched output at 20 PPS with 10 joules per pulse input (5 joule threshold and 1% slope efficiency).

Twenty pulse per second operation was achieved when the laser rod was cooled to -15° centigrade at 20° centigrade, repetition rate was limited to 15 PPS. Q-switched outputs of up to 100 millijoules have been achieved from a 3 x 42 mm rod. Rods grown with properly refined feed materials showed no susceptibility to damage.

The composition 50% Erbium, 6.7% Thulium, 0.34% Holmium has exhibited a 6.5 joule threshold and a 2.5% slope efficiency.

The risetimes of Indium Arsenide and Mercury Cadmium Telluride detectors were measured and the detectors used to observe Q-switched pulses of 20 nanoseconds FWHM.

SUMMARY

The results of a 12 month program to develop multiply sensitized Ho:YLF as a Q-switched laser material are presented. This material, called "αβYLF", is the only material in which efficient laser operation at 2 microns has been reported at room temperature. Lasing threshold of 6.5 joules with a 2.5% slope efficiency is reported.

Crystals were grown by the Top-Seeded Solution Technique, a modification of the Czochralski process. Extensive analysis of the effects of feed purity and growth technique on the crystalline quality and damage susceptibility of this material are presented.

Extensive spectroscopic measurements are reported with direct observation of sensitization quantum yields of three; the implications for optimization of the material for specific applications are discussed.

Repetitively pulsed operation at up to 20 Hz (-15°C) is reported with operation up to 15 Hz at room temperature and 0.7 watts output at 10 Hz from a 3 x 22 mm rod. Q-switched operation of different material compositions is reported (calcite with $LiNbO_3$).

A calculation of the thermal loading at fracture of a uniformly heated rod cooled at the surface is presented.

PREFACE

This is a Final Technical Report describing the work performed under Contract No. DAAB07-73-C-0066, ARPA Order 1868, Amendment I, over the period 15 December 1972 through 14 December 1973 entitled "Development of Ho:YLF as a Laser Material." The work was performed for the Electronics Components Laboratory, U. S. Army Electronics Command, Ft. Monmouth, New Jersey under the guidance of Mr. V. Rosati, contracting officer's designated representative.

The work was performed by the Electro-Optics Division of Sanders Associates, Nashua, N. H. Subcontracting services were provided by the Center of Material Sciences and Engineering, Crystal Physics Laboratory, Dept. of Electrical Engineering, Massachusetts Institute of Technology.

The principal investigators of the program were E. P. Chicklis, R. C. Folweiler, and Dr. C. S. Naiman. Mr. J. C. Doherty assisted with the laser measurements and Ms. S. Lichtensteiger the spectroscopic measurements. The subcontracting efforts were under the direction of Dr. A. Linz. Dr. H. P. Jenssen conducted and analyzed some of the spectroscopic measurements. Crystals were grown by Dr. D. R. Gabbe with the assistance of R. Mills.

TABLE OF CONTENTS

TABLE OF CONTENTS (Cont)

Section 4

Spectroscopy

Section 5

Laser Measurements

TABLE OF CONTENTS (Cont)

LIST OF ILLUSTRATIONS

LIST OF ILLUSTRATIONS (Cont)

LIST OF TABLES

LIST OF TABLES (Cont)

TECHNICAL REPORT ECOM-73-0066-F
OCTOBER 1974

Reports Control Symbol
OSD-1366

Research and Development Technical Report
Report ECOM-73-0066-F

DEVELOPMENT OF MULTIPLY SENSITIZED Ho:YLF AS A LASER MATERIAL

FINAL REPORT

FOR PERIOD: 15 DECEMBER 1972 - 15 JANUARY 1974

CONTRACT NUMBER DAAB07-73-C-0066

Prepared By

E. P. Chicklis – R. C. Folweiler – C. S. Naiman – D. R. Gabbe – A. Linz – H. P. Jenssen

SANDERS ASSOCIATES, INC. - DEFENSIVE SYSTEMS DIVISION
95 Canal Street - Nashua, New Hampshire 03060 Tel. (603) 885-3010

SPONSORED BY
ADVANCED RESEARCH PROJECTS AGENCY - ARPA ORDER No. 1868, AMENDMENT 1

THIS RESEARCH WAS SUPPORTED BY THE ADVANCED RESEARCH PROJECTS AGENCY OF THE DEPARTMENT OF DEFENSE AND WAS MONITORED BY THE UNITED STATES ARMY ELECTRONICS COMMAND UNDER CONTRACT No. DAAB07-73-C-0066.

Prepared For

UNITED STATES ARMY ELECTRONICS COMMAND - FORT MONMOUTH, NEW JERSEY 07703

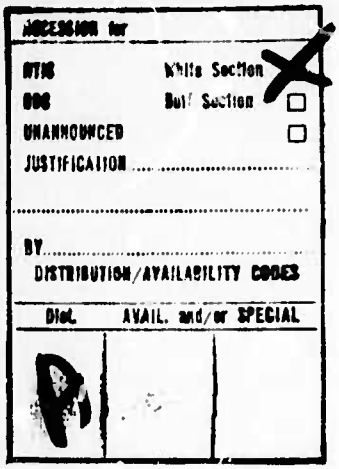

NOTICES

Disclaimers

The findings in this report are not to be construed as an official Department of the Army Position, unless so designated by other authorized documents.

The citation of trede names and names of manufacturers in this report is not to be construed as official Government indorsement or approval of commercial products or services referenced herein.

Disposition

Destroy this report when it is not longer needed. Do not return it to the originator.

X

SECTION 1

INTRODUCTION

The results of a twelve month program to investigate the material properties and two micron laser performance of multiply sensitized Ho:$LiYF_4$($\alpha\beta$YLF) are presented. The program goals were:

(a) investigation of repetitively pulsed operation at and near room temperature

(b) investigation of Q-switched performance and of the material susceptibility to damage under Q-switched irradiation

(c) investigation of the effects of compositional variations on laser performance and energy transfer efficiency

(d) investigation of the effects of growth parameters on laser damage susceptibility and crystalline quality

(e) measurement of the response times of HgCdTe and InAs photodiodes

The key results of this program are summarized below.

- Dramatic improvements in the optical quality, uniformity, and yield of YLF boules have been obtained as the result of the use of argon as the furnace atmosphere. The effects of oxides in the melt are described with dramatic experimental evidence showing the rejection

of oxides from the growing crystal. In preliminary results microscopic scattering inclusions (visible only under He-Ne irradiation) have been eliminated with the use of specially purified feed, resulting in optical quality comparable to Nd:YAG.

- Q-switched outputs of up to 100 mJ in a single pulse have been obtained without laser damage to the material. Analyses of a boule in which laser damage was previously observed[1] were inconclusive. However, a boule was grown from feed from the same manufacturers lot, but was zone-refined as an additional processing step. Laser rods fabricated from this boule did not damage at Q-switched outputs far in excess of levels previously observed.

- Sensitization quantum yields of three were measured directly in αβYLF. This accounts for the high efficiency in this material and is the result of the low (compared to oxide hosts) probability for multiphonon relaxation in this fluoride host. The decay modes of each level of αβYLF up to $^4S_{3/2}$(Er) have been measured. Energy conserving resonant transfer is the dominant relaxation mode of excited ions in YLF. The effects of variations in the sensitizer and activator concentrations on sensitization and laser efficiency are described. The model of energy transfer described in a previous report[1] has been experimentally verified.

- The calculated thermal loading at fracture of a uniformly heated YLF rod cooled at the surface is 11 watts/cm. Because of the efficient sensitization in this material, the energy decrement between the pump bands and the upper laser level is not taken up by lattice phonons (heat) and it is estimated that the total laser output at fracture is equal to the thermal load.

- Q-switched outputs of up to 100 mJ in a single spike are reported from a 3 x 42 mm rod. Q-switched performance was found to critically depend on the operation of $LiNbO_3$. Laser damage was not observed in the laser material or calcite polarizer but surface damage was found in the $LiNbO_3$.

- In repetitively pulsed operation a maximum of 0.7 watts was observed at 10 Hz from a 3 x 22 mm rod. In another experiment 20 Hz operation at -15°C was obtained (long pulse) for a brief period. Material limitations were not encountered in these experiments.

- A threshold of 6.5 joules with a 2.5% slope efficiency (95%R) was observed in a rod of composition 50% Er, 6.7% Tm, 0.34% Ho in long pulse operation at room temperature. Four other compositions were investigated and one composition was found to have a significantly lower threshold than previously observed.

- The risetimes of a Philco InAs and two HgCdTe diodes were measured. Two micron Q-switched pulsewidths of ~ 20 ns FWHM were detected.

αβYLF provides a viable two micron laser source for many applications. This is the only available source which can provide high peak power in the wavelength region which is retinal safe, covert to photo cathode surfaces, and operate with efficiencies consistent with lightweight packaging. A complete systems analysis of 1.06 and 2.06 micron designator/rangefinders has shown[2] that the performance of the two systems is nearly equal. For the rangefinder case sufficiently high laser material efficiency has already been demonstrated[1] for con-

struction of a hand held device. The designator case may require further improvements in laser efficiency through optimization of the material composition and strong emphasis on lightweight packaging and cooling technology.

SECTION 2

CRYSTAL GROWTH

Crystals of αβYLF ($LiY_{1-x-y-z}Er_xTm_yHo_zF_4$) were grown by the Top-Seeded Solution technique, a modification of the Czochralski technique, in a highly purified inert atmosphere. A complete description of the growth technique is provided in references 1 and 3. During this program crystal growth efforts were directed at

(a) growth of a sufficient number of high quality rods for laser testing

(b) determination of the effects of feed purity on the laser damage susceptibility

(c) determination of the effects of growth conditions on crystalline quality.

A major advance in the optical quality and yield of YLF boules has resulted from the use of argon as the furnace cover gas (instead of He). Five boules have been grown in this and other programs using Ar with complete absence of bubble type inclusions observed using a He atmosphere. Furthermore, the uniform quality of boules has vastly improved the rod yield/boule. Recent experiments using recrystallized feed have resulted in crystals with optical quality comparable to Nd:YAG, viz., complete absence of observable scattering under He-Ne illumination. Program results are discussed below.

2.1 LASER BOULES

A summary of the laser boules grown for this program is presented below. Boules 185f through 206f were grown in a highly purified helium atmosphere. Boule 224f was grown using argon. Photos of some representative boules are shown in Figures 1, 2, and 3.

#185f $LiY_{0.6266}Er_{0.2}Yb_{0.1}Tm_{0.07}Ho_{0.0034}F_4$

This crystal exhibited numerous inclusions due in part to feed purity and possibly to seed rod failure. Feed was non-zone-refined Lindsay, except for Yb and Tm which were zone refined Research Chemicals. Only two rods were of suitable quality.

#193f $LiY_{0.628}Er_{0.2}Yb_{0.1}Tm_{0.067}Ho_{0.005}F_4$

A clear center section rod was obtained.
The rest of the crystal was filled with inclusions.
Feed was non zone-refined Lindsay material. This crystal was grown in a small furnace in a molybdenum crucible.

#194f $LiY_{0.628}Er_{0.2}Yb_{0.1}Tm_{0.067}Ho_{0.005}F_4$,

This run was aborted due to failure of the seed rod cooling system. A by-product of this failure was inboard water leakage into the furnace which contaminated the melt.

#199f $LiY_{0.4296}Er_{0.5}Tm_{0.067}Ho_{0.0034}F_4$

Zone-refined Lindsay feed was used. Oxyfluoride in the melt limited the length of the crystal.

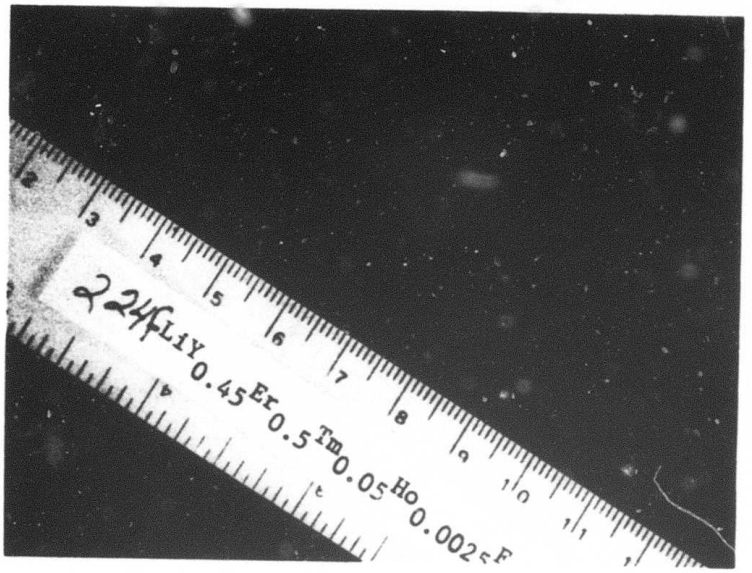

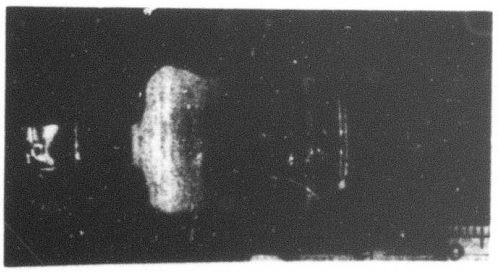

Figure 1 αβYLF Boules 224f, 193f

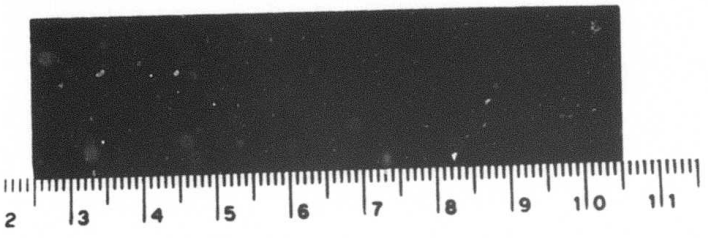

BOULE 206 f

$LiY_{0.428}Er_{0.5}Tm_{0.067}Ho_{0.005}F_4$

D-113

Figure 2 αβYLF Boule 206f

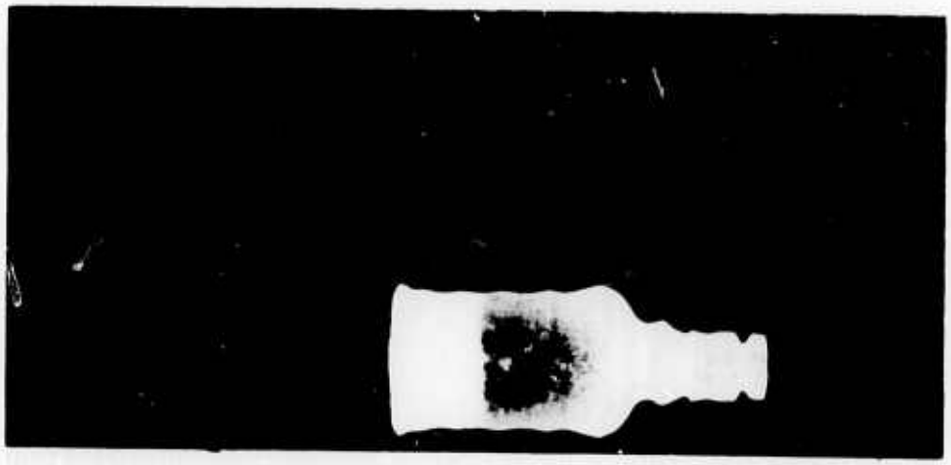

199f

D-214

Figure 3 αβYLF Boule 199f

#201fa $LiY_{0.4296}Er_{0.5}Tm_{0.067}Ho_{0.0034}F_4$

Zone-refined Lindsay feed was used. Adverse thermal gradient conditions led to formation of numerous inclusions. The crystal and residue in the crucible were reused for run 201fb.

#201fb $LiY_{0.4296}Er_{0.5}Tm_{0.067}Ho_{0.0034}F_4$

A second crystal was pulled from melt #201f. The gradient conditions were modified. Eight rod blanks of approximate dimensions 3 x 30 mm were obtained.

#204f $LiErF_4$

Research Chemicals zone-refined feed was used. This boule was used for feed in boule 206f.

#206f $LiY_{0.418}Er_{0.5}Tm_{0.067}Ho_{0.005}F_4$

Zone-refined Research Chemicals feed was used. One 25 mm and two 43 mm rods of excellent quality were obtained.

#224f $LiY_{0.4475}Er_{0.5}Tm_{0.05}Ho_{0.0025}F_4$

Zone refined Lindsay Rare Earth feed was used and growth was in an argon atmosphere. The uniformly excellent quality of the boule allowed utilization of the entire boule. Cutting is not yet complete, but at least 15 3 x 30 mm rods can be obtained.

2.2 FEED PREPARATION

The earliest boules of αβYLF were grown from rare-earth fluorides obtained from the American Potash and Chemical Co. The materials were of questionable quality with respect to non-rare-earth impurities. In particular, metallic iron was found in some samples and many of them turned gray upon hydrofluorination, suggesting carbon contamination and, indeed, heavy surface contamination was observed on the melt surfaces. Research Chemicals, Inc. was investigated as a supplier and their material was found to be generally better with regard to those impurities causing melt surface contamination.

The original αβ crystals grown with American Potash feed were Q-switched without laser damage.[4] Rods from one boule grown with Research Chemical feed exhibited very low damage thresholds in active Q-switched testing. Furthermore, in passive tests of spectroscopic samples of different growth runs large differences in damage susceptibility were observed between samples grown with Research Chemicals and American Potash feed - independent of the sample compositions.[1] In order to insure the availability of damage resistant laser rods for this program during the first part of this program, feed was purchased from Lindsay Rare-Earth Division* of Kerr-McGee Chemical Corporation, formerly American Potash. Simultaneously an investigation of the mechanism(s) of damage formation in crystals grown with Research Chemicals feed was carried out.

The assumption that the "damage problem" was impurity related was adopted in view of the results discussed above. However, chemical analysis (by mass spectroscopy) did not reveal the presence of any

* Kerr-McGee discontinued the Lindsay operation in 1973, and has sold the remaining rare-earth stock.

impurity potentially responsible for the damage. The results of scanning electron microscope analysis, discussed in Appendix II, are incomplete and have yet to produce definitive results. Because of the demonstrated effectiveness of zone-refining in feed purification,[1] a batch of zone-refined Research Chemicals feed was utilized for growth of an αβYLF boule (206f). Rods cut from this boule were Q-switched repeatedly at up to 100 mJ in a single 20-50 ns pulse without any evidence of damage to the laser rods. This result indicates that the previously observed low damage resistance was impurity related and that zone-refining is a very important technique in the overall feed purification - crystal growth process.

2.3 CRYSTALLINE PURITY

2.3.1 ABSORPTION SPECTRA

IR transmission spectra of a number of samples were recorded to determine whether impurities with absorption peaks in this region are present in detectable concentrations. The results of mass spectrographic analysis indicated very low concentrations of oxygen and DY^{3+}. Moreover, purification with respect to oxygen and rare earth ions was observed[1] as a result of zone-refining, a process now routinely used to prepare feed material.

The IR absorption spectra of a number of samples of different αβYLF boules were examined and showed no trace of any IR absorption beyond 2 μm. Figures 4 and 5 show representative spectra of YLF samples investigated.

A further indication of the purity of YLF grown by this technique is provided by the results of laser operation of YLF laser materials. High

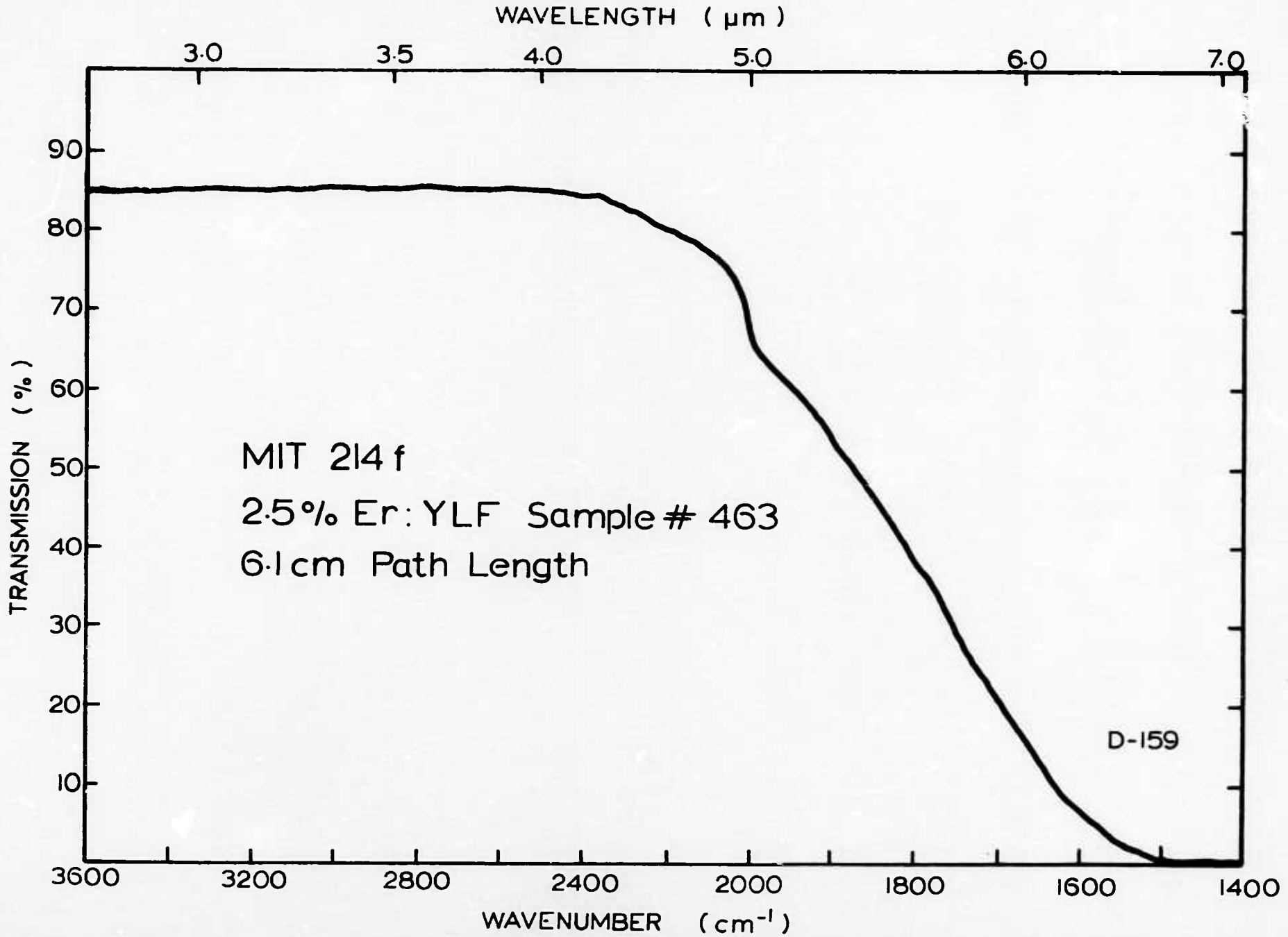

Figure 4 IR Transmission Spectrum of Boule 214f

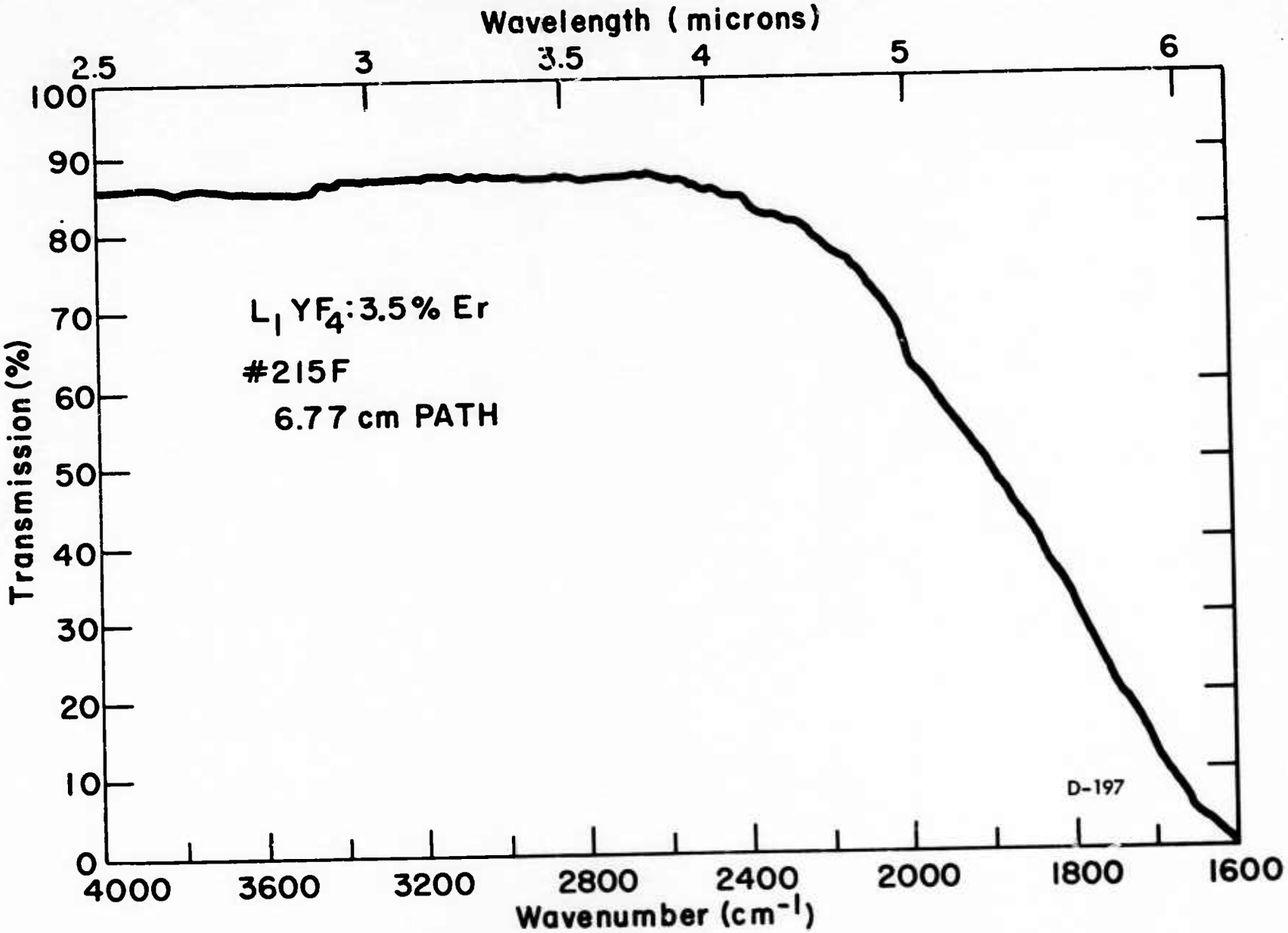

Figure 5 IR Transmission Spectrum of Boule 215f

current density, unfiltered Xe flashlamps with clear fused quartz envelopes are used in pumping αβYLF and Er^{3+}:YLF.[3] In experiments with Tb^{3+} YLF, a room temperature laser with emission at 0.55 μm, dye laser flashlamps are used for pumping (typically 50 joules in 1 μs) to provide the intense ultraviolet emission needed to pump the material.[5] In all the experiments conducted, no evidence of degradation of the optical quality of YLF rods has been observed indicating the complete absence of impurities which are affected by ultraviolet emission.

2.4 CRYSTAL CHEMISTRY

Phase diagrams for the systems LiF-REF_3[6] and LiF-YF_3[7] have been published and our experience indicates that these diagrams are essentially correct. Our data for the LiF-TbF_3 and LiF-GdF_3 systems indicates that the peritectics occur at somewhat higher LiF concentrations than reported by the Oak Ridge investigators. Figure 6 shows the LiF-YF_3 phase diagram. In the system LiF-YF_3 there is only one compound, $LiYF_4$, which melts incongruently at 819°C. The peritectic composition occurs at 49 mole % YF_3. The eutectic composition and temperature are 19 mole % YF_3 and 695°C, respectively. The systems LiF-REF_3 vary, as the size of the rare earth ion decreases, from a simple system with one eutectic, through a system with one incongruent compound, $LiREF_3$, and finally to a system with one congruently melting compound and two eutectics. All of the $LiREF_4$ compounds have the Scheelite structure. As might be expected, lattice constants vary little over the range of existing compounds. The phase diagram shows no solid solution formation between $LiYF_4$ and LiF and this concurs with our experimental evidence.

In those systems where $LiREF_4$ forms, it can be grown from a melt whose composition lies within the field bounded by the peritectic and

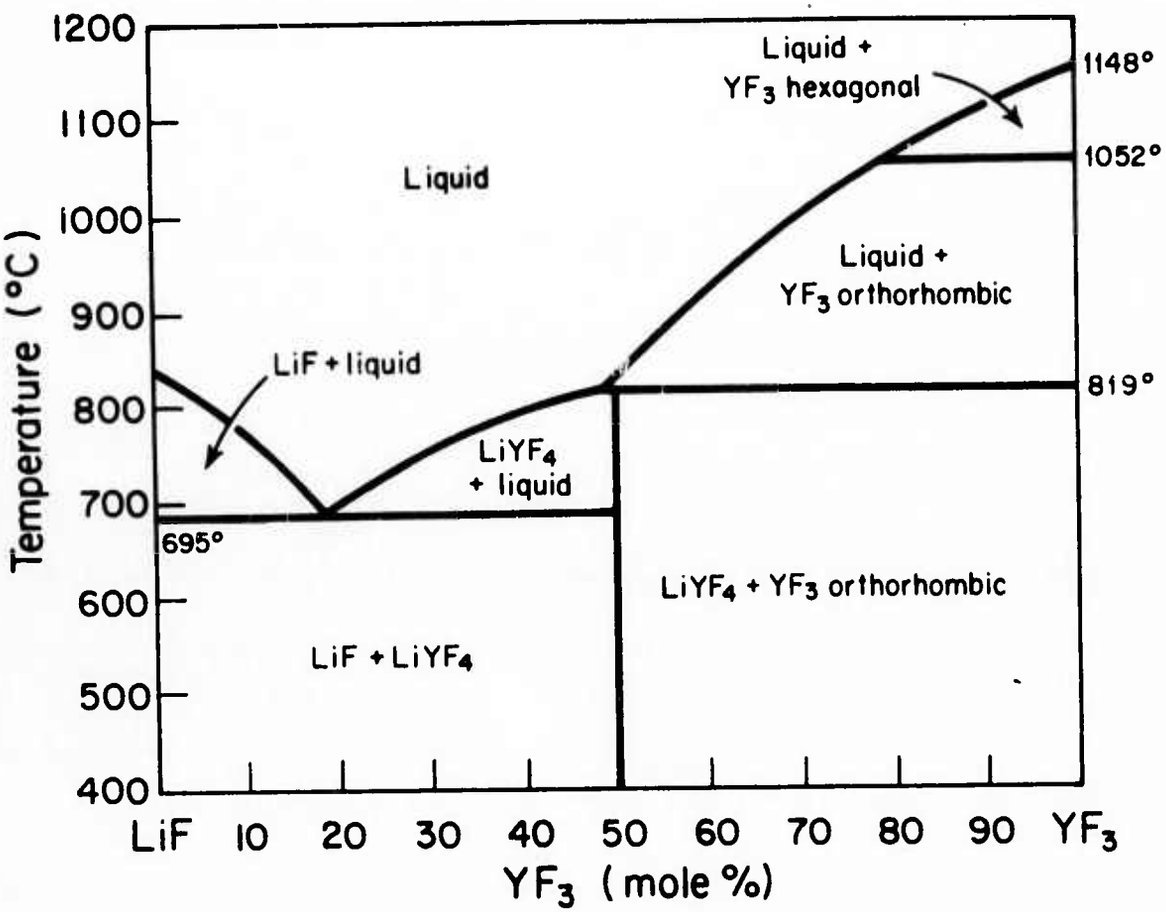

D-56

Figure 6 Phase Diagram of $LiF-YF_3$

eutectic or by the two eutectics. Our observations on systems $LiF-YF_3$ made during crystal growth experiments show that substitution of as much as 50% of the Y by rare earths heavier than Sm alters the system very little, i.e., the melting point and incongruent behavior of $Li(Y,RE)F_4$ remain about the same. Since the $LiREF_4$ phase field occurs on the LiF-rich side of the incongruently melting compounds and predominates on the LiF-rich side of the congruently melting ones, all crystals are grown from LiF-rich melts.

Little is known about the behavior of oxides* in fluoride melts and their effect on phase stability in the solid-solid and liquid-solid systems. Henderson[8] has prepared rare earth trifluorides containing $10-50_{ppm}$ by weight of oxygen. This represents an order of magnitude reduction of oxygen compared to what was probably present in previous preparations. These purer fluorides show the same orthorhombic-hexagonal phase transitions as the less pure substances, indicating that at the trace level oxygen does not affect this property.

At higher oxide concentrations, possibly as low as 0.2 mol %, oxyfluorides can form. During a crystal growth experiment the oxyfluoride phase can cocrystallize with the $LiYF_4$ phase. This means that the system $LiF-YF_3-Y_2O_3$ is at such a composition that two solid phases are in equilibrium with the liquid phase. At lower oxide concentrations there probably exists a two-phase region where $LiYF_4$ is in equilibrium with a liquid containing oxide. Several things might happen during crystallization from such a melt. At high temperatures a solid solution $LiYF_4$-oxyfluoride could form from which an oxide phase could precipitate upon cooling. Or local concentrations at the

* The state of oxygen in the fluorides may exist $O^=$ or a separate oxide phase, or OH^-, for example. In the ensuing discussion the generic terms oxide and oxygen are used without implying anything about the state of oxygen in the system.

crystal-melt interface of oxide rejected from the growing crystal could drive the system into the three-phase region - $LiYF_4$ - oxyfluoride - melt, resulting in precipitation of an oxyfluoride phase followed by its incorporation into the crystal. This behavior is closely related to constitutional supercooling. Under such conditions, it is possible to pull a crystal consisting of alternate bands of clear and opaque material.

Of special interest to this discussion is the behavior observed during growth of boule 199f, grown from zone-refined $LiREF_4$ compounds prepared from Lindsay rare-earth trifluoride feed. The small crystal that was grown,shown in Figure 3, has a very sharp boundary between a clear, almost scatter-free, top section (first part grown) and an opaque section. The scattering in the clear top section was less than is commonly observed in other YLF crystals grown in this and in other laboratories. The effect was observed during the growth run and could be reproduced by partly melting back and re-growing the crystal. This sharp boundary is indicative of passing from a composition region where one solid phase is in equilibrium with the melt to a composition region where two solid phases are in equilibrium with the melt. The two-phase region is encountered as the oxide content of the melt increases due to rejection of this species from the growing crystal. An x-ray powder pattern of the bottom, opaque part of the crystal has the extra line at d = 3.1Å. The powder pattern of the clear top is normal. The $LiYF_4$ feed was suspect and an x-ray powder pattern of this material had an extra line at d = 3.1Å, corresponding to an intense reflection of YOF. This line also appears when $LiYF_4$ is heated in air above 600°C.

Additional evidence was obtained from an experiment in which $LiYF_4$ with a known amount of Y_2O_3 added was crystallized in a normal freezing configuration. The starting materials were $LiYF_4$ single crystal chips grown from zone-refined YF_3, Harshaw LiF and Research Chemicals 99.99% Y_2O_3. In the first experiment the 10 grams of $LiYF_4$ was mixed with 0.5 mol % Y_2O_3 and crystallized at ~ 0.6 cm/hour. The central portion of the normally frozen specimen consisted of clear sub-cm size grains of $LiYF_4$ (confirmed by x-ray powder pattern analysis), while the end third was translucent and had an anisotropic appearance characteristic of an oriented needle-like precipitate. The head of the charge was a mixture of YF_3 and $LiYF_4$. We believe this precipitate to be an oxy-fluoride. A reflection for the spacing d = 3.1A was observed in the powder pattern.

These results indicate that:

(1) oxide is rejected from $LiYF_4$ as it crystallizes;

(2) the presence of oxide in the melt does not necessarily mean that a clear, nearly scatter-free, crystal cannot be grown;

(3) the relation between trace amounts of optical scattering and oxide content of the melt is not simple.

In connection with item 3, it should be pointed out that much work has been done in alkali halides on OH^- precipitation in the presence of other impurities. For example, it was found that formation of a hydroxide precipitate requires that both OH^- and Mg^{++} or Ca^{++} be present as impurities[9]. Other studies have dealt with the infrared absorption in LiF of complexes between OH^- and Mg^{2+}[10]. These studies strongly suggest that in YLF the formation of light scattering precipitates is not only a function of the oxide content of the crystals but also depends upon other impurities as well.

Possibly two types of precipitation phenomena should be distinguished; the first resulting from gross amounts of oxide leading to formation of a rare-earth oxyfluoride or similar phase; the second caused by the presence of other trace impurities which may interact with trace oxygen. However, the nature of the trace scattering centers is not at all clear at this time. The work aimed at analyzing the scattering centers is discussed in Appendix II. Work on the fluoride-oxide systems at low oxide concentrations has been hampered by the great difficulty in obtaining accurate oxygen analyses. Recent contacts have indicated that it is possible to obtain accurate low level oxygen analyses.(11)

2.5 CRYSTALLINE QUALITY

The technique utilized to grow YLF crystals, described in reference 1, has produced excellent optical quality material for laser applications. In general crystals are optically clear and free of refractive index gradients and low angle grain boundaries. A view through a 7.5 cm boule of Er:YLF is shown in Figure 7. However, defects have been observed in YLF and their characteristics are discussed below.

2.5.1 BUBBLES

In prior growth runs, using helium as the furnace atmosphere, isolated bubbles and bands of localized bubbles have been observed. The former type are frequently of elongated shape (order of tenths of millimeters in diameter) oriented parallel to the c-axis.

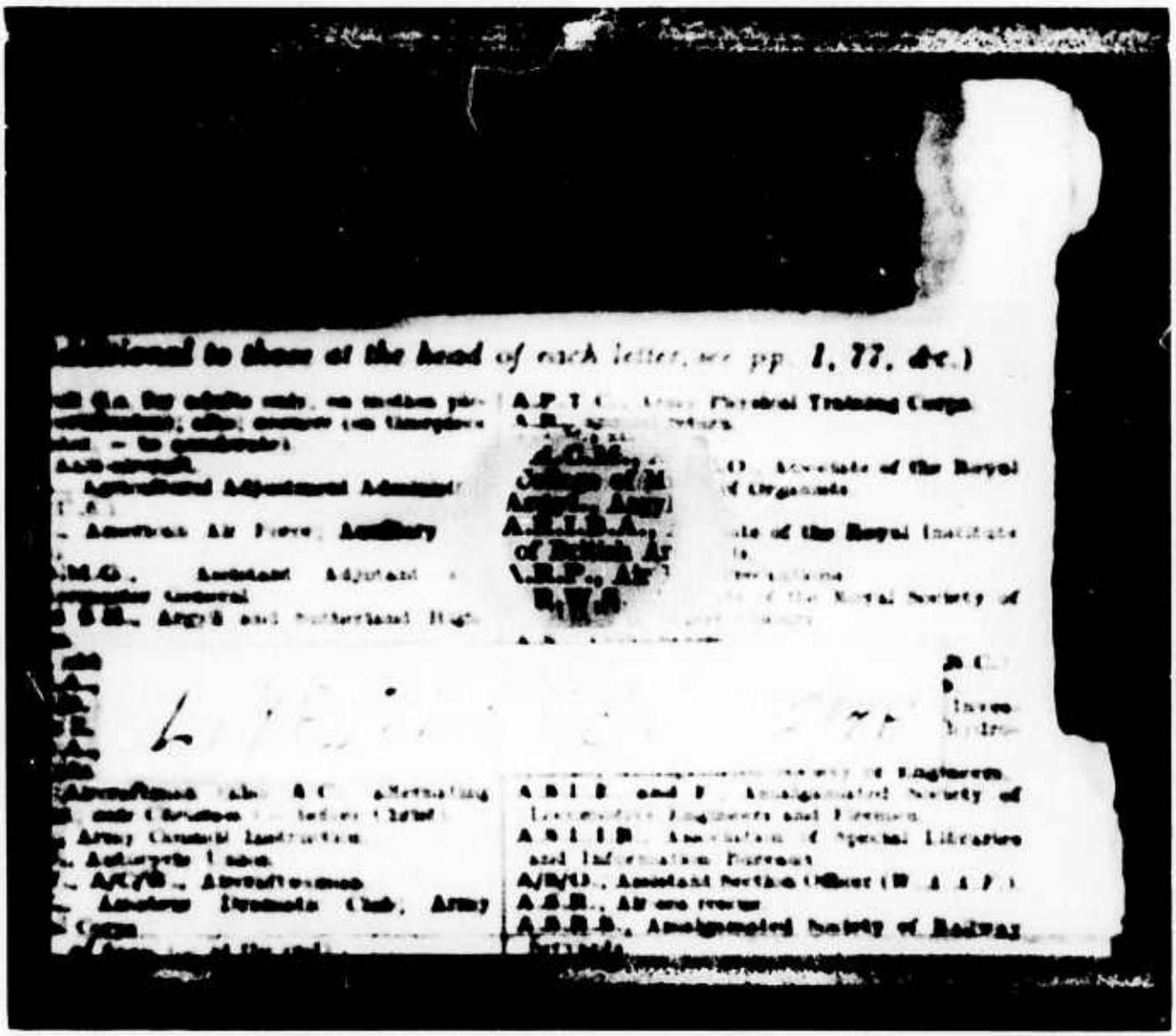

Figure 7 View Through 7.5 cm of YLF

The latter type are much smaller and frequently have formed in sufficiently high density to limit the useable length of the boule. Optical and scanning electron microscope (SEM) analyses (see Appendix II) have confirmed that these types of inclusions are bubbles.

Until recently the major problem in YLF growth runs for laser rods has been the variable rod yield per boule due to these large bubbles and bands of bubbles across the whole growth plane. This problem has apparently been eliminated with the use of argon as the furnace atmosphere (instead of helium). Boules grown with an argon atmosphere have exhibited excellent uniformity with nearly complete elimination of large bubbles and complete elimination of the bands of bubbles. This has been consistently observed through a total of five large boules, each greater than 50 mm in length.

2.5.2 MICROSCOPIC SCATTERING INCLUSIONS

What appears to be a fine precipitate has also been observed in some crystals under He-Ne illumination. Sometimes this type of inclusion displays optical anisotropy, in other instances the precipitate appears as a light haze. The distribution of these types of defects is not uniform; their formation may be associated with a combination of impurities and thermal instabilities in the melt. The characterization of this type of defect as a "precipitate" may be misleading as this type of scattering center may consist partly of very fine bubbles.

It is emphasized that this type of inclusion is not visible to the unaided eye, requiring either He-Ne illumination with appropriate index matching or magnification.

Recently use of recrystallized feed material in a growth run in an argon atmosphere has resulted in a YLF boule with virtually none of the scattering inclusions discussed above. The optical quality of the boule was comparable to that of Nd:YAG when the scattered radiation of a HeNe probe beam was viewed. This very significant result does point to a relationship between inclusion formation and feed purity but additional studies are required.

2.5.3 REFRACTIVE INDEX DEFECTS

YLF crystals grown by this technique are characterized by very low fringe counts, hence path distortions, when analyzed with interferometric measurements. Some poor quality material has exhibited apparent refractive index gradients but this has only been observed in one αβYLF boule and the source of the problem is unknown. Furthermore, viewed under a polarizing microscope, YLF boules have exhibited none to very low angle grain boundaries. This is the result of careful seeding and growth from a rigorously clean melt.

SECTION 3

THERMAL AND MECHANICAL PROPERTIES

Most of the relevant thermal and mechanical properties of YLF have been measured on this and other[1],[3] programs and are shown in Table 3-1. During the course of this program the strength of samples of αβYLF were measured with the result:

$$\text{STRENGTH} = 3.3 \pm 0.32 \times 10^7 \text{ N/m}^2.$$

In addition an analysis of the thermal loading at fracture of a YLF rod uniformly heated and cooled at the surface was carried out. The results are that at thermal fracture the heat input to a YLF rod is 11 watts/cm.

TABLE 3-1

MATERIAL AND OPTICAL PROPERTIES

YLF ($LiYF_4$)

and

YAG ($Y_3Al_5O_{12}$)

MECHANICAL	YLF	YAG
Density (gm/cm^3)	5.07 ($\alpha\beta$YLF)	4.47
Hardness (Mohs)	4-5	8.5
Elastic Modulus (N/m^2)	7.5×10^{10}	33.3×10^{10}
Strength (N/m^2)	$3.3 \times$	
THERMAL (300°K)		
Thermal Conductivity W/cm-°K	0.06	0.13
Thermal Expansion Coefficient - $°C^{-1}$	a axis : 13×10^{-6} c axis : 8×10^{-6}	6.9×10^{-6}
OPTICAL		
Index of Refraction $\lambda = 0.6$ µm	$n_o = 1.443$ $n_e = 1.464$	1.8347
UV Absorption	<0.2 µm	∿0.38 µm
CRYSTALLINE STRUCTURE	Tetragonal (Scheelite)	Cubic (Garnet)

3.1 STRENGTH MEASUREMENT

The strength of αβYLF has been re-measured using a group of samples that were prepared in a manner to minimize the effect of surface damage. The samples were cut from boule 140f and finished by lapping with diamond abrasive. A final chemical polish of Syton* was used to leave a damage free surface on the side that was to be placed in tension during the test. An attempt was made to chamfer the tension edges, but difficulties were encountered in the procedure.

Surface microcracks and scratches are known to reduce the observed strength of all materials tested in tension, but their effect is greatest on material that have little plastic flow before fracture. A scanning electron microscope was used to examine the tension surface of samples 2 and 3 after completion of the strength measurements. Very little cracking was observed anywhere, although the fracture surfaces did appear to originate from flaws at the edges that probably existed prior to testing. The tension surface of sample 3 was of such high quality that it was very difficult to focus the microscope on it at 63,000X without the aid of a small scratch or dust particle. Sample 2 showed some surface pits, indicating that it was not as well polished.

The strength was measured in an Instron testing machine using a carefully aligned four-point test fixture. Sample dimensions were approximately 0.06 inches thick by 0.19 inches in breadth. The modulus of rupture was calculated using the formula

$$\sigma_f = \frac{3P(c-a)}{2bt^2}$$

*T-M Monsanto Co.

where σ_f = modulus of rupture

P = load at fracture

c = distance between outer load points

a = distance between inner load points

b = specimen width

and t = specimen thickness.

The observed strength of the samples is shown in Table 3-2. All samples broke between the inner load points.

The data represents reasonably low scatter for strength measurement.

TABLE 3-2

STRENGTH OF αβYLF

Composition $Li\ Y_{0.34}\ Er_{0.50}\ Tm_{0.067}\ Ho_{0.034}\ F_4$

Boule 140f

SPECIMEN	STRENGTH psi
1	4630
2	4250
3	5500
4	4650
Average	4760

Strength of αβYLF = 4760 ± 460 psi

$= 3.28 \pm 0.32 \times 10^7$ Newtons/meter^2

3.2 ESTIMATED POWER LOADING AT FRACTURE

The thermal loading at fracture of a uniformly heated laser rod cooled at the surface can be calculated using measured material parameters. This calculation is extremely important as it defines the level of average power obtainable in a given host material. The calculation is predicated on the assumption of a uniformly heated, isotropic material. In the case of αβYLF in a flashpumped cavity the assumption of uniform heating is approximately correct for 3 mm diameter rods as the effective absorption coefficient of αβYLF is ~ 1 mm^{-1}* . YLF, however, is not isotropic. This is not expected to result in a severe discrepancy between predicted and actual thermal performance. The major uncertainty is involved in estimating the fraction of the heat load which can be extracted as laser output. This is discussed below.

The ultimate limitation on the amount of power which can be extracted from a solid state laser material is determined by the heat load for which the rod will fracture. Following Henningsen's analysis[12], we can obtain an estimate of the thermal load of a cylindrical rod at fracture under the following assumptions:

(a) The rod is heated uniformly and cooled at the surface.

(b) The rod is isotropic.

From (a) and (b) the temperature distribution is obtained:[12]

$$T(r) = \frac{1}{4k} Q \ (r_o^2 - r^2) \qquad (3\text{-}1)$$

* Determined by a measurement of the peak 2 μm fluorescence of an αβYLF sample as a function of thickness of other αβYLF samples placed in the pump beam.

where:

$T(r)$ = temperature at distance r from the axis

r_o = rod radius

k = thermal conductivity

Q = heat/volume dissipated in the rod

This temperature gradient is accompanied by a stress distribution given by:[12]

$$\sigma_r(r) = \frac{2aE}{(1 - \mu)16k} Q(r^2 - r_o^2)$$

$$\sigma_\theta(r) = \frac{2aE}{16(1 - \mu)k} Q\,(3r^2 - r_o^2) \qquad (3\text{-}2)$$

and

$$\sigma_z(r) = \frac{2aE}{16(1 - \mu)k} Q(4r^2 - 2r_o^2)$$

where:

$\sigma_r(r)$ = radial stress at distance r

$\sigma_\theta(r)$ = tangential stress at distance r

$\sigma_z(r)$ = axial stress (stress parallel to rod axis) at distance r

E = Young's modulus

μ = Poisson's ratio

a = thermal expansion coefficient

From these relations, it is seen that the radial component of the stress

vanishes at the rod surface, but the tangential and axial components do not. Thus the rod surface is under tension; at a certain heat load the tension at the surface will exceed the tensile strength of the material causing the rod to crack.[12]

At the rod surface ($r = r_o$) the net stress is given by:

$$\left|\vec{\sigma}_n\right| = \frac{\sqrt{2}\ Ea}{4\pi k(1 - \mu)}$$

Rod fracture will occur at the Q for which $\left|\vec{\sigma}_n\right|$ equals the tensile strength of the material (defined as σ). Noting that $P = QA$, where P is the input power dissipated as heat and A is the rod cross-section, we obtain the condition for rod fracture at $r = r_o$:

$$\sigma = \frac{\sqrt{2}\ aE}{4\pi k(1 - \mu)} \frac{P}{\ell}$$

That is, rod fracture due to the thermal gradient produced by surface cooling depends only on Young's modulus, the power/unit length, thermal conductivity, Poisson's ratio thermal expansion coefficient, and the tensile strength, but is independent of rod cross-section and the surface temperature.

Rearranging, we can compute the power loading/length at which the material will fracture:

$$\frac{P}{\ell} = \frac{4\pi k(1 - \mu)\sigma}{\sqrt{2}\ aE} \qquad (2\text{-}5)$$

Using the measured values of k, E, μ, a (along the a axis and σ as shown in Table 3-3, we obtain:

P/ℓ = 11 watts/cm for YLF

TABLE 3-3

PHYSICAL PROPERTIES OF YLF and YAG

	YLF	YAG*
Thermal Conductivity, k W/cm - °C (20°C)	a axis: 0.06	0.13
Thermal Expansion Coefficient, α $°C^{-1}$	a axis: 13×10^{-6} c axis: 8×10^{-6}	6.9×10^{-6}
Young's Modulus, E N/m^2	7.5×10^{10}	3.3×10^{11}
Poisson's Ratio, μ	0.33	0.3
Tensile Strength, σ N/m^2	3.3×10^{7}**	1.7×10^{8}

* Airtron Data Sheet
** Assumed equal to the Modulus of Rupture

	YLF*	YAG
Thermal Loading at Fracture P/ℓ (watts/cm)	11	60

* Assumed isotropic with a axis α

compared to:

P/ℓ = 60 watts/cm for YAG

Then for a 60 mm YLF rod the thermal loading at fracture is 66 watts - independent of cross section. For an adequate safety margin we choose to operate at 0.2 the maximum loading and obtain:

P = 13 watts of heat in 60 mm YLF rod at 0.2 the fracture thermal loading.

We must now estimate the amount of heat per watt of laser output generated in the material. In a "properly designed system" 1.5 watts of heat/watt of laser output in Nd:YAG is reported in reference (12). In the case of αβYLF the internal heat generation per watt output power is not known. Attempts at measurement of the heat rise in a rod pumped at modest average power have been unsuccessful[13].

A crude estimate may be obtained by noting that in Nd:YAG the energy decrement between the pump bands and the upper laser level is taken up by the emission of phonons to the lattice[14]. In αβYLF, on the other hand, resonant transfer[1] and emission are the dominant relaxation modes for levels with energy gaps > 2000 cm^{-1} above adjacent levels.[15] The strong pump bands (0.35 - 0.55 μm) in αβYLF relax to the upper laser level (2μm) by processes which nearly conserve energy. For example, for each Er^{3+} ion initially excited to $^4S_{3/2}$ (18130 cm^{-1}) three Ho ions are excited to $^5I_7$ (4850). The net result is 14550 cm^{-1} of energy available in laser output and 3550 cm^{-1} as heat. As a result for each $^5I_7$ excitation (4850 cm^{-1}) we have 1180 cm^{-1} of heat deposited in the crystal. This result has been confirmed with radiometric mea-

surements of the input power and the 2 μm fluorescence power output when selected levels are pumped; this is discussed in Section 4.

Because the relaxation modes from all the excited levels have not yet been determined we adopt the conservative assumption that the heat load from levels above $^4S_{3/2}$ results in twice the thermal load of the $^4S_{3/2}$ relaxation. That is for each $^5I_7$ excitation we assume an additional 1180 cm^{-1} of heat, for a sub total of 2360 cm^{-1}. Furthermore, we assume that only one-half of the stored energy in the upper laser level is extracted as laser power, the rest lost to spontaneous emission. As a result the energy associated with each laser photon is accompanied by an equal amount of heat deposited in the crystal.

As a result we predict:

13 watts of laser output is obtainable in a
60 mm rod at 0.2 x the fracture loading

or

11 watts of laser power per cm of rod length
at thermal fracture.

This estimate does not include the effects of local stress concentration due to surface microcracks. Such surface imperfections can reduce considerably the thermal load at fracture. The magnitude of this effect is difficult to calculate but can be minimized by careful fabrication.

To check the correspondence of this analysis with reality we note that in Section 5 experiments are described in which ~ 0.7 watts output from a 2.2 cm long YLF rod was obtained using a 95% R output mirror.

Under these conditions the total circulating power, P_t, inside, P_{in}, and outside, P_{out}, of the resonator is

$$P_t = P_{out} + P_{in} = P_{out} \left[1 + \frac{1}{1-R}\right]$$

or $P_t \cong 15$ watts.

This corresponds to 6.8 watts/cm without fracture compared to the calculated fracture load of 11 watts/cm.

SECTION 4

SPECTROSCOPY

Spectroscopic measurements were directed at determining the useful pump bands of αβYLF in flashpumped operation and at verifying the model of energy transfer proposed in reference 1 . In Xe flashpumped operation the most important pump bands lie between 0.2 - 0.55 μm; radiometric measurements of the quantum yield from these higher lying states positively show that the energy transfer mechanisms are nearly energy conserving. Quantum yields up to three have been directly measured.

4.1 αβYLF PUMP BANDS

Figure 8 shows the fluorescence excitation spectrum of a representative sample of αβYLF (composition: 50% Er, 6.7% Tm, 1.7% Ho). Care must be exercised in interpreting these data as the sample used in the measurement was too thick (most of the peaks are optically dense) to allow for accurate amplitude information. Most of the pump bands are due to Er^{3+} absorption with a few strong bands due to Tm^{3+}. By contrast direct Ho^{3+} absorption is very weak due to the relatively low Ho^{3+} concentrations necessitated by laser considerations.

Excitation spectra of αβYLF samples revealed transfer to the $^5I_7$ (Ho) manifold from all the absorption bands (see Figure 8). However, in pulsed operation the speed of transfer as well as the effi-

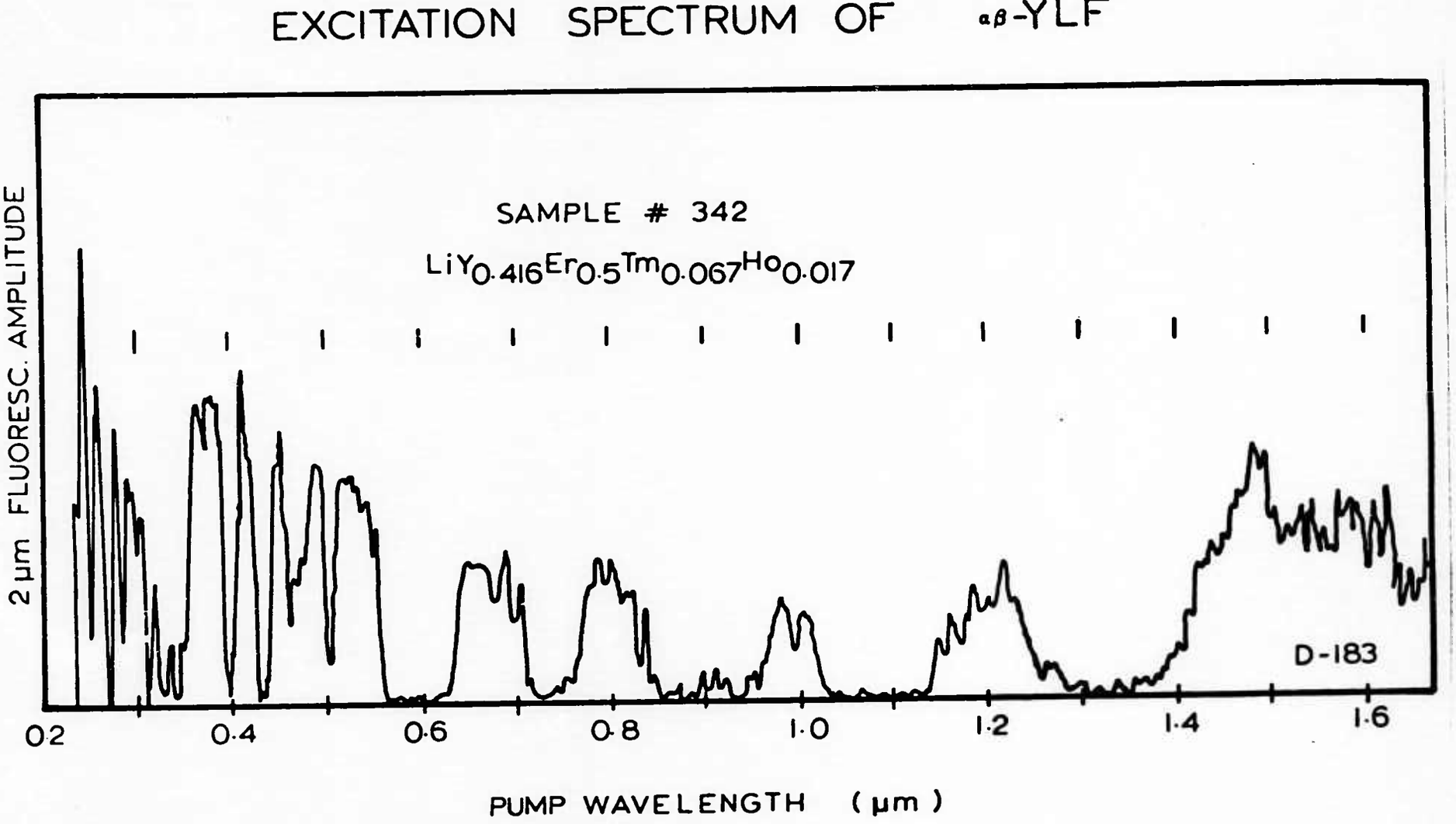

*Lowell Noble, ILC Corp.

Figure 8 Excitation Spectrum of αβ-YLF

ciency determine the useful pump bands; continuous excitation spectra provide no information about transfer rates. For example, in excitation spectra, the $^4I_{11/2}$ (Er^{3+}) manifold at $\lambda \sim 1$ μm appears as a strong peak. However, the lifetime of this manifold in "αβ" compositions is typically ~ 1 ms which is far too slow for useful sensitization of the Ho^{3+} laser line despite the fact that the $^4I_{11/2}$ (Er) → $^5I_7$ (Ho) branching ratio is ~ 0.5.

4.1.1 EXPERIMENTAL

A simple estimate of the useful αβYLF pump bands was made. An EG&G FX-33 Xe flashlamp was pulsed at 500V, 25 μf, L=0 (pulsewidth ~ 20 μs) and the peak fluorescence measured using different filters in the pump beam. A quartz lens was used to focus the light into the sample; the fluorescence was detected with a cooled InAs photodiode with a bandpass filter centered at 2.06 μm.

A series of Corning filters were utilized with nearly identical characteristics except for the cut-on wavelength. All the filters are opaque above the cut-on region and exhibit >80% transmission to beyond 2 μm.

The spectral output of the lamp can be estimated from Figure 9 from reference (16) which shows the absolute irradiance vs λ of Xe discharges as a function of fill pressure and current density. Note that the irradiance is in units of quanta/sec. The current density utilized for these measurements was ~ 3000 amps/cm^2 in a 450 torr lamp.

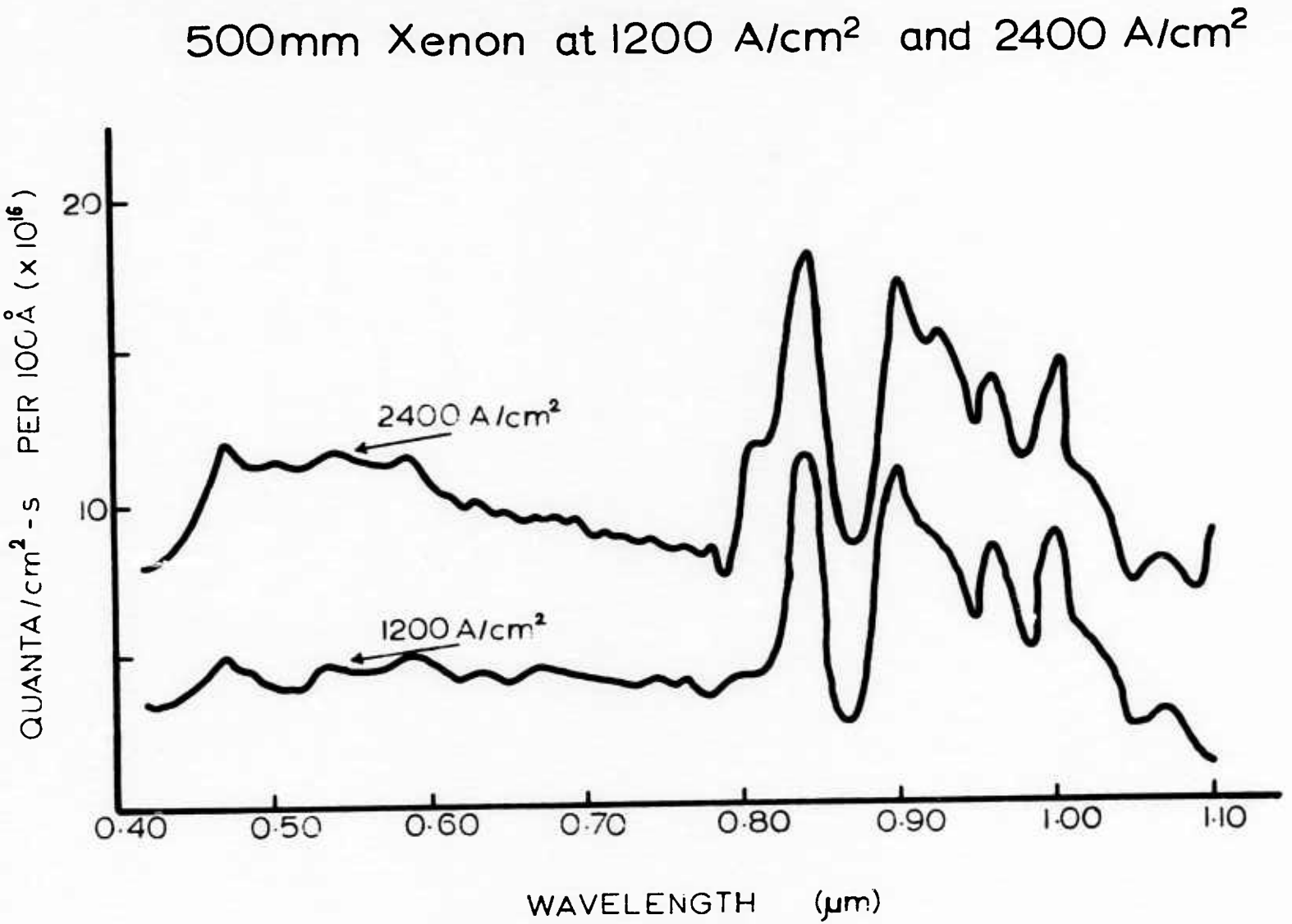

D-84

Figure 9 Emission Spectra of Xe Flashlamps

4.1.2 RESULTS

Table 4-1 lists results normalized to the fluorescence amplitude through the 9-54 filter. The cut-on wavelength was arbitrarily defined as the point at which the filter transmits 50%. The fluorescence amplitude was measured at the peak some 100 μs after the trigger to the lamp, and indicates the useful fluorescence. Pump bands which feed slowly (too slowly for pulsed laser operation) are eliminated in this manner.

In Table 4-2, the excitation efficiency defined as the percent fluorescence observed by pumping in a band with the indicated bounds to pumping from 0.280 - 2 μm is tabulated. Note that ∿67% of the pumping under these conditions occurs in the 0.28 - 0.57 band (actually somewhat higher as states above 0.28 μm, not included due to experimental difficulties, also contribute). Thus, it appears that operating at the highest current density in Xe flashlamps to shift the emission toward the blue would result in the highest pumping efficiency. However, for fixed energy input, higher current densities are obtained by either decreasing the pulsewidth and/or the bore size. For bore sizes much below 2.5mm the electrical/optical conversion efficiency tends to degrade [17]; for pulsewidths less than ∿100 μs degradation in the energy transfer is reported to occur [18] - although the source of the apparent decreased transfer efficiency is not yet known.

The results clearly indicate that the important pump bands are the blue-uv states in flashpumped operation. However, the near IR pumpbands ($\lambda > 0.65$ μm) do account for 30% of the excitation energy, and a change of 30% of the input energy above threshold

TABLE 4-1

PULSED EXCITATION DATA

CORNING CS #	CUT-ON AT 50% TRANSMITTANCE	MEASURED PEAK *	EXCITATION EFFICIENCY
9-54	0.280 μm	4.8 mV	100.0% †
0-54	0.315	4.2 mV	87.5%
0-52	0.360	4.0 mV	
3-74	0.425	3.5 mV	73.0%
3-72	0.455	2.9 mV	60.4%
3-71	0.480	2.75 mV	
3-69	0.520	2.25 mV	46.8%
3-66	0.570	1.6 mV	33.3%
2-62	0.605	1.6 mV	
2-58	0.650	1.5 mV	31.2%

† Normalized to unity, pump bands above 0.280 have been excluded.

* Estimated error ±10%.

TABLE 4-2

PUMP BAND EFFICIENCIES

PUMP BAND	EXCITATION EFFICIENCY
0.280 - 2 μm	100%*
0.280 - 0.570	67%
0.570 - 2μ (∿ gold reflectivity)	33%
0.400 - 2μ (∿ silver reflectivity)	80%

* Normalized to unity in this band.

can very significantly change the output. For example, in a number of experiments using different pump cavities, the output above threshold was observed to decrease by approximately a factor of two when water was introduced into the pump cavity. Water absorbs for $\lambda > 1$ μm; and the pumping efficiency is decreased by only 10-20%. Nevertheless this relatively small change in the pumping rate transforms to a significant change in the output energy above threshold (see Figure 19 , for example).

4.2 DETERMINATION OF PUMP BAND QUANTUM YIELDS

Radiometric measurements have confirmed the nearly energy conserving energy transfer mechanism in αβYLF proposed in (1). That is, an Er^{3+} ion initially excited to $^4S_{3/2}$ relaxes in three steps simultaneously exciting three Tm thence Ho ions. By pulsing $^4I_{9/2}$ (Er) directly with a short flash pulse and observing the rise of the fluorescence as a function of Tm^{3+} concentration, it was found that direct Er-Tm ($^4I_{9/2} \rightarrow {}^4I_{13/2} : {}^3H_6 \rightarrow {}^3H_4$) dominates even in low (1%) Tm^{3+} concentration. The experimental results, conclusions and implications on laser operation are discussed below.

4.2.1 INTRODUCTION

The multiply sensitized Ho:YLF laser relies on efficient energy transfer. Useful absorption in the laser crystal is provided mainly by Er^{3+} and in part by Tm^{3+}. The active laser ion, Ho^{3+}, is very dilute and does not absorb much of the pump radiation . In order to optimize the relative concentrations of the different ions it is necessary to know in detail what energy transfer steps are involved and their concentration dependence. Basically, we have a three-level

system with an upper and a lower laser level and a pump band. Laser threshold is reached when a certain population in the upper laser level is obtained. The upper laser level is fed by the pump band. If, by a pulse of excitation, we obtain N_o excitations in the pump band, N_u, the upper laser level population, will be as a function of time:

$$N_u = \eta N_o \ [\exp(-t/\tau_u) - \exp(-t/\tau_p)] \qquad (4\text{-}1)$$

where η is the efficiency of the pump band in feeding the upper laser level, τ_p and τ_u are the lifetimes of pump and upper laser level, respectively. For efficient operation we want η to be as large as possible and $\tau_p << \tau_u$.

In the present system the pump band consists of several energy levels of different types of ions. For each level we have a different η and τ_p. Also, since the feeding from most of the levels is not direct but via other levels, the simple model expressed by Eq. 4-1 is not exact. It is usually found that one step in the relaxation process is much slower than the others, and using the characteristic time for this process in Eq. 4-1 gives a good approximation.

A pump band level can relax by one of three processes: emission of radiation, multi-phonon relaxation to the next lower level, or by transfer. Of these, energy transfer is the most desirable because it is nearly energy conserving. An example of this is diagrammed below. One of two identical neighboring ions

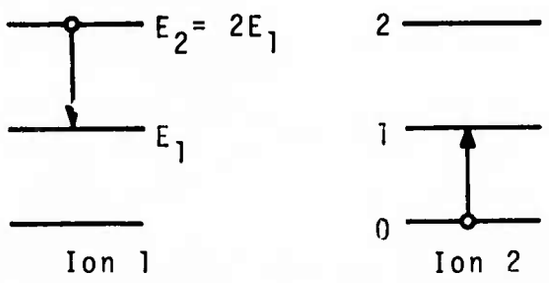

is excited to level 2. After transfer both ions are excited to level 1. In this process the energy is conserved and the quantum yield is 2. Experimentally what is observed is that when level 2 is pumped, only fluorescence from level 1 is observed. However, this could be the case also without transfer. If there are intermediate levels between levels 1 and 2, multi-phonon relaxation could completely quench fluorescence from level 2 and again only fluorescence from level 1 is observed, providing a quantum yield of one in the latter case. To distinguish between these two processes the quantum yield has to be measured. Assume that we can pump level 1 at a rate W_1 sec^{-1} and observe a fluorescent intensity I_1 from level 1 with a detection system. Next we pump level 2 at a rate W_2 and observe a fluorescent intensity I_2 from level 1. The quantum yield is then:

$$\eta = \frac{I_2/W_2}{I_1/W_1} \tag{4-2}$$

The method described above does not tell us anything about the transfer rate, which we want to be much faster than the decay rate from the upper laser level. For this we need to observe the time dependence of the fluorescence after a pulse of excitation. If level 2 does have some fluorescence, the time dependence can also be used to measure the transfer efficiency. Assume level 2 of ion 1 has a lifetime τ in the absence of ion 2 and τ' with ion 2 present. The difference is then due to transfer and the transfer efficiency is:

$$\varepsilon = \frac{\tau'^{-1} - \tau^{-1}}{\tau'^{-1}} \tag{4-3}$$

Note that this is not the same as the quantum yield. If the indicated transfer process is the only possible one, however, we can infer a

quantum yield of 2ε for the transfer process. So far we have discussed only energy transfer that conserves energy (resonant transfer). Most energy transfer processes are more or less non-resonant. The only true resonant process is energy migration, where the transfer is between the same levels of equal ions. Transfer rate depends both on concentration and degree of resonance (or non-resonance). Depending on the relative concentrations of sensitizer and activator ions, the transfer rate can be limited by diffusion time (low activator concentration) or by sensitizer-activator transfer time (high activator concentration). If the last case is the limiting factor, no improvement can be made. If the diffusion time is the limiting factor, either the sensitizer concentration or the activator concentration, or both, can be increased in order to increase the transfer rate. In alphabet-YLF the Ho concentration is limited to a fairly low value, since it is a three-level laser. The Er and Tm concentrations can be varied, however, and should be optimized for best laser performance.

4.2.2 EXPERIMENTAL TECHNIQUES AND RESULTS

Figure 10 shows the energy levels of Er^{3+}, Tm^{3+} and Ho^{3+} in YLF up to 20,000 cm^{-1}. The problem is to find out how the different levels relax and how efficient they are in feeding the upper laser level, Ho $^5I_7$. The crystals used in this study are listed in Table 4-3. Energy levels of successively higher energy starting with the Ho $^5I_7$ itself were studied.

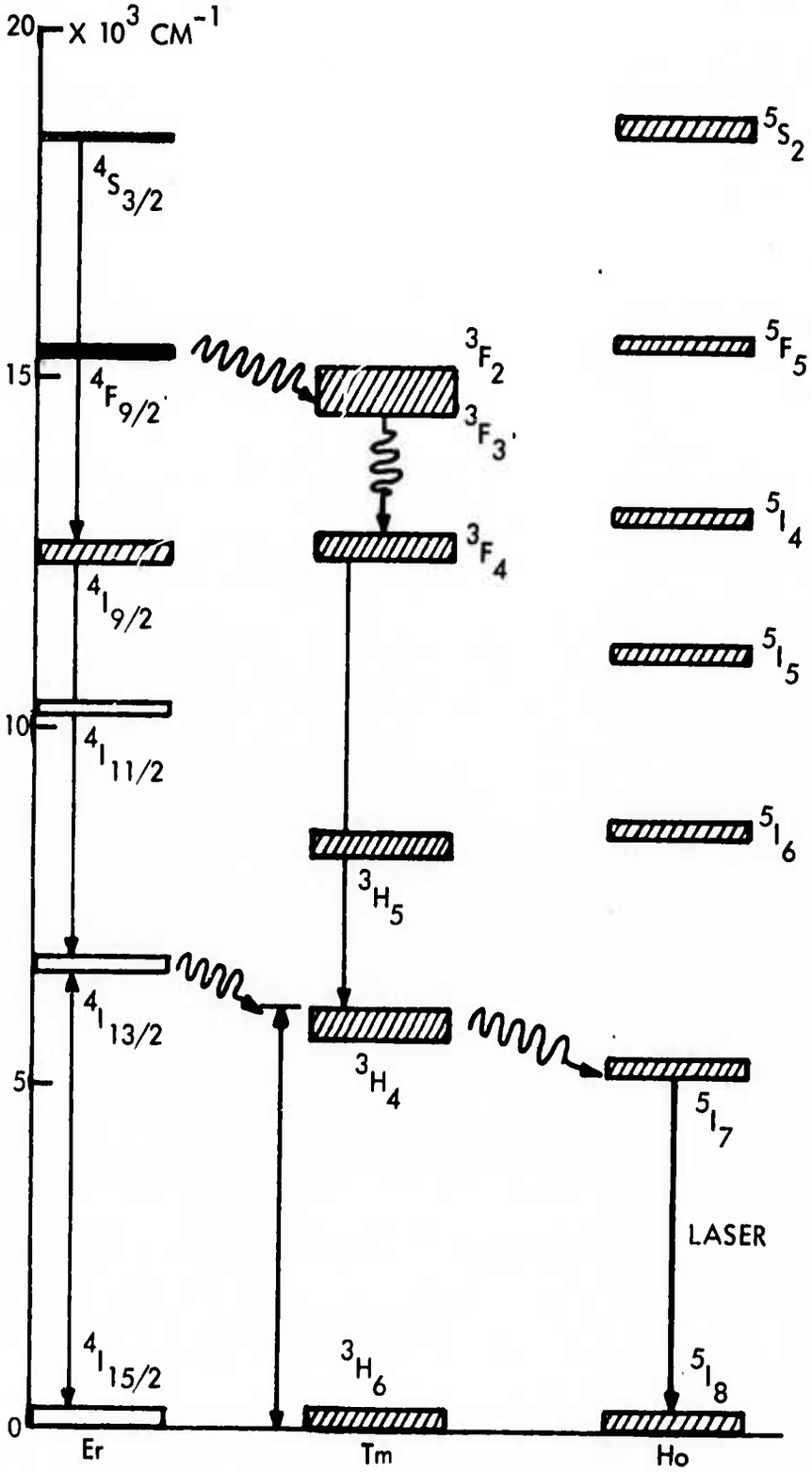

Figure 10 Levels of Er, Tm, Ho

TABLE 4-3

COMPOSITION OF ALPHABET YLF CRYSTALS
USED IN THIS STUDY

(The numbers give the fraction of Y-sites occupied by the ions.)

Boule #	Er	Tm	Yb	Ho
140f	0.5	0.067	-	0.0034
159f	0.5	0.01	-	0.003
169f	0.5	0.02	-	0.003
171f	0.5	0.035	-	0.003
193f	0.2	0.067	0.1	0.005

Time dependence of fluorescence was obtained by using a repetitively pulsed xenon flashlamp for excitation. The pump light was passed through a monochromator and appropriate filters for selective pumping. The 2 μm fluorescence was detected with a liquid nitrogen cooled InAs detector with a 2 μm bandpass filter. The signal was amplified and averaged on a computer of average transients.

Quantum efficiency measurements were obtained by use of a continuous pump source (1000 W xenon or 650 W. tungsten) through a scanning monochromator, simultaneously monitoring the fluorescence from the crystal, the intensity of the incident pump light, and the pump light transmitted through the crystal.

The rest of this section summarizes the results for the different energy levels investigated.

Ho $^5I_7$: The room temperature lifetime of this level is 15.5 ± 0.5 ms in YLF doped with only Ho. Because of the large energy gap to the ground state ($^5I_8$), the lifetime is due only to spontaneous emission.

In all the alphabet crystals investigated, the lifetime was shorter than 15.5 ms, ranging from about 9 to 14 ms. The quenching is caused in part by the presence of Tm through reversible transfer, $^3H_4 \leftrightarrow {}^5I_7$ and in part by the presence of quenching impurities. Because the spontaneous rate from this level is so slow even very weak quenching can be observed. However, the effect of quenching on laser operation is negligible provided fast transfer rates are maintained.

Tm $^3H_4$: The Tm $^3H_4$ - Ho $^5I_7$ transfer is a resonant transfer process evidenced by overlap of Tm fluorescence and Ho absorption (see Figure 11). The reverse process is also resonant at room temperature when the upper levels of Tm $^3H_6$ and Ho $^5I_7$ are thermally populated (Figure 12). As described in an earlier report,[1] this leads to a thermal distribution in the combined Tm $^3H_4$ and Ho $^5I_7$ levels when the transfer rate is fast compared to the normal relaxation rates of the two levels. Neglecting impurity quenching the observed lifetime for both levels will then be the same and somewhere between the two individual lifetimes. The highest efficiency in feeding $^5I_7$ from $^3H_4$ is obtained for Tm^{3+} concentrations of 1-2%. At higher Tm^{3+} concentrations (at room temperature) strong Tm^{3+} emission is observed when the Ho^{3+} concentration is low. For example, with 6.7% Tm and 0.34% Ho the Tm^{3+} emission is about equal in strength to the Ho^{3+}. However, the buildup time of the $^5I_7$ fluorescence decreases as the Tm and/or Ho concentrations increase. From Figure 13 it is seen that with 3.5% Tm the buildup time is ~ 700 μs, with 6.7% Tm it is ~ 100 μs.

Er $^4I_{13/2}$: This level is strongly quenched by $Tm^{3+}(^3H_4)$ via phonon assisted transfer. Figure 14 shows the levels involved; the difference in energy is about 300 cm^{-1}. As the Er^{3+} concentration is generally

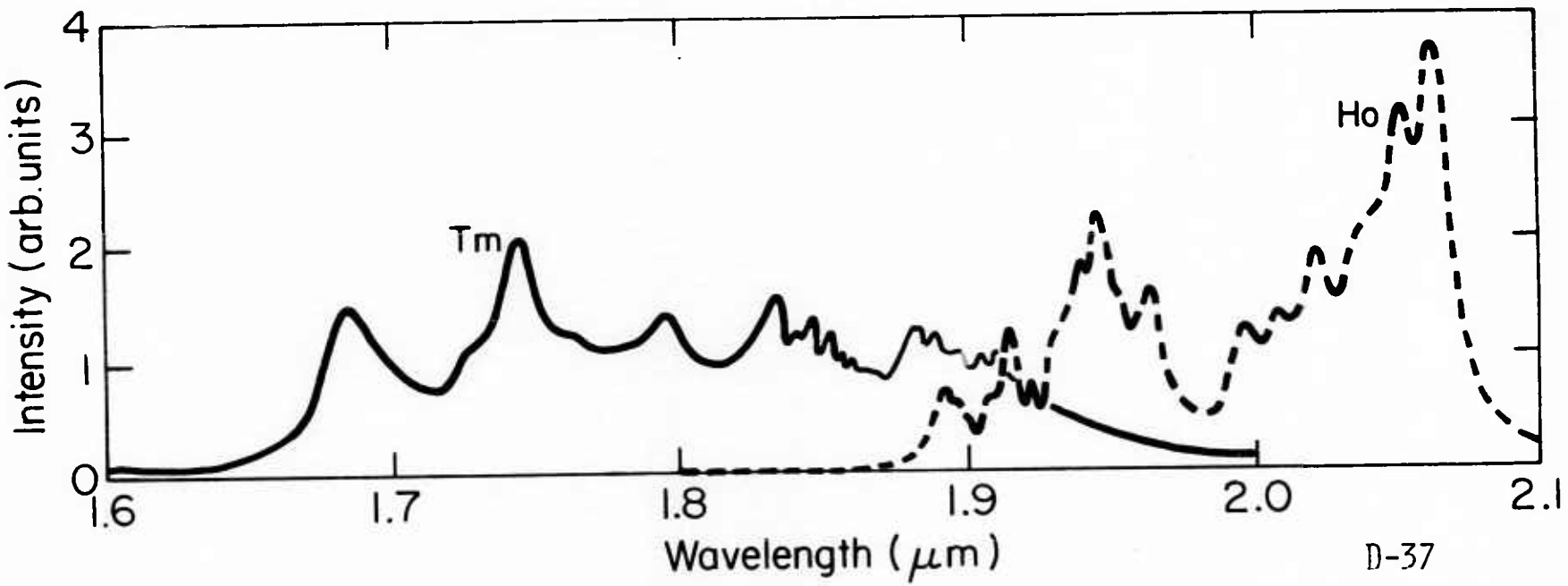

Figure 11 Tm($^3H_4$) and Ho($^5I_7$) Overlap

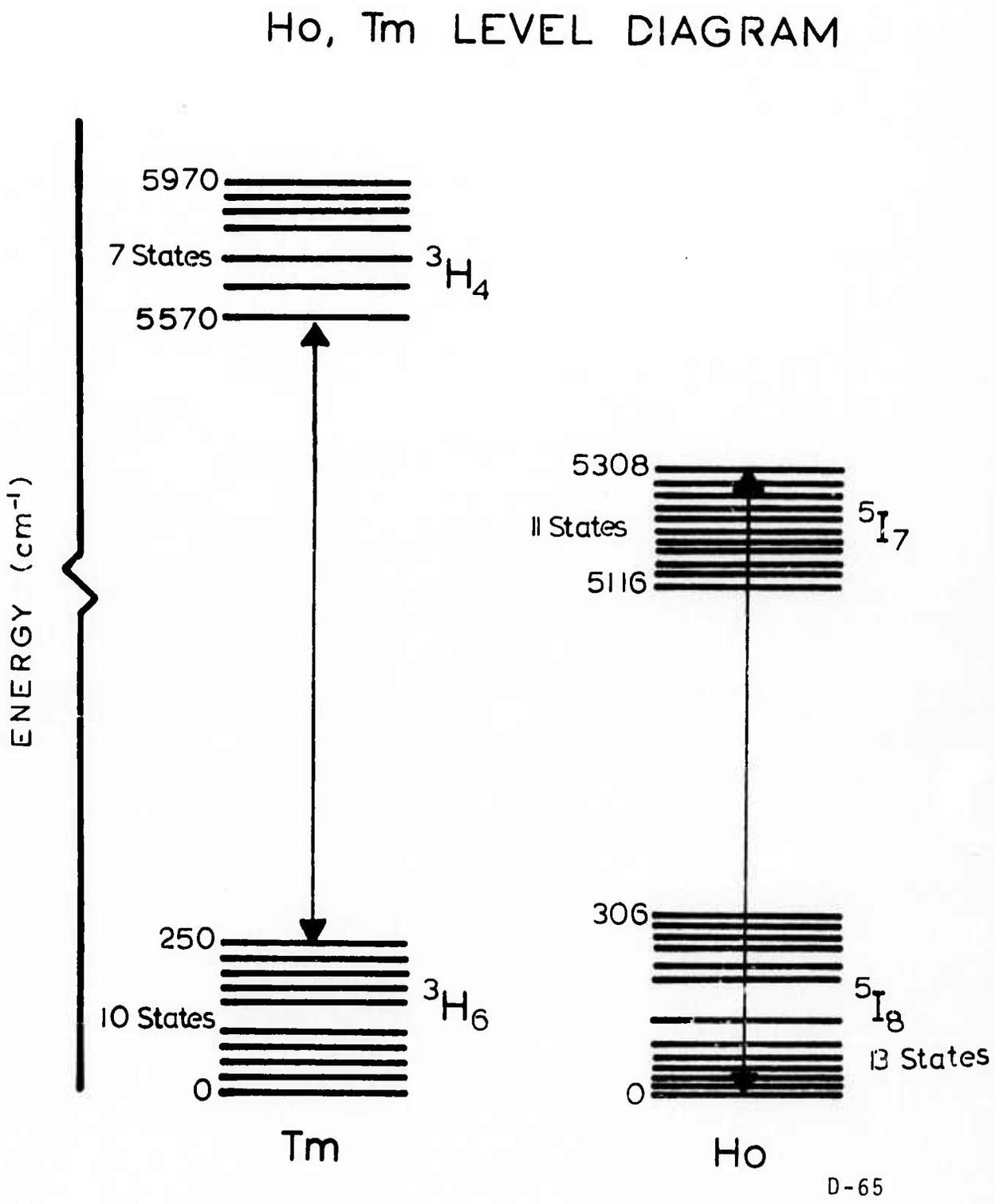

Figure 12 Ho($^5I_7$) - Tm($^3H_4$) Resonance

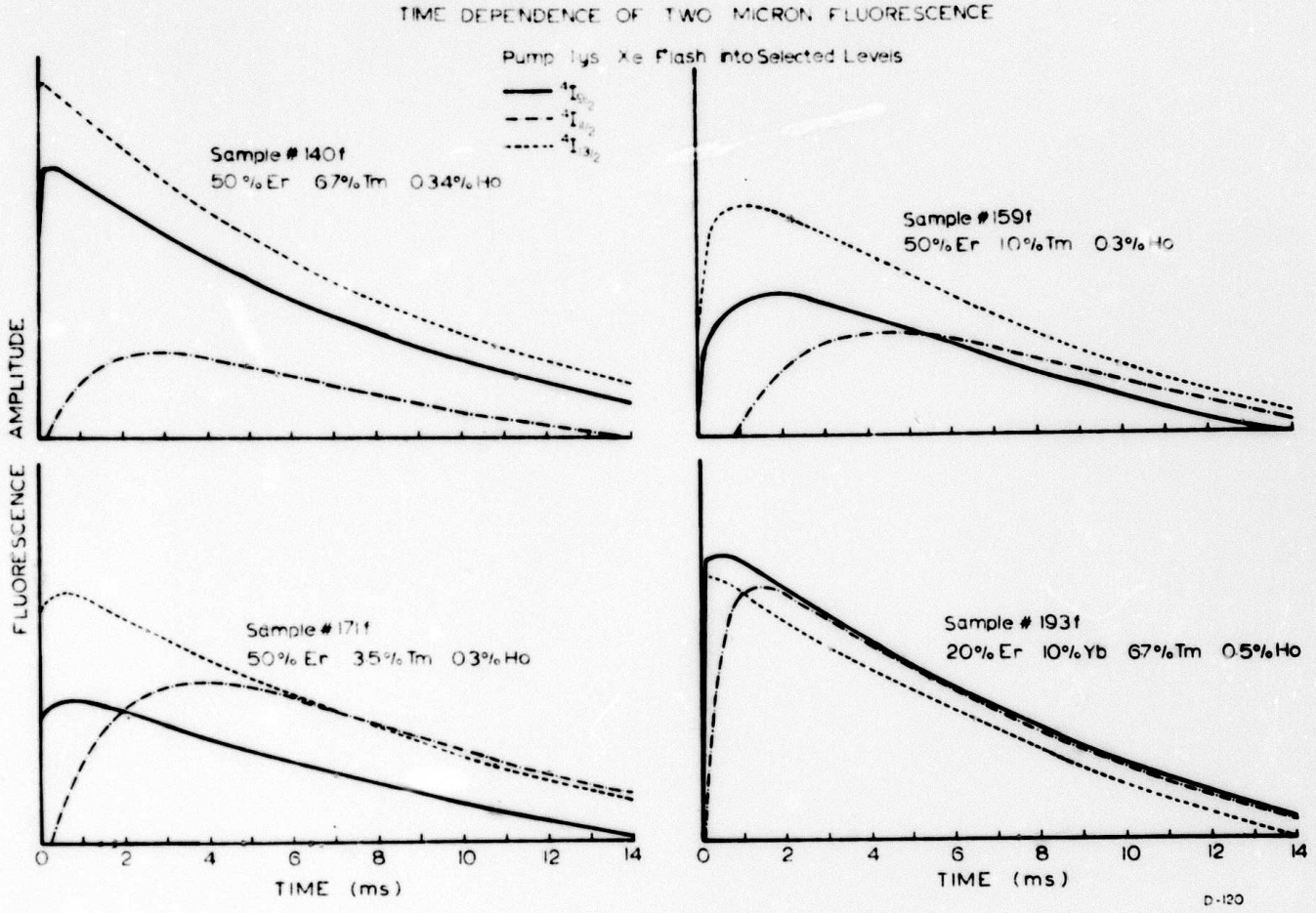

Figure 13 Time Dependence of Two Micron Fluorescence

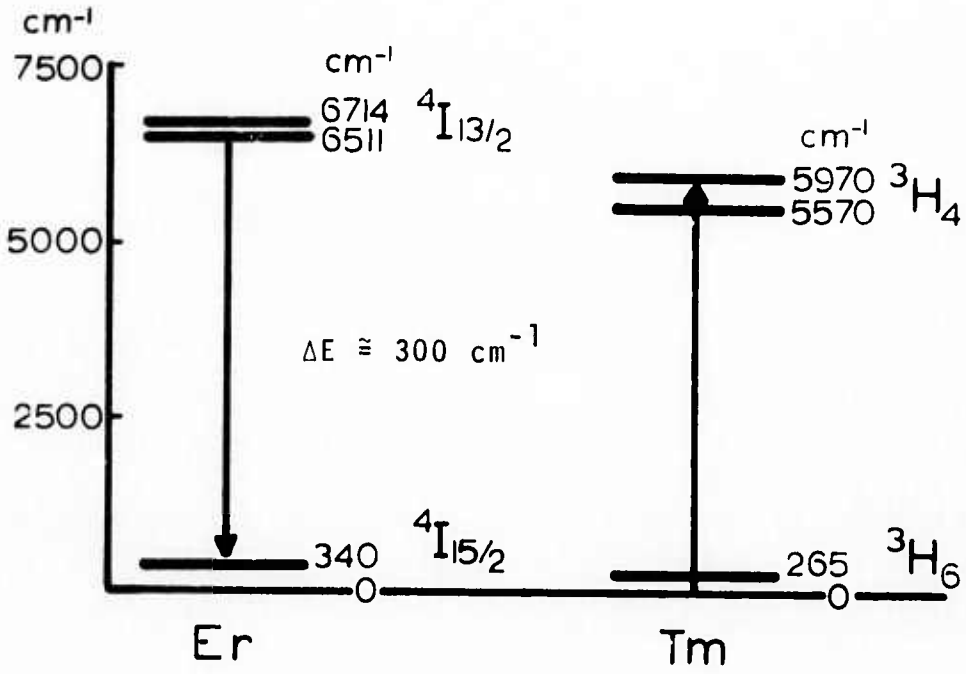

Figure 14 Er($^4I_{13/2}$) - Tm($^3H_4$) Transfer

very high, the $^4I_{13/2} \rightarrow {}^3H_4$ transfer time is insensitive to Tm^{3+} concentration as Er-Er migration is very rapid. For Tm^{3+} concentration above 1% the transfer yield from $^4I_{13/2}$ is near unity.

Tm $^3H_5$: No fluorescence was detected from the Tm $^3H_5$ level in any of the crystals. The multi-phonon relaxation rate from this level to $^3H_4$ should be of the order of 10^4 sec^{-1}.[15] There are no resonant or near resonant transfer processes that could quench this level. Thus all excitations in Tm $^3H_5$ relax to $^3H_4$ with unity quantum efficiency.

Ho $^5I_6$: Because of the low Ho concentration in the crystals investigated, it was impossible to selectively excite the $^5I_6$ level and at the same time observe any fluorescence from this level. Again because of the low Ho concentration it is of little importance what happens to these levels since their contributions in pumping of the laser are insignificant. Nearly resonant transfer from the Ho $^5I_6$ to Tm $^3H_5$ could quench the Ho $^5I_6$ level.

Er $^4I_{11/2}$: This very important level, while not contributing to sensitization, provides the key to understanding the transfer sequence. There are no resonant or near-resonant transfer processes in this system that can quench the Er $^4I_{11/2}$ level. In YLF doped with only Er, the $^4I_{11/2}$ lifetime is 3.6 ms. $^4I_{11/2}$ relaxes radiatively to the ground state $^4I_{15/2}$ and to $^4I_{13/2}$ and by multi-phonon relaxation to $^4I_{13/2}$; the quantum yield of the combined relaxation to $^4I_{13/2}$ is 0.5. In αβYLF crystals $^4I_{11/2}$ is not strongly quenched (lifetime ~ 1 ms). Despite the long lifetime of this intermediate level, the 2 μm fluorescense rise when the higher Er^{3+} levels are pumped is ~ 100 μs - (see Fig. 15) - positively ruling out internal relaxation within each Er^{3+} ion to $^4I_{13/2}$ with subsequent transfer to the Tm^{3+}.

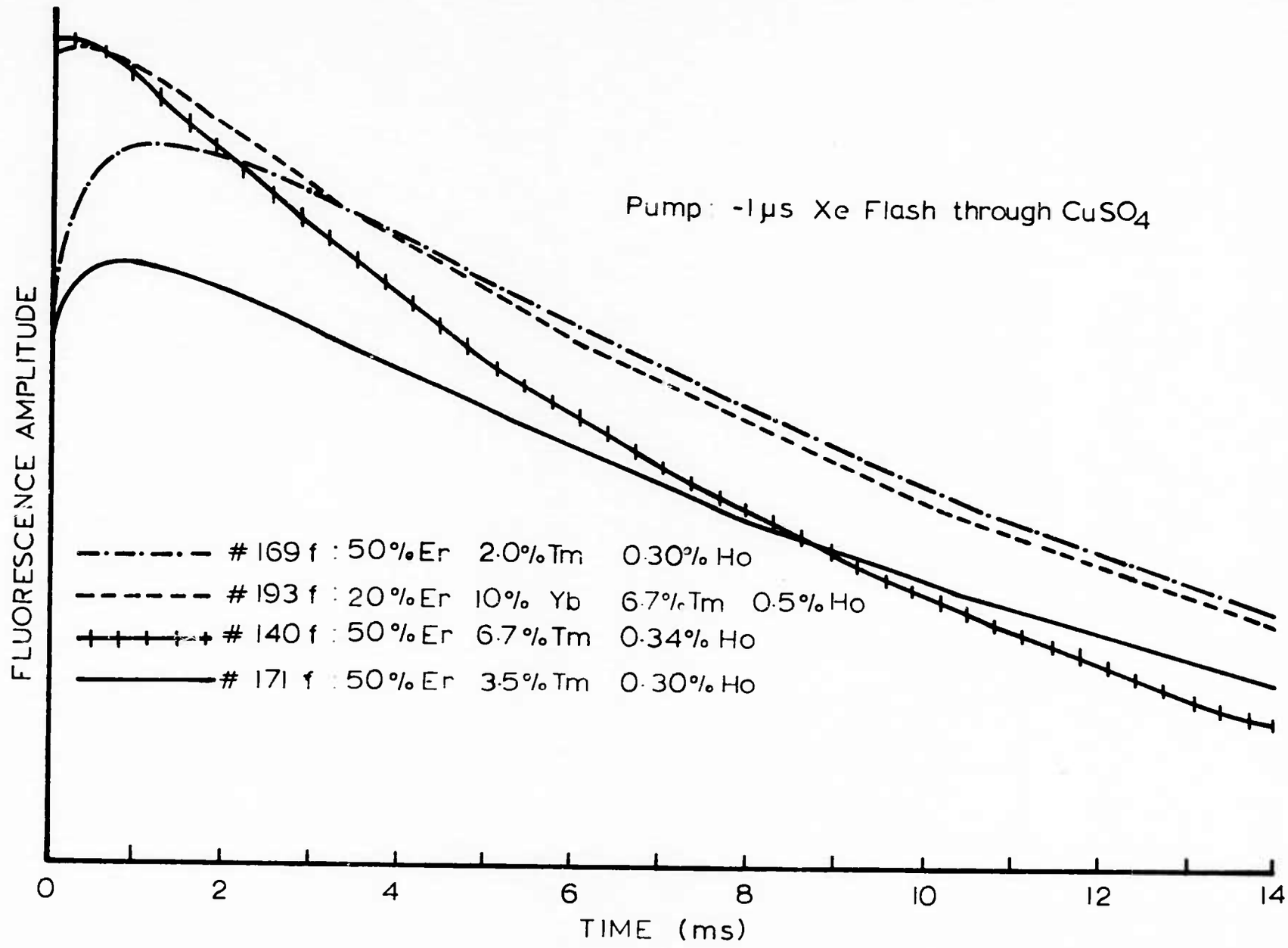

Figure 15 Time Dependence of Two Micron Fluorescence in αβYLF Samples - Levels Above $^4S_{3/2}$ Pumped

Quenching of $^4I_{11/2}$ is due to the Tm $^3H_5$ and the Ho $^5I_6$ levels. The measured quantum efficiency of $^4I_{11/2}$ in feeding $^5I_7$ is ~ 0.8 but the rate is too slow for effective laser sensitization. Addition of Yb does increase the rate (crystal 193f in Figure 13); however, the rate is still too slow and Yb quenches $^4S_{3/2}$ competing with other more efficient transfer schemes in flash pumped operation.

In Figure 13 the 2 μm fluorescence rise is shown when selective levels are pumped with a short flash pulse. Note that when $^4I_{11/2}$ is pumped the 2 μm rise is very long; in typical long pulse oscillations the laser emission is completed before the maximum due to $^4I_{11/2}$ is reached.

Er $^4I_{9/2}$: The lifetime of Er $^4I_{9/2}$ is short (10-100 μs) even in lightly doped crystals. This is because of multi-phonon relaxation to $^4I_{11/2}$ of almost unity quantum efficiency. In the alphabet crystals, however, it is found that the multi-phonon relaxation efficiency decreases with increasing Tm concentration. Figure 15 shows the $^4I_{13/2}$ fluorescence under selective pumping of $^4F_{9/2}$, $^4I_{9/2}$ and $^4I_{11/2}$ with a fast pulse. In this crystal (1% Tm) the multi-phonon relaxation efficiency is down to 0.3. At Tm concentrations greater than 3.5%, no $^4I_{11/2}$ fluorescence is observed when $^4I_{9/2}$ is pumped. At the same time the quantum efficiency of $^4I_{9/2}$ in feeding Ho $^5I_7$ approaches 2. The transfer process here is the resonant process Er $^4I_{9/2} \rightarrow {}^4I_{13/2}$, Tm $^3H_6 \rightarrow {}^3H_4$ followed by Er $^4I_{13/2} \rightarrow$ Tm $^3H_4 \rightarrow$ Ho $^5I_7$ and Tm $^3H_4 \rightarrow$ Ho $^5I_7$.

Tm $^3F_2$, $^3F_3$ and $^3F_4$: Because of the small gaps between these levels everything relaxes very rapidly to $^3F_4$. Because of the closeness of Tm $^3F_4$ and Er $^4I_{9/2}$ it is difficult to separate these levels. But here also the resonant process Tm $^3F_4 \rightarrow {}^3H_4$, Er $^4I_{15/2} \rightarrow$ Er $^4I_{13/2}$ yields a quantum efficiency of 2.

50%Er 1%Tm 0.3%Ho

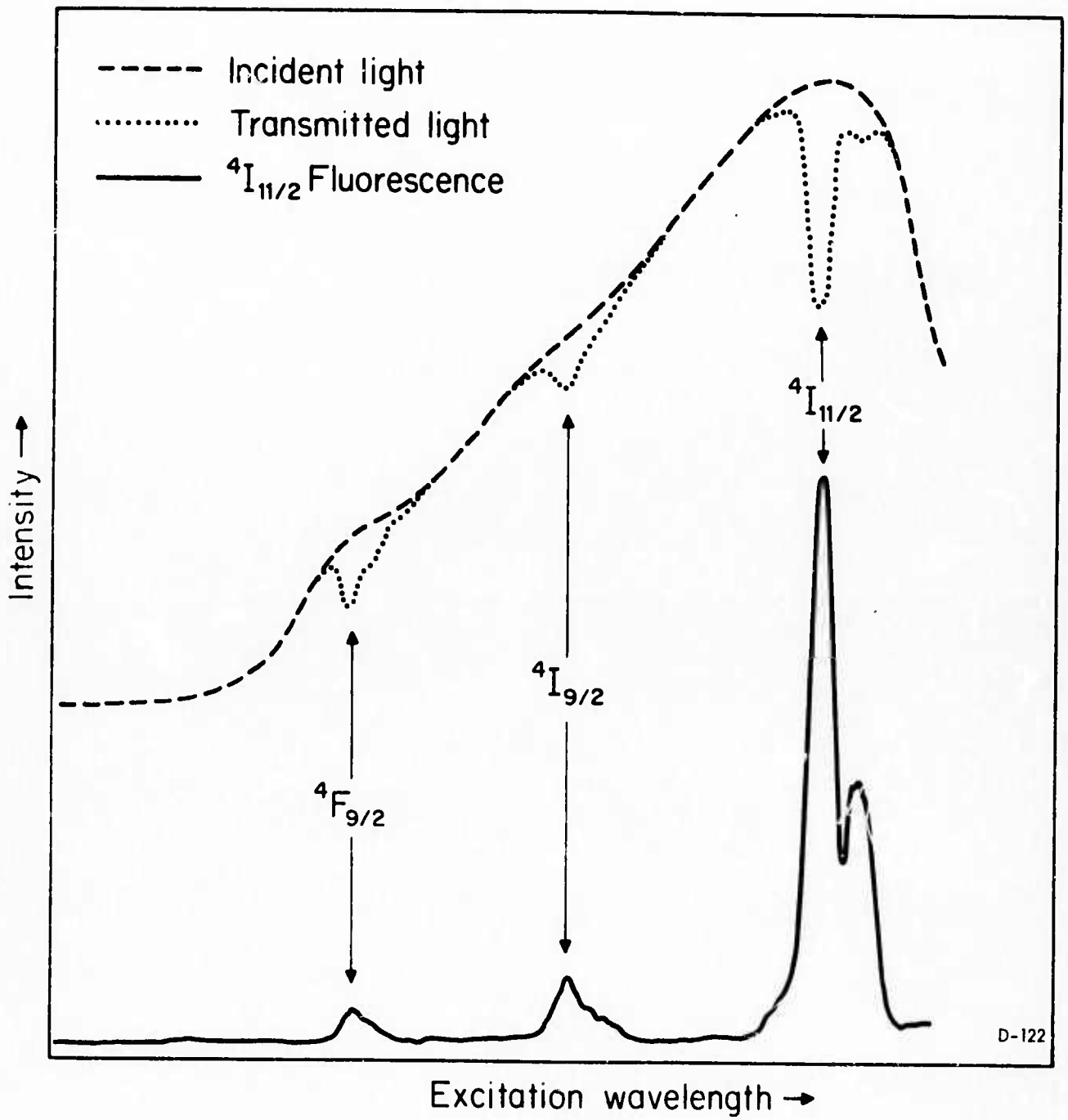

Figure 16 Two Micron Fluorescence Excitation Spectrum (Quantum Measurement) Efficiency

Er $^4F_{9/2}$: As with $^4I_{9/2}$, this level has a quantum efficiency of 2 in feeding Ho $^5I_7$ for Tm concentrations greater than 2%. The quenching of $^4F_{9/2}$ is through transfer to Tm $^3F_2$ or by the resonant transfer scheme

$$^2F_{9/2} \rightarrow {}^4I_{13/2}(Er): \; {}^3H_6 \rightarrow {}^3H_5(Tm).$$

Er $^4S_{3/2}$: The quantum efficiency of $^4S_{3/2}$ was found to be 3 for Tm concentrations greater than 3.5%, and with the same dependence on Tm concentration as was found for Er $^4I_{9/2}$. The most likely processes here are[1]

(a) $^4S_{3/2} \rightarrow {}^4I_{9/2}(Er): \; {}^3H_6 \rightarrow {}^3H_4(Tm)$

(b) $^4I_{9/2} \rightarrow {}^4I_{13/2}(Er): \; {}^3H_6 \rightarrow {}^3H_4(Tm)$

(c) $^4I_{13/2} \rightarrow {}^4I_{15/2}(Er): \; {}^3H_6 \rightarrow {}^3H_4(Tm)$

The net result being three ions excited to $^3H_4$ per initial $^4S_{3/2}$ excitation; the last step is

(3) $^3H_4 \rightarrow {}^3H_6(Tm): \quad (3) \; {}^5I_8 \rightarrow {}^5I_7(Ho)$

Instead of step (a) the following may occur:

(a') $^4S_{3/2} \rightarrow {}^4I_{13/2}(Er): \; {}^4I_{15/2} \rightarrow {}^4I_{13/2}(Er)$

with the same steps (b) and (c). Steps (a) and (a') are experimentally indistinguishable and yield the same net result. Both processes probably occur.

Other Levels

Levels above $^4S_{3/2}$ were not investigated but a number of resonances could yield quantum yields up to four. For example:

$$^2P_{3/2} \rightarrow {}^2H_{9/2}(Er): \; {}^4I_{15/2} \rightarrow {}^4I_{13/2}(Er)$$

$$^2H_{9/2} \rightarrow {}^4S_{3/2}(Er): \; {}^3H_6 \rightarrow {}^3H_4(Tm)$$

are possible resonant or near resonant transitions which would yield quantum yields of 4. These processes were not investigated as their concentration dependence is probably very weak at the high Er concentrations utilized in laser crystals.

4.2.3 DISCUSSION OF RESULTS

The decay modes of each level up to $^4S_{3/2}$ in αβYLF have been measured. Direct radiometric measurement of quantum yields of up to three have been obtained in appropriately doped αβYLF confirming the transfer mechanism proposed in reference 1. The results of the spectroscopic investigation, particularly with reference to variations in the Tm^{3+} concentration, are in general agreement with laser testing of rods of different composition.

The implications for laser design are as follows:

- Spectroscopic measurements must be interpreted with care. For example, if the peak fluorescence amplitude of samples of different Ho^{3+} concentrations were compared radiometrically, the composition with the highest 2 μm fluorescence amplitude would not result in the most efficient laser operation.[18] This is simply due to the fact that in a three level system lasing action depends on population inversion, whereas fluorescence amplitude depends only on upper level population. For Ho concentrations between 0.1 - 2% the Ho fluorescence increases with concentration - but the upper level population required for threshold increases faster.[1]

- The optimum composition for laser operation does not necessarily correspond to the composition with the highest energy transfer

efficiency. This again follows from the three level character of the laser transition; the number density of ions, N_7, which must be pumped at threshold is linear in the active ion density. To optimize laser efficiency requires maintaining low active ion densities with high transfer efficiency.

- Direct measurement of the Er-Tm transfer yield shows that the efficiency in feeding Tm $^3H_4$ is as high as possible with 50% Er, Tm > 4%.

- The Er^{3+} concentration is determined by pump uniformity considerations. The transfer efficiency is insensitive to the Er^{3+} concentration at doping levels above ~ 20%.

- The optimum Tm^{3+} concentration is determined (apart from the minimum required for complete quenching of the Er^{3+}) by the last step of the transfer sequence - $^3H_4 \leftrightarrow {}^5I_7$. To maintain rapid transfer at Ho^{3+} concentrations < 0.3% requires fairly high Tm^{3+} concentrations (in this way high migration rates in the Tm^{3+} minimize the effect of the range dependence of the transfer rate). However, as the Tm:Ho population ratio increases, the transfer yield diminishes as evidenced by increasing Tm^{3+} emission.(1)

- Maintaining very high transfer rates (much faster than the $^5I_7$ decay rate) is essential for efficient laser operation. It has been shown(1) that for a pump band with a transfer rate of 2.5×10^3 sec^{-1} feeding with unit quantum efficiency a metastable level with a decay rate of 10^2 sec^{-1} (values appropriate to the composition 50% Er, 2% Tm 0.3% Ho), the peak inversion is 20% smaller than in the case of an infinitely fast transfer rate. Measurements of the $^5I_7$ decay rate

near threshold, however, have revealed that the decay rate is considerably faster near threshold due to amplified spontaneous emission. The decrease in the peak inversion is then considerably larger in laser operation (with a measured lifetime of 4 ms near threshold the peak inversion is 45% smaller); furthermore if the radiative rate of the pump band is taken into account losses due to slow transfer rates are even more severe. To determine whether a composition will be an efficient pulsed laser material a necessary (but not sufficient) condition is a rapid buildup (< 100 μs) of the 2 μm fluorescence.

Optimum material composition is defined as that which can yield performance suitable for hand held operation. For certain applications where constraints on input energy are not as severe higher Ho^{3+} concentrations will yield higher Q-switched energy storage capability. For example, 500 mJ has been switched[4] from a rod of dimensions ~ 3 x 30 mm of composition 50% Er, 6.7% Tm, 1.7% Ho but the input energy required would be 20-30 joules in an optimized pump cavity.

SECTION 5

LASER MEASUREMENTS

The intent of laser measurements during this program were

- determination of the effects of feed purification techniques on the laser damage susceptibility of the material
- continued studies of the effects of compositional changes on laser efficiency
- demonstration of repetitively pulsed operation in the 1-20 Hz range
- investigation of Q-switched behavior
- evaluation of detector bandwidths (HgCdTe, InAs)

The key results of the program were:

- Demonstration of Q-switched outputs of up to 100 mJ (3mm rod, 50% R) in a single spike without damage to the laser material or the calcite polarizer. However, surface damage was observed in the two $LiNbO_3$ crystals used at ~ 100 mJ (3 mm aperture, 50% R). The source of laser damage observed in a previous αβYLF boule[1] at much lower power densities was apparently eliminated by the use of zone refined feed.
- Comparative measurements of the laser efficiency of three different material compositions show that the addition of Yb^{3+}

decreases laser efficiency in Xe flashpumped operation. This is believed to be due to quenching of $^4S_{3/2}$ (Er^{3+}) by $^2F_{9/2}$ (Yb^{3+}). On a company funded program thresholds 14% below that observed in boule 140f were observed in the composition

50% Er 5% Tm 0.25% Ho

- Repetitively pulsed operation at 20 Hz was obtained at -15°C. At 20°C operation up to 15 Hz was obtained, and at 10 Hz 0.7 watts output was obtained from a 3 x 22 mm rod. The temperature dependence of the threshold was determined from 0 - 40°C.

- Evaluation of HgCdTe detectors using back biasing voltages from 0 - - 0.7 volts revealed risetimes > 100 ns. Philco L4530 InAs divices exhibited risetimes of < 20 ns.

5.1 COMPARISON OF NEW COMPOSITIONS

Two new compositions were grown and compared to the most efficient composition previously evaluated[1] (140f:409).

Boule #	S/A Code	Composition	Remarks
185f	447	20% Er, 10% Yb 6.7% Tm, 0.34% Ho	American Potash feed not zone refined except for Tm F_3 - zone refined Research Chemicals
193f	452	20% Er, 10% Yb 6.7% Tm, 0.5% Ho	American Potash feed, not zone refined
140f	409	50% Er, 6.7% Tm, 0.34% Ho	Research Chemicals feed, not zone refined

It is emphasized that comparison of laser performance of different compositions can be misleading as isolating the effects of composition alone is extremely difficult. Factors which can strongly influence laser performance include pump conditions (flashlamp current density, pumping geometry, rod quality, size and finish and optical alignment).

In comparative tests it is not always possible at the present time to employ rods of the same size and optical quality. However, in all cases, the pump lamp is longer than the rod and none of the rod is shadowed; thus the threshold should be nearly independent of length. The effects of optical quality are difficult to account for in such a comparison. It should be noted, however, that lasing threshold in αβYLF is far less sensitive to the presence of scattering than for a four level laser (Nd glass or YAG).

One of the most serious experimental difficulties encountered in such a comparison is resonator alignment ambiguities. Using a He - Ne alignment laser, it is not possible to positively identify the optimum mirror positions. Instead, the resonator is "tweaked" by observing the output energy for fixed input as small changes in the mirro. positions are made. This is a very tedious procedure in an uncooled cavity, as an adequate interval between shots must be maintained in order for the rod to return to ambient temperature. The comparative data presented are the "best" data that could be obtained for each rod.

In Table 5-1 and Figures 17 and 18, a comparison is shown between these three compositions. In all cases, rods of the 409 composition exhibited the lowest threshold and highest slope efficiency. The 409/447 comparison is somewhat ambiguous due to the misalignment between the faces of the 447 rod.

5.1.1 PERFORMANCE OF 409d.1

The most efficient room temperature data obtained to date are shown in Figure 19. These data were obtained in a separate program[18] and indicate the high efficiency which can be obtained in a more favorable pumping geometry described below:

Lamp:	ILC 3 x 20 mm 3000 Torr Xe
Bank:	75 μf, 38 μH, pulsewidth 140 μs FWHM
Cavity:	Front surface silvered cylinder length = 27 mm diameter 10 mm
Trigger Mode:	Parallel to cavity/simmered
Resonator:	flat/flat - 95% R
Rod Size:	3 x 14 mm - clear polished barrel
Temperature:	71°F

Simmer mode operation was obtained using a quasi-simmer circuit as degredation of the silver pump cavity reflector could not be avoided when the lamp was continuously simmered. The improvement in laser operation using a simmered lamp is in good agreement with the improved electrical/radiant conversion efficiency of Xe flashlamps operated in the simmered mode.[18]

TABLE 5-1

LASER PERFORMANCE vs. COMPOSITION

ROD	COMPOSITION	PERFORMANCE	REMARKS	CONDITIONS
409d.1	50% Er, 6.7% Tm 0.34% Ho	6.5 joule threshold 11 J in/43 mJ out	3x14 mm, polished O.D. excellent optical quality	3x20 mm, 3000 Torr Xe lamp 75 µf, 80 µh pulsewidth: 140 µs FWHM Cavity: 18 mm second Surface silver onto pyrex 95% R flat Max.R: 1 m Radius, 72°F
447.1	20% Er, 10% Yb 6.7% Tm 0.34% Ho	7.3 joule threshold 11 J in/12 mJ out	3x15 mm, polished O.D. some inclusions, slight misalignment of rod faces	
409a.2	50% Er, 6.7% Tm 0.34% Ho	14 joule threshold	3x16 mm, rough ground O.D.	3 x 54 mm, 2000 Torr Xe 100 µf, 100 µh 37 mm front surface cavity lead resistance ~0.4 ohms 74°F 95% R flat/flat
447.2	20% Er, 10% Yb 6.7% Tm, 0.34% Ho	17 joule threshold	3x16 mm, polished O.D. poor optical quality, slight misalignment of faces	
409d.1	50% Er, 6.7% Tm 0.34% Ho	Threshold <7 joules 12 joules in/62 mJ out	3x14 mm, polished O.D.	2.5x25 mm, 3000 Torr Xe 50 µf, 46 µh 18 mm second surface Ag cavity 95% R flat/flat 74°F
452	20% Er, 10% Yb 6.7% Tm 0.50% Ho	10 joules threshold 12 joules in/33 mJ out	3x25 mm, polished O.D. Excellent optical quality	

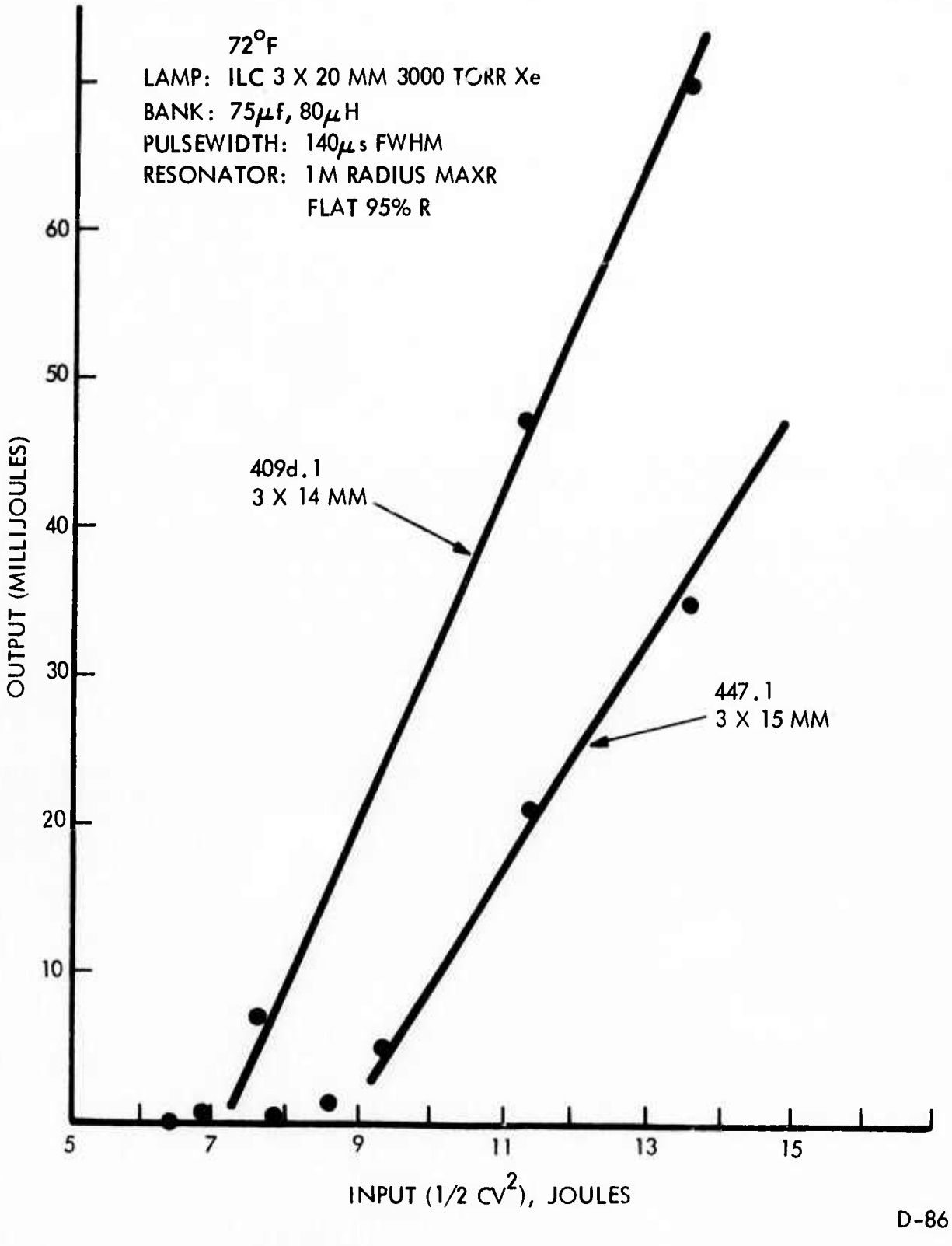

Figure 17 Efficiency Comparison Rods 409d.1 and 447.1

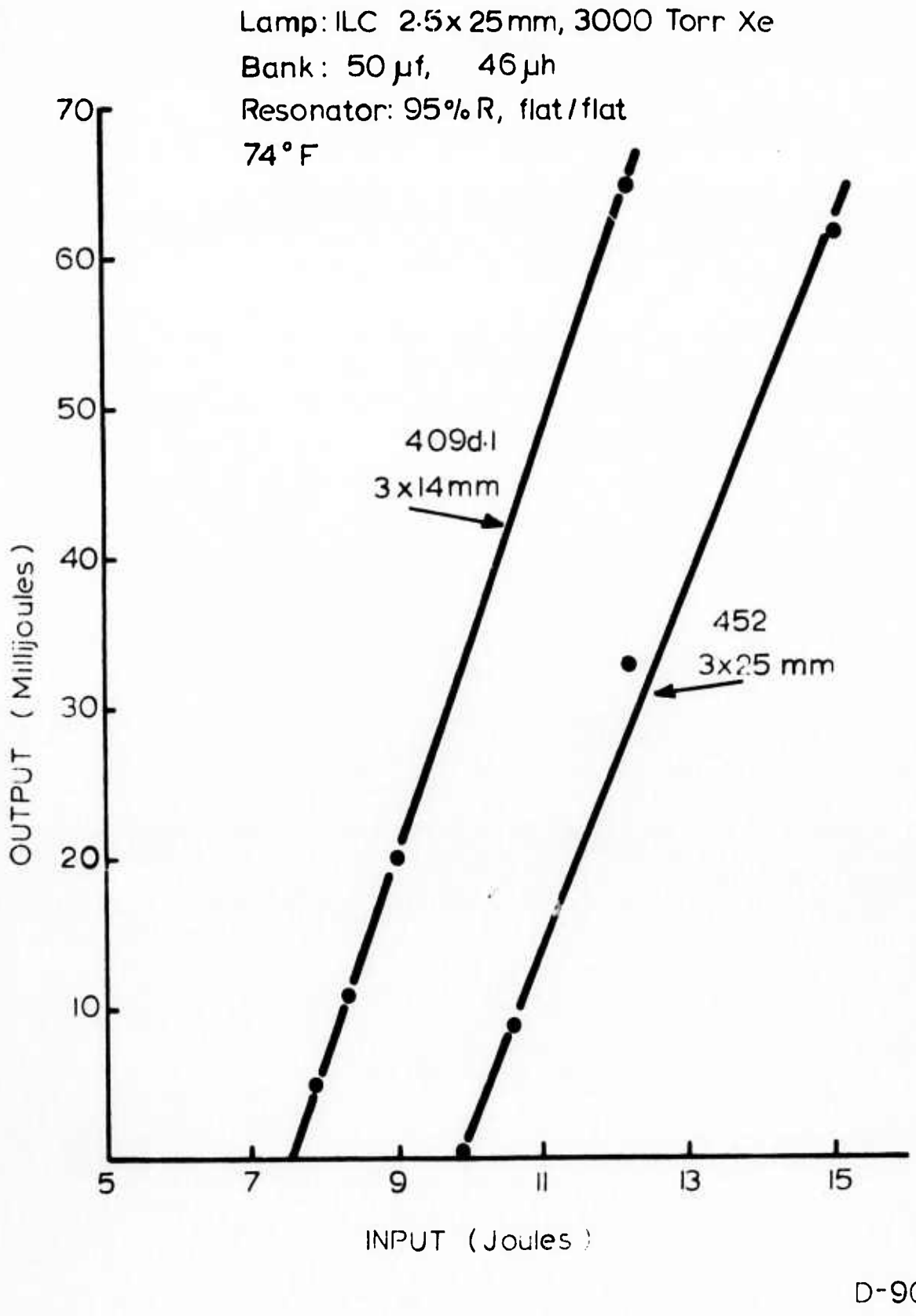

Figure 18 Efficiency Comparison Rods 409d.1 and 452

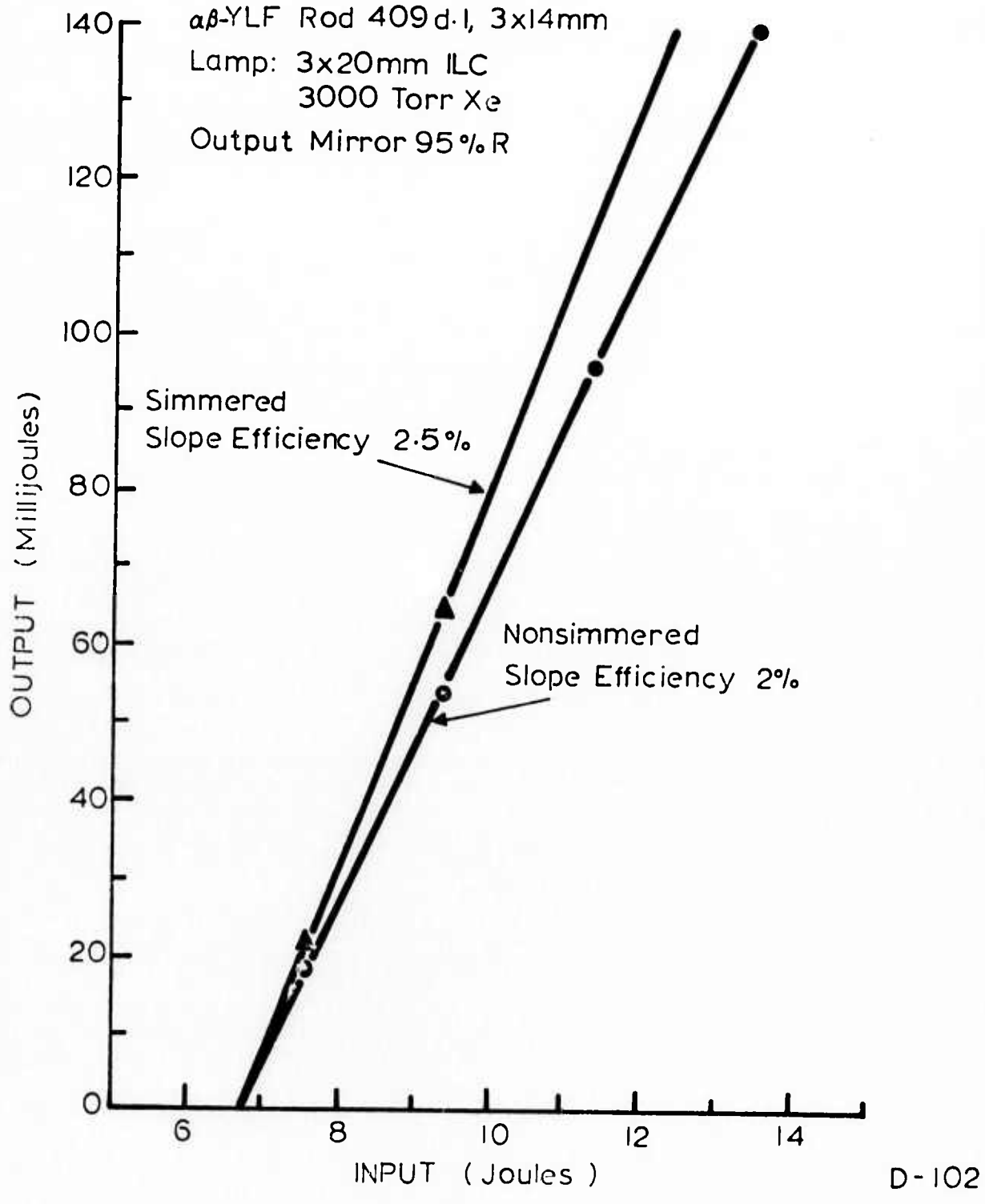

Figure 19 Effect of Simmer Mode on Two Micron Laser Output

5.1.2 COMPARISON OF 409f.3 AND 474.5

Long pulse measurements were made in the pump cavity described above using a non-simmered lamp. Both rods were 3 x 15 mm and of excellent optical quality. The compositions of the rods were

409f.3 :	50% Er	6.7% Tm	0.34% Ho	(140f)
474.5 :	50% Er	5% Tm	0.25% Ho	(224f)

Measurements were made on a company funded[19] program as rods from the boule (grown on this contract) were obtained after the end of this program. Threshold for the new composition with reduced Ho and Tm concentration was 14% lower than in the previously "optimum" composition, 140f. In this new composition the Ho^{3+} concentration was reduced by ~ 25% and the Tm:Ho population ratio of 140f maintained. The lower long pulse threshold in the newer composition was expected[1]; the important parameter which must be determined is the extractable energy in Q-switched operation.

5.2 REPETITIVELY PULSED OPERATION

Experiments were carried out in a number of water cooled pump cavities in order to determine performance of the material in the 1-20 Hz range. The pump cavities were in no way optimal and the efficiencies reported herein could be very substantially improved. However, the results indicate that αβYLF is capable of operation in the 1-20 Hz region at modest output powers (1-10 watts) at or near room temperature. Realization of performance suitable for device applications, particularly for hand-held system, will require technological developments parallel to those expended for light weight Nd:YAG systems.

5.2.1 16 pps OPERATION: SPHERICAL PUMPING CAVITY

Rod 409c.2 (3 x 23 mm, rough ground O.D.) was mounted in an 8 inch spherical pumping cavity with an aluminum reflective surface (Liberty Mirror Coating No. 749). Approximately 8 mm of the rod ends were shadowed by the metal "O" ring holders. The rod and lamp were cooled in separate loops with the flow rate over the rod only 0.5 ℓ/min. Other pump conditions were:

Flashlamp:	ILC 3 x 50 mm, 2000 Torr Xe
Bank:	50 μf, 200 μh
Trigger Mode:	Parallel
Resonator:	1 meter radius max, flat 96% R attached to rod

Threshold was approximately 20 joules in single shot; at 16 pps the input power was approximately 320 watts with ∿0.3 watts output. Operation at 16 pps was obtained for only ∿30 sec due to degradation of the attached dielectric mirrors.

An analysis[13] of the heat flow in the present setup (0.8 ℓ/min H_2O at 10°C with an assumed laser rod heat load of 20 watts, 1.0 mm annulus over the rod) indicates that a factor of two reduction in rod surface temperature can be obtained simply by increasing the flow rate to ∿ 6 ℓ/min.

5.2.2 10 Hz OPERATION

In long pulse operation 0.7 watts were obtained from 3 x 22 mm of unshadowed αBYLF rod at 10 Hz. The efficiency obtained was largely determined by the pump conditions which were:

Pump Cavity:	8 inch diameter aluminized sphere Liberty Mirror Coating No. 749
Rod:	456.5, 3 x 27 mm, MIT Boule No. 201f 50% Er, 6.7% Tm, 0.34% Ho
Holders:	Stainless/O-ring seal - 5 mm of rod shadowed
Lamp:	ILC 3 x 50 mm, 3000 Torr, Xe
Storage Bank:	25 μf, 130 μh, parallel triggered
Resonator:	Plane parallel, attached coatings - max/95% R
Cooling:	Separate loops over lamp and rod Flow rate over rod - 3 ℓ/min (0.8 gal/min) at 18°C

Threshold in this pumping cavity was below the minimum energy (voltage) required to flash the lamp under these conditions: 23 joules. The input versus output power is shown in Figure 20 ; at ~ 550 watts input, 700 mW output was obtained with an incremental efficiency of ~ 0.2%, despite the use of a lamp 2X longer than the rod. Up to this point, no damage to the rod was observed. However, during operational checks at 50 J/pulse - 20 Hz (1 kW), the rod fractured. It is not known whether the fractures initiated at surface microcracks or were indicative of the material limitation. Such microcracks greatly increase the stress at the surface of a uniformly heated rod cooled only at the surface.

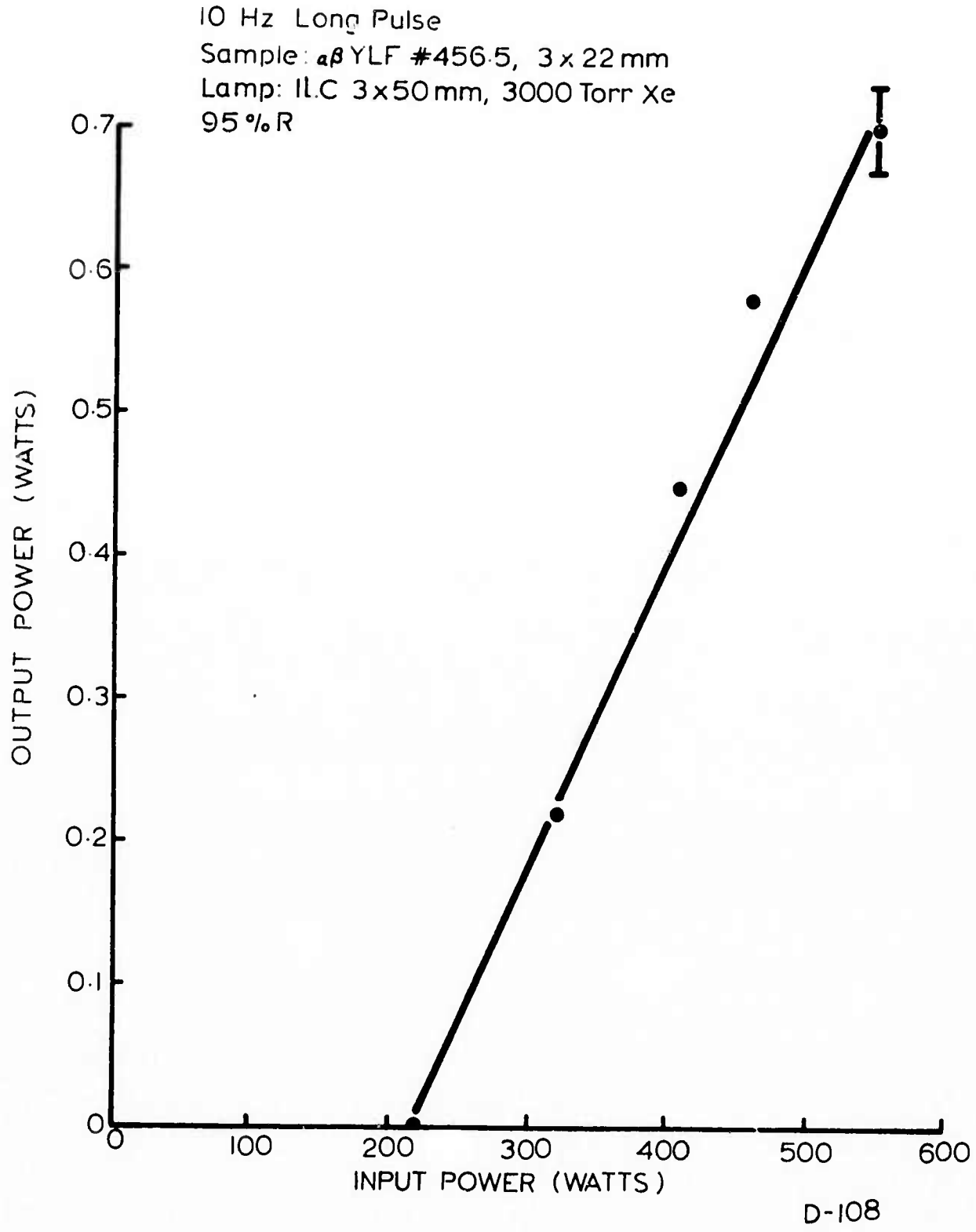

Figure 20 Two Micron Output vs Input Power

5.2.3 20 Hz OPERATION

In order to determine the effects of temperature on lasing threshold and slope efficiency, long pulse experiments were carried out under the following conditions:

Rod:	462.2, 50% Er 6.7% Tm 0.5 Ho
Coolant:	denatured alcohol heat exchanged to dry ice/methanol
Pump Cavity:	silvered ellipse, lamp and rod cooled with separate jackets
Flashlamp:	ILC 3000 Torr Xe (3.5 x 55 mm)
Rod holders:	Stainless with "O" ring seals.

Unfortunately a number of experimental difficulties were encountered and reproducible data were not obtained. However, at -15°C operation at 20 Hz, long pulse, was obtained. The output at 20 Hz and below was not stable due to mechanical difficulties and measurements of average output power were not attempted.

5.2.4 TEMPERATURE DEPENDENCE OF 2 μm LASER PERFORMANCE

Determination of the temperature dependence of laser threshold and slope efficiency were carried out using the following experimental conditions:

Cavity:	Water flooded, front surface cylinder
	flashlamp/rod separation (centers): 11.1 mm
	length 38 mm, radius: 9.65 mm
	flow rate: < 1.9 ℓ/min
	rod holders: stainless/"O" ring, ~ 5 mm of rods shadowed

Lamp:	ILC 3 x 25 mm, 3000 Torr Xe
Trigger Mode:	Parallel to cavity
Bank:	50 μf, 100 μh, 170 μs FWHM
Rod:	409C.2 3 x 23 mm, 50% Er, 6.7% Tm 0.34% Ho
Resonator:	Mirrors coated onto rod, 96% R.

Temperature of the coolant water was varied using a Korad K-1 cooler. The results shown in Figure 21 indicate an increase of ~ 0.3 joules/°C in threshold over this temperature range in this pumping cavity. Note that the incremental increase in laser threshold is dependent on the overall pumping efficiency. From these data we obtain a normalized temperature dependent threshold rate of change of

1% per °C per joule threshold at 20°C.

Note that this is applicable to a rod of this composition using a "low loss" resonator. With a lower reflectivity output mirror, for example, the threshold temperature dependence would be considerably weaker.

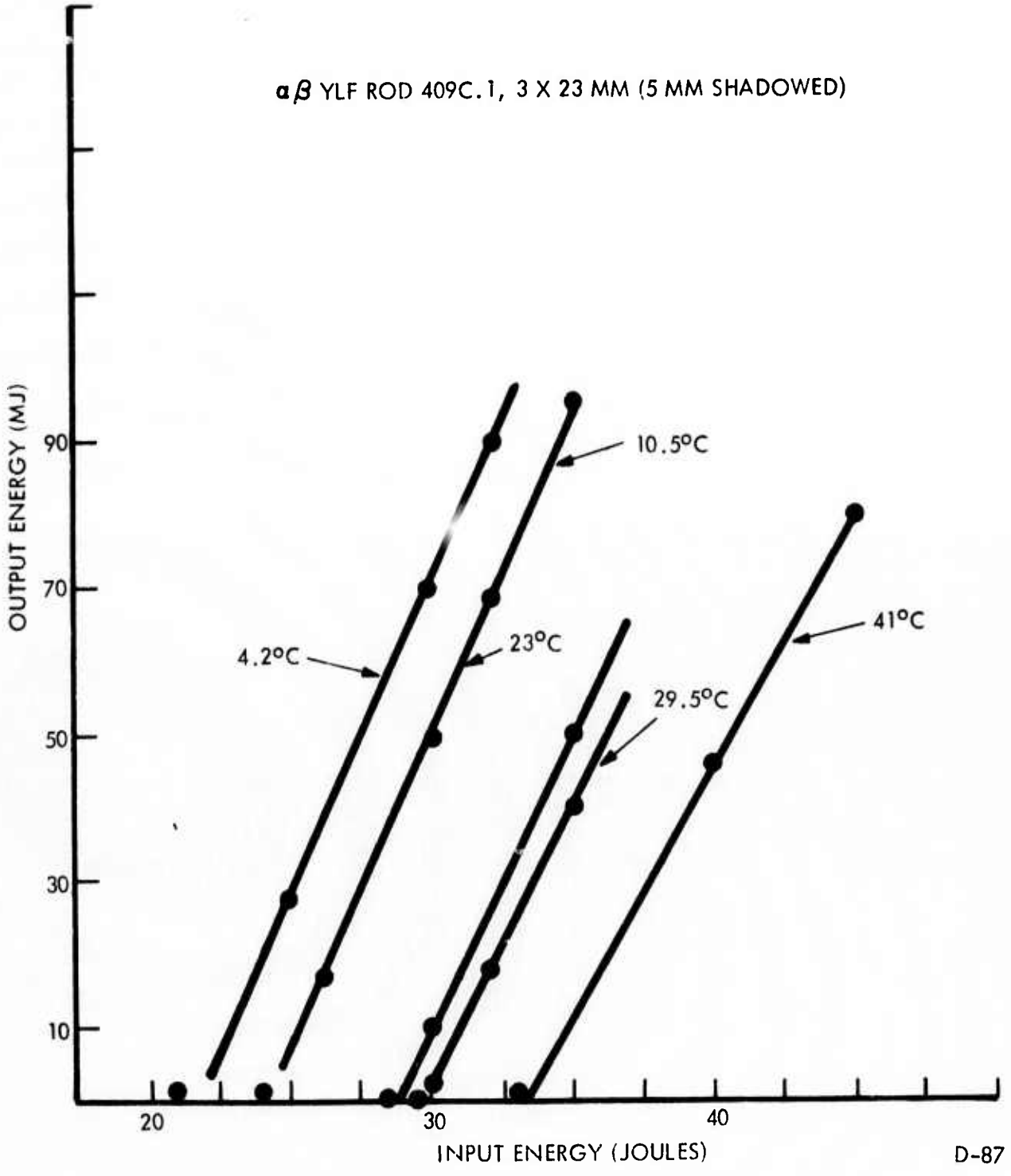

Figure 21 Temperature Dependence of Two Micron Laser Performance

5.2.5 BEAM DIVERGENCE MEASUREMENTS

Measurements of the beam divergence at 3 pps in the water cooled cavity described in 5.2.4 were made in long pulse operation (rod 409d.2, flat/flat resonator, length 29 cm). Measurements were made at three distances using a Barnes InAs with a 25 μm pinhole over the diode. Visual alignment and location of the beam was obtained using the reflection of the rod face of a He - Ne alignment laser aligned normal to the rod face. Measurement of the beam width was made by scanning along one axis (X) to locate the midpoint; then scanning perpendicular to the X scan at the X midpoint; measuring the total width; then measuring the total width along the X axis, perpendicular to the Y axis at the Y axis midpoint. The data are tabulated below:

TABLE 5-2
BEAM DIVERGENCE MEASUREMENT

DISTANCE FROM OUTPUT MIRROR	X/2*	Y/2*	θ†
R_1: 56 cm	0.20 cm	0.18 cm	0.8 mr
R_2: 595 cm	0.75 cm	0.65 cm	1.0 mr
R_3: 1661 cm (54.5 ft)	1.54 cm	1.40 cm	0.8 mr

* X,Y = full width (total distance along axes for which spiking was observed)

† θ = half angle (to total extinction) divergence using X/2 = r

The divergence was calculated from the expression:

$$r = R\theta + r_o$$

where

r_o = aperture radius (1.5 mm at the mirror output)

θ = half angle beam divergence

R = distance from output mirror

r = beam radius at R

Note that the table lists the half angle divergence measured to the full extinction of the laser spiking. As the intensity profile of the beam is not known the full angle beam divergence to the half power points cannot be accurately inferred from these data. The condition in the far field

$$R >> \frac{r^2}{2\lambda} = 53 \text{ cm}$$

was satisfied at R_3. Thus, the worst case full angle raw beam divergence is 1.8 mr; the full angle divergence to the half power points is probably much closer to ~ 1 mr.

The low divergence is indicative of the low strain and lack of index inhomogeneities of this material. This results from growth in the melt under concommitantly smaller thermal gradients than in growth of YAG, for example. Fringe counts of YLF are typically considerably less than one per inch.

5.3 Q-SWITCHED MEASUREMENTS

Q-switched measurements were made with a number of rods of different compositions. The major focus of these measurements, in addition to providing baseline performance data of this material and determining the effects of feed purification technique on the damage susceptibility of the material, was to determine the effects of composition on Q-switched performance. In particular determination of the ratio of Q-switched to long pulse output as a function of Tm:Ho population ratios is of great importance in determining the optimum material composition. While rather extensive Q-switched data were obtained, the determination of the Q-switched output as a function of Tm:Ho population ratio was rendered somewhat ambiguous due to experimental difficulties discussed below.

5.3.1 BACKGROUND

αβYLF would appear to be an excellent Q-switched laser material. The storage time is extremely long (10-15 ms spectroscopic lifetime) and the splitting of the upper manifold provides for very high energy storage/unit volume. This latter property requires some discussion. The upper manifold ($^5I_7$) is split into 11 doubly degenerate states with a total splitting of 191.5cm^{-1}. Threshold is determined by the thermal occupation factor of the upper laser level (0.13 at room temperature). Above threshold the excess population stored in the entire manifold is available (the thermal relaxation time between levels is much faster than the time scale of Q-switched or long pulse oscillation times) to replenish the depleted inversion as the loss due to stimulated emission increases.

However, in this sensitized system another factor must be considered. Energy transfer times between rare earth ions in crystals are generally slow compared to Q-switched oscillation times. In this specific system the excitation energy is shared between the excited $^3H_4$ (Tm) and $^5I_7$ (Ho) levels[1]. In long pulse oscillations the combined energy stored in these manifolds can be extracted (long pulse oscillation characteristic times are typically 10 μs - 1 ms). Oscillation times in Q-switched operation, however, are probably too fast to make use of the energy stored in the Tm^{3+}. Since the energy stored in the Tm^{3+} depends on the Tm:Ho population ratio, the magnitude of this effect can be observed by determining the extractable energy per unit volume as a function of composition in long pulse and Q-switched operation. Experiments were performed with rods of four different Tm:Ho concentration ratios: 3.9:1, 13.4:1, 19.7:1, and 6.6:1. The extractable energy in Q-switched operation was found to be extremely sensitive to resonator conditions, particularly the operating conditions of the $LiNbO_3$, and a relationship between the long pulse to Q-switched extractable energy as a function of composition was not established. In addition surface damage of the $LiNbO_3$ was observed at output levels above 50 mJ. Results are discussed below.

5.3.2 ROD 452.1

Q-switched operation was obtained under the following conditions:

Rod:	452.1, 3 x 35 mm 20% Er, 10% Yb, 6.7% Tm, 0.5% Ho - uncoated
Lamp:	ILC 3 x 35 mm, 3000 Torr, Xe
Resonator:	Plane parallel, length = 60 cm
Q-Switch:	Lasermetrics Model No. 902 $LiNbO_3$
Polarizer:	Calcite Glan Prism
Cavity:	Flooded, front surface silvered cylinder ℓ = 38 mm, r = 9.65 mm Flow rate <0.5 gal/min
Rod Holders:	Stainless/O-ring seal - 5 mm of rod shadowed

At 45 joules input, 43 mJ output was obtained long pulse - the low efficiency was due to the pump cavity. The effects of resonator alignment, Q-switched voltage and Q-switch delay time were investigated. The optimum delay time was found to be 400 ± 100 μs after the trigger to the lamp for a ~ 200 μs flash pulse duration. Variations of the resonator alignment and retardation voltage affected the energy output and the number of spikes. Under the optimum conditions, determined by trial and error, 1/2 of the long pulse output energy was obtained in a single Q-switched pulse at the same input. The long pulse output was that obtained with the polarizer and $LiNbO_3$ in the cavity.

The maximum output which could be obtained in a single pulse was 20 mJ with 95% R. At higher input levels, after pulsing was observed; in fact long pulse oscillations could not be held off completely under static conditions (1/4 wave voltage on - but not switched) at this

input level. This suggests that better results might be obtained with AR coated rods but the major problem, discussed below, was oscillations in the $LiNbO_3$ transmission.

More than 400 shots were taken at peak powers ~ 1 MW without evidence of damage to the rod, polarizer or $LiNbO_3$. Note that the rod was grown using Lindsay Rare Earth feed (not zone refined).

5.3.3 RODS 71.344 and 462.2

Measurements were made with rods of two compositions in order to evaluate the effects of the Tm:Ho concentration ratio on the amount of energy which can be extracted in the Q-switched mode. Unfortunately, in the experiments described below, differences in the laser output in Q-switched and long pulse operation could not be attributed to rod composition alone. Rather the characteristic of $LiNbO_3$ operating as an electro-optic shutter appears to be the major factor limiting the extractable energy in Q-switched operation and the net efficiency at the present time.

5.3.3.1 Rod 71.344

The composition of this material is:

50% Er - 6.7% Tm - 1.7% Ho;

the original composition formulated by Johnson, et al.[20] for CW operation at LN_2 in "αβYAG". A YLF rod of this composition had previously been operated Q-switched with the same efficiency in long pulse[4] but with a rotating mirror. Q-switched operation of this composition was obtained under the following conditions to determine the switched behavior using $LiNbO_3$.

Rod:	71.344: 3 x 25 mm, 5 mm shadowed, no coatings
Lamp:	3000 Torr Xe, 3 x 35 mm
Cavity:	Silvered ellipse, lamp and rod water cooled in separate quartz jackets
Resonator:	plane parallel, length 53 cm
Polarizer/ Q-switch:	Calcite/$LiNbO_3$ - Lasermetrics EOM-902

The results obtained in this rather inefficient pump cavity are shown in Figure 22. The long pulse data were taken with the calcite/$LiNbO_3$ in the resonator; the switched outputs with a 300 μs delay after the initiation of the flashlamp whose total duration was 320 μs. At 50 joules input to the lamp, where the long pulse output was 50 mJ, less than 1 mJ output was observed with the voltage on the $LiNbO_3$ but not switched. Optimum resonator conditions (alignment, polarizer, and 1/4 wave voltage) were determined by the minimum in long pulse output with static voltage on the $LiNbO_3$. Most of the energy output in Q-switched operation was obtained in a single spike; weak long pulse oscillations were not completely suppressed, but accounted for < 10% (estimated from photographs of the output) of the energy.

In previous Q-switched operation of this composition material using a rotating mirror, the Q-switched threshold and slope efficiency were nearly the same as in long pulse. This together with data discussed below indicates that Q-switched performance is limited by the dynamic optical retardation characteristics of $LiNbO_3$.

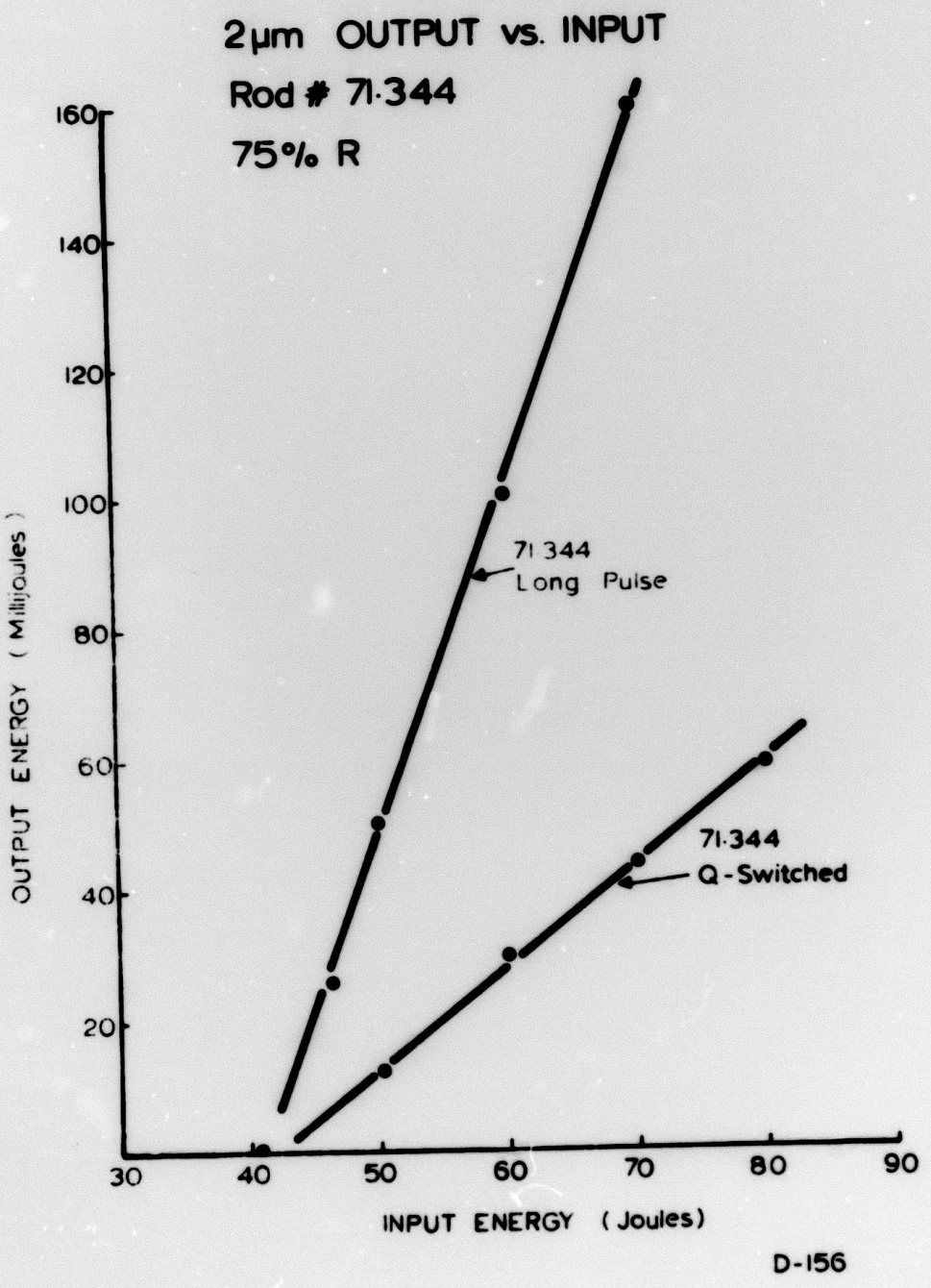

Figure 22 Q-Switched and Long Pulse Output vs Input

5.3.3.2 Rod 462.2

The composition of this material is

50% Er, 6.7% Tm, 0.5% Ho

The experimental setup was as follows:

Rod: 462.2, 3 x 42 mm, 5 mm shadowed

Lamp: 3000 Torr Xe, 3 x 35 mm

Cavity: Silvered ellipse; lamp and rod water cooled in separate quartz jackets

Resonator: Plane parallel, length 50 cm

Polarizer/Q-switch: Calcite/$LiNbO_3$

In comparison between Q-switched and long pulse operation it was found that most of the long pulse output could be obtained in Q-switched operation; however, the output consisted of many spikes. For example, at 32 joules input (37 mJ long pulse, 35 mJ Q-switched using a 300 μs delay) the Q-switched output consisted of up to seven giant spikes spaced 10 μs apart. Confirmation of giant spiking was obtained using two detectors - one monitoring all spikes through the rear mirror, and one sufficiently far removed from a diffuse target so that only giant spikes could be observed.

Long pulse (with polarizer and $LiNbO_3$ in the resonator) and Q-switched output under these conditions were as follows:

TABLE 5-3

Q-SWITCHED AND LONG PULSE OUTPUTS

INPUT ENERGY	OUTPUT*	
	Long pulse+	Q-Switched"
28 J	threshold	threshold
32 J	37 m J	35 m J

* 75 % R

\+ Polarizer and Q-switch in resonator

" multiple spikes

At higher inputs some (long pulse) after pulsing was observed which persisted up to 100 μs. In general, most of the Q-switched energy was in the first pulse; the secondary giant pulses were somewhat erratic under fixed resonator conditions. Such multiple spikes were observed with Q-switch delays from 0 - 600 μs after the flashlamp initiation (flashlamp duration 160 μs). In long pulse operation oscillations began at 270 μs after the trigger to the lamp. The maximum energy extracted under these conditions was at a Q-switch delay of 300 μs; at 600 μs delay approximately half the maximum output was obtained.

Multiple pulse behavior using $LiNbO_3$ to Q-switch Nd:YAG is reported in references 21 and 22. The multiple spiking was attributed to a piezooptic effect induced by the voltage on the crystal. The net effect is to increase the switching time and cause anomalies in the transmission (see Appendix III). This effect can be minimized[22] by applying a reverse voltage to the crystal.

A reverse bias was applied by floating the $LiNbO_3$ above ground and applying a reverse bias of 1.38 KV with a high voltage D.C. supply. The initial voltage on the Q-switch supply was increased (to 3.1KV) to

maintain a net quarter wave retardation. The result was an immediate decrease in the number of giant spikes and a more reproducible output.

Fig. 23 shows the single shot output in long pulse and Q-switched operation with the $LiNbO_3$ back biased. The Q-switched output was for the most part contained in a single spike. Both the long pulse and Q-switched data in Fig. 23 were taken with a damaged Q-switch in the resonator. The damage consisted of two large surface pits which obscured 10-20% of the rod cross section.

5.3.4 LASER DAMAGE

In addition to the problems encountered with transient effects in $LiNbO_3$, laser damage in Q-switched operation was observed in the two crystals available (both obtained from LASERMETRICS). Careful damage studies in $LiNbO_3$ are not a part of this program; moreover, local peak powers may be much higher in "hot spots" than the estimates obtained from the energy output divided by the pulse width.

Bass et al.[23] have studied the passive surface and bulk damage thresholds for $LiNbO_3$ under carefully controlled conditions (at λ = 1.06 and 0.69 μm) and conclude:

(a) internal damage is produced at the same or lower levels of irradiation than required for surface damage

(b) the damage resistance, defined as the maximum power level for which the probability for damage is vanishingly small, for $LiNbO_3$ is 6 MW/cm^2 for a multimode pulse and 350 MW/cm^2 for a single mode (TEM_{00}) pulse at λ = 1.06 μm. The difference in the two levels is attributed to the non-uniform intensity distribution in a multimode beam - that is $LiNbO_3$ will not damage at uniform power levels of

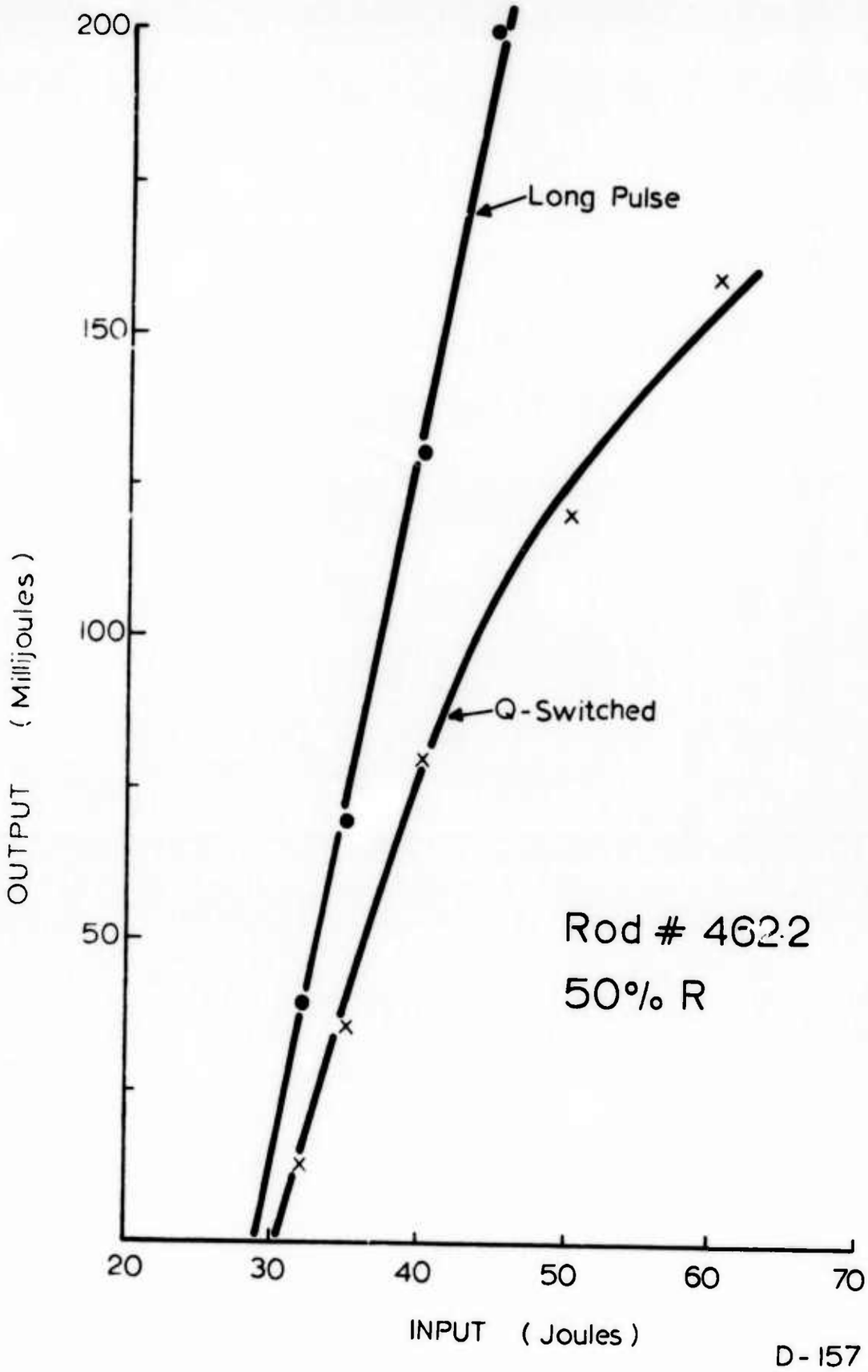

Figure 23 Q-Switched and Long Pulse Outputs

350MW/cm^2. In a multimode beam the apparent lower damage resistance is due to sufficiently high local powers (hot spots).

Damage observed in the $LiNbO_3$ crystals used in these experiments was confined to the surfaces of the crystals (see Fig. 24). The approximate level where damage was observed with near unit probability/shot was ~ 100 mJ Q-switched. This corresponds to a peak power (assuming a 50 ns square pulse) of 2 MW and a peak power density of some 30 MW/cm^2 outside of the resonator. Inside the resonator with a 50% R output mirror the "average peak power density" is some 60 MW/cm^2.

From laser beam patterns on Polaroid film it is clear that the laser was not operating in the TEM_{oo} mode. Therefore local power densities might be much higher. Correlation of these observations with the results of Bass et al.[23] is premature as these results at 2 μm were not sufficiently well controlled. However, in contrast to the conclusion (a) stated above, only surface damage was observed in these experiments. This may indicate that inadequate surface cleaning and/or poor coatings were responsible at least in part for these results.

Damage to the calcite polarizer was not observed. Figure 25 shows a transmission spectrum through a 2 cm thick sample of uncoated calcite (data supplied by Karl Lambrecht Corp.). Output oscillations of Ho:YLF lie between absorption bands.

No laser damage was observed in the YLF rods used in these experiments. Rod 71.344 was cut from a boule grown in 1968 using American Potash (not zone refined) feed. Rods from this boule have previously been Q-switched (up to 500 mJ from a 3 x 30 mm rod) using a rotating mirror without any material damage. The only boule in which laser

DAMAGE CRATERS

($LiNbO_3$ Q-Switch)

MODEL 902 M

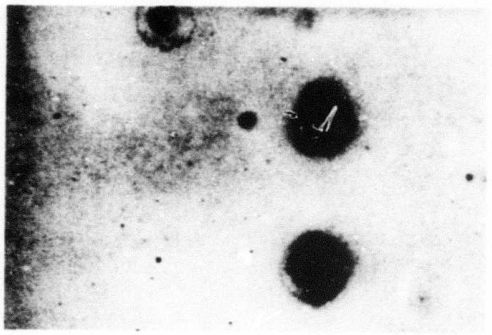

→1mm←

REAR SURFACE

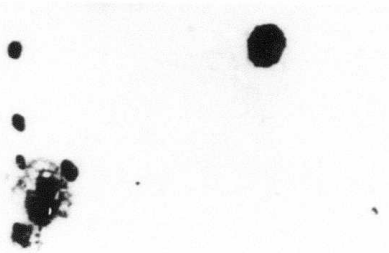

FRONT SURFACE

MODEL EOM 902

REAR SURFACE

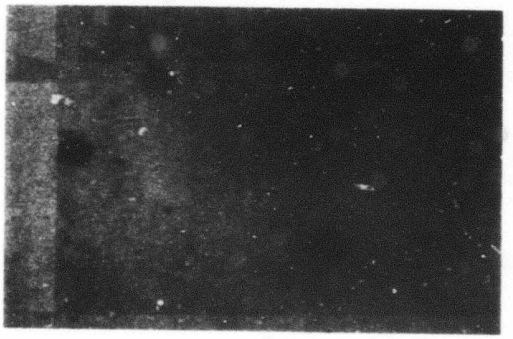

FRONT SURFACE

D-160

Figure 24 $LiNbO_3$ Damage Sites

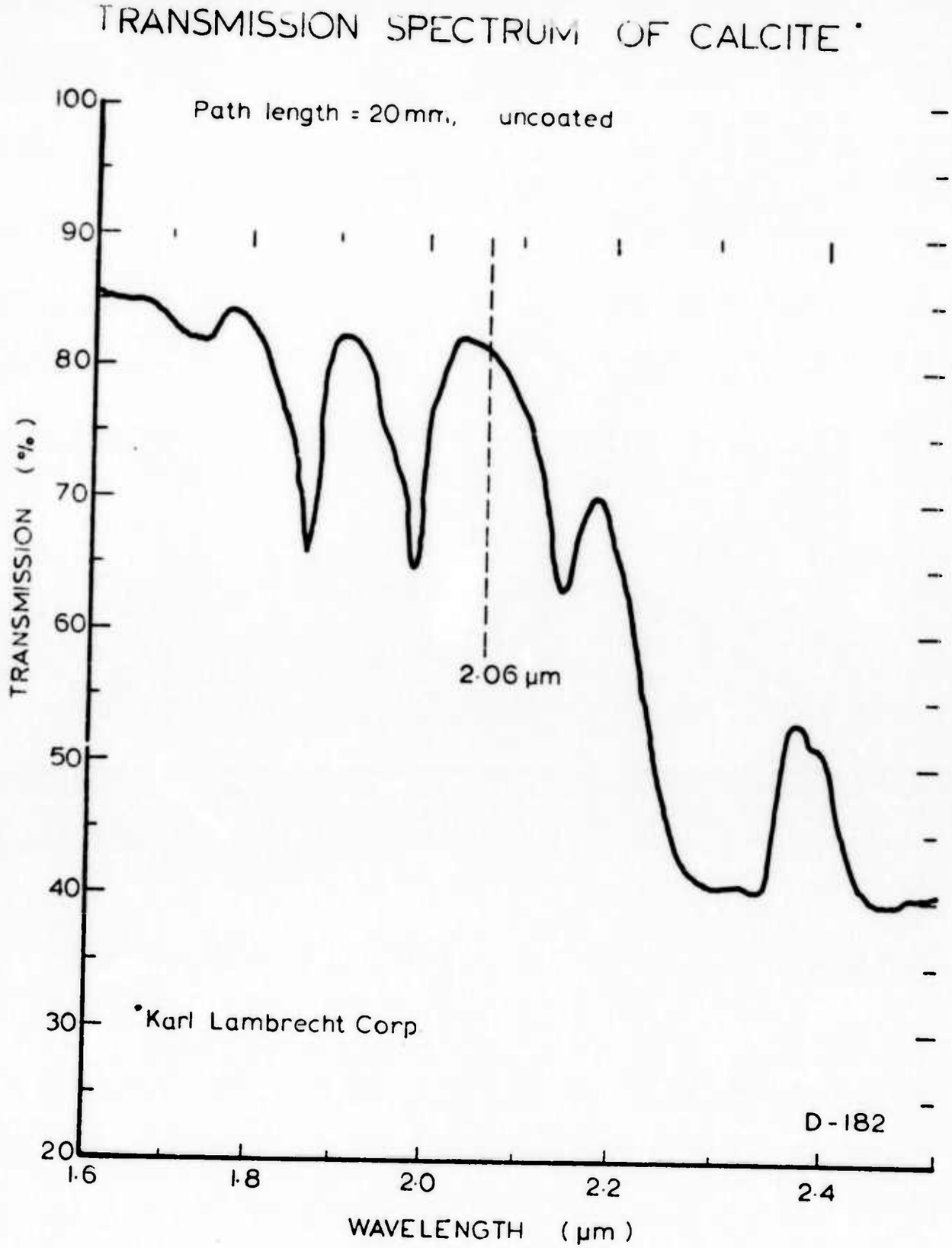

Figure 25 Transmission Spectrum of Calcite

damage has been observed is 140f (feed material Research Chemicals - not zone refined). Rod 462.2 was grown from zone refined Research Chemicals feed. Up to 100 mJ was switched in a single spike and repetitively switched operation at 3-5 Hz for an extended period at 10-30 mJ was obtained. No laser induced damage was observed. This result suggests that some impurity(s) in Research Chemical feed initiated damage formation, and zone refining of the feed before growth eliminates the offending impurity. However, as positive identification of such impurities is lacking, these conclusions are speculative.

5.4 DETECTOR RISETIMES

The response of HgCdTe and InAs diodes to 2 μm Q-switched pulses was investigated. In preliminary experiments using both detector materials, typical pulses observed were asymmetric with faster apparent risetimes than decay times. In those experiments the output voltage of a TIXL151 preamp across 50Ω was measured with a Tektronix 7904 oscilloscope. Under these conditions the output voltage (E_o) is

$$E_o = I_d R_T$$

where I_d is the diode current and R_T is the transimpedance of the TIXL151(4.7 K ohm). Typical peak voltages were 10 mV corresponding to diode currents of ~ 2 μA. As the advertised nep's of the HgCdTe are typically ~ 5×10^{-12} watts/$Hz^{1/2}$ with responsivities of ~ 1 amp/watt, 2 μA output corresponds to a current 4×10^5 above the dark current. Dynamic range data on the diodes are not available from the manufacturers. Manufacturer's data for the diodes are shown in Table 5-4.

TABLE 5-4

HgCdTe Diode Properties

Diode Number	Cut Off Wavelength	Manufacturer
H-1[†]	2.08 μm	Honeywell Radiation Center
ADL-1*	2.8 μm	Arthur D. Little Type ADL-28-10-4B

† Active area 5×10^{-4} cm^2, junction capacity 13.7 pF at -0.10 volt

* Active area = 4.6×10^{-4} cm^2

In order to eliminate the possibility of saturation of the diodes additional amplification was provided. The complete circuit includes a TIXL151 preamp, a 733 wideband amplifier, and an emitter follower. The effective transimpedance of the entire unit was found to be 178K ohm. Thus for a 10 mV output the diode current is only 6×10^{-8} amps with the additional amplification stage.

Measurement of the risetime of the detector electronics was made using a Rutherford B16 pulse generator. Figure 26 shows the response of the amplifier circuitry to a square wave input as well as the output of the pulse generator directly across 50Ω. These measurements indicate that the rise and fall times of the detector electronics are < 20 ns.

The risetime of the HgCdTe diodes with the associated electronics was then examined using a 0.9 μm light emitting diode. The output of the diode observed with a Si photodiode (SGD-100) followed by the same circuitry is shown in Figure 27 together with data observed with the HgCdTe diodes designated H-1 and ADL-1. The data in Figure 27 were obtained with a back bias of 0.5 volts; similar risetimes were observed using back biasing voltages from 0 - 0.7 volts. The measured rise and decay times for both diodes are > 200 ns when irradiated with 0.9 μm radiation.

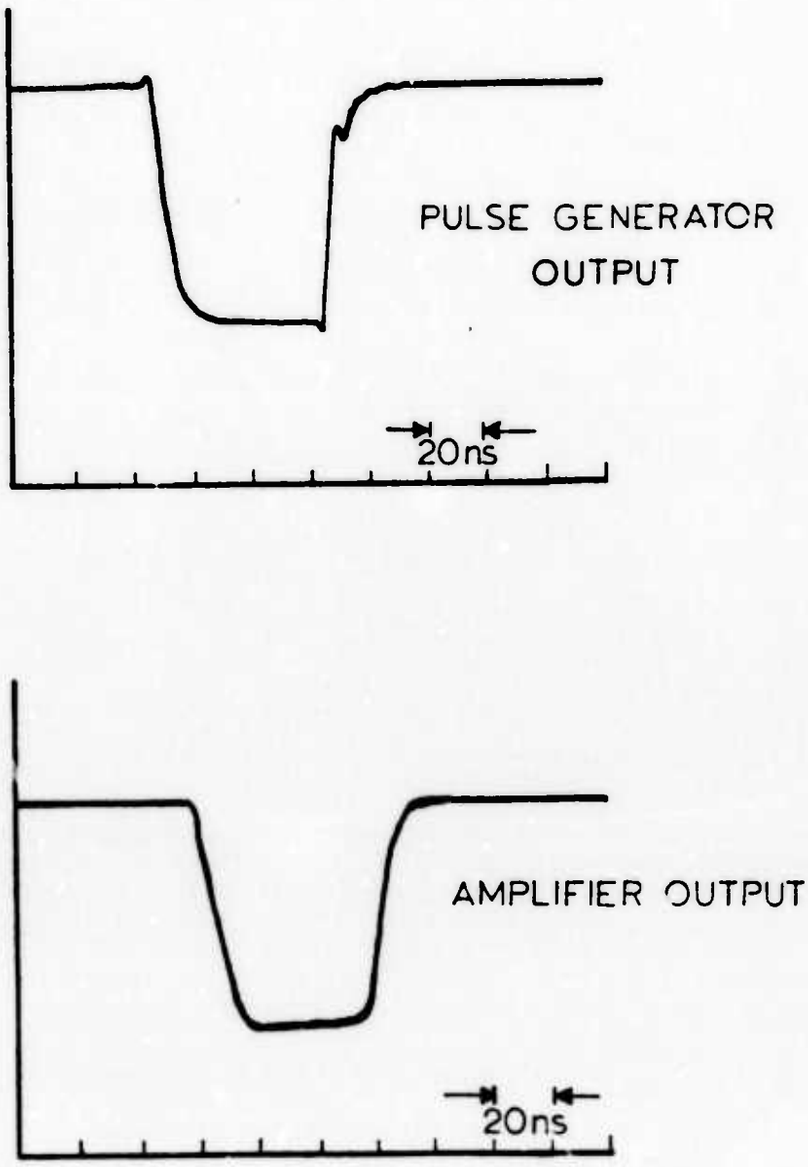

Figure 26 Amplifier Response Times

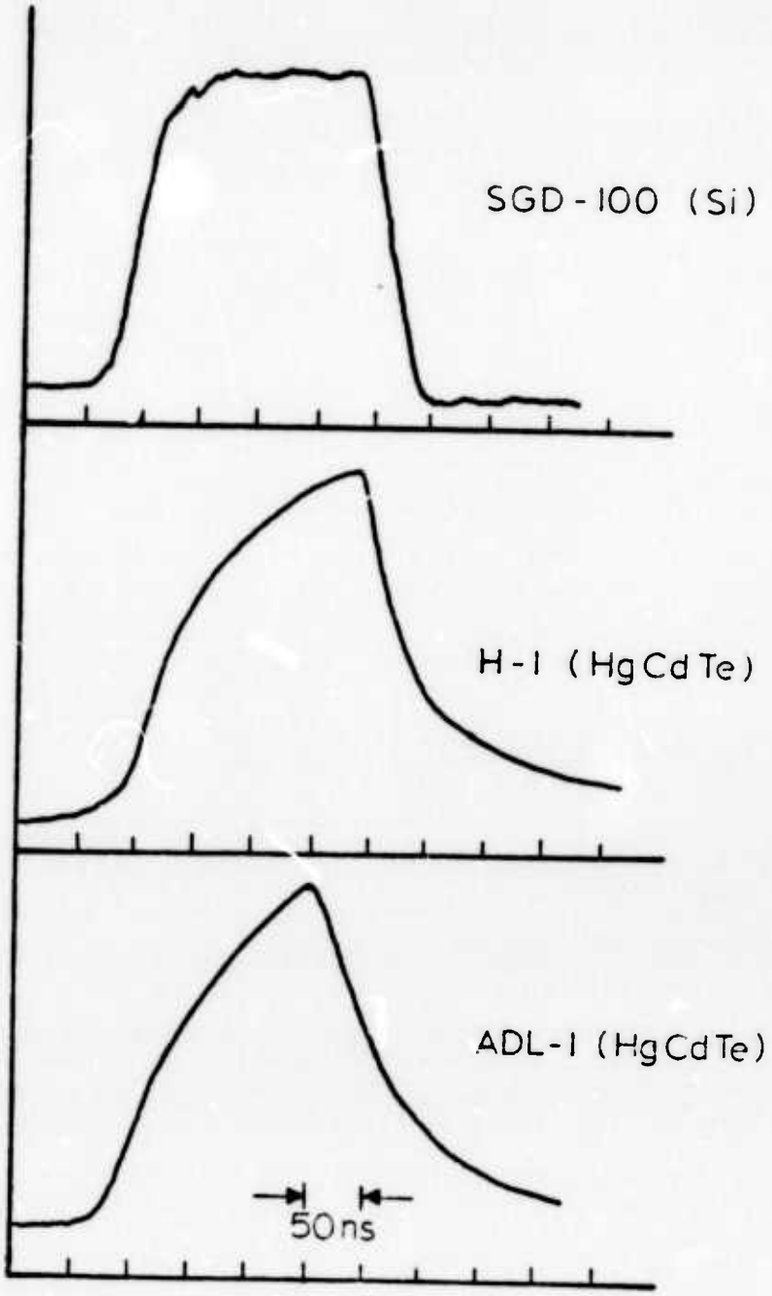

Figure 27 Detector Risetimes
Excitation Source: LED(λ = 0.9μm)

In detection of Q-switched 2 μm spikes risetimes of ~ 20 ns with decay times of ~ 100ns were observed. The "risetimes" were obtained from photographs of Q-switched pulses and were defined as the time interval between which the pulse rose from 10 - 90% of the peak value. However, this definition can be misleading.

Consider the response of an RC circuit to a step function of amplitude E_o (see Fig. 28). The voltage (E) rises according to

$$E = E_o \{1 - \exp(-t/\tau)\}$$

where τ is the RC time constant of the circuit. It is easy to show for an exponential rise that

$$\tau_r = 2.2\tau$$

where τ_r is the risetime of the pulse (time interval during which the pulse rises from 10 - 90% of the peak value). Then for an input pulse of duration $T < \tau$ the peak voltage at $t = T$

$$E(T) = E_o \{1 - \exp(-T/\tau)\}.$$

For $t > T$ the voltage pulse decays according to

$$E(t) = E(\tau) \{\exp -t/\tau\}.$$

Note that $E(T) < E_o$. This is shown graphically in Fig. 28. For input pulsewidths $T < \tau$ it is seen that the output of this circuit is an asymmetric pulse whose apparent risetime (τ_r^*) reflects the pulsewidth, and whose decay time reflects the true "RC time constant" of the circuit.

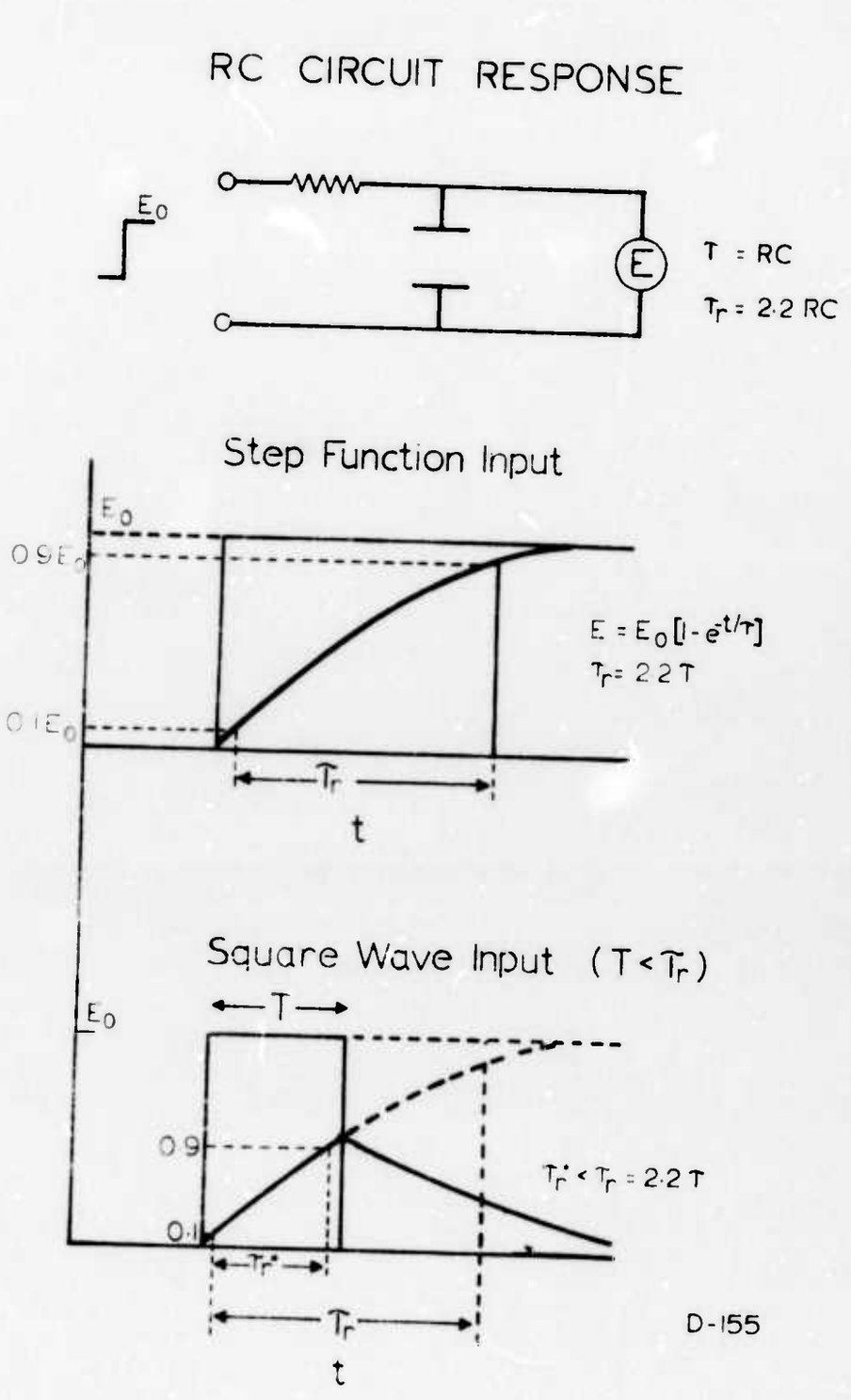

Figure 28 RC Circuit Transient Response

Using the RC circuit analogy to describe the response of the HgCdTe diode we note that a risetime (or decay time) of 100 ns corresponds to an equivalent "time constant" of 220 ns. Suppose a 20 ns wide pulse of intensity P_o (watts) is incident on the detector. The diode output current (I_D) rises according to

$$I_D = RP_o \{1 - \exp(-t/\tau)\}$$

where R is the diode responsivity (amps/watt). The peak current at t = 20 ns is

$$I_D = RP_o \{1 - \exp(-20/220)\}$$
$$\sim (0.1R)P_o$$

Thus the effective responsivity is reduced by an order of magnitude.

If we wish to use such a diode for a rangefinder we note that, using the RC circuit analogue, the range resolution is determined by the laser pulsewidth; however, the responsivity will be degraded. In the specific example cited for a 20 ns Q-switched 2 μm pulse detected with a diode with a 100 ns risetime the minimum power which can be detected by the diode is reduced by an order of magnitude, requiring a comparable increase in transmitted power.

In view of the similarity of the observed 2 μm Q-switched pulse shapes using the HgCdTe diodes and the output of a simple RC circuit to a short driving pulse, it appears that these diodes can be characterized by risetimes of ~ 100 ns. This roughly corresponds to the 90% - 10% time interval in the tail of the decay of these devices irra-

diated with 2 μm and 1 μm Q-switched pulses. From the observed rise of 2 μm Q-switched pulses, pulsewidths from 20 - 50 ns are inferred in this analogy.

Recent experiments conducted with a Philco L4530 InAs diode using the same amplification circuitry revealed risetimes of approximately 10 ns. The 2 μm Q-switched pulses were approximately 20 ns wide (FWHM) and symmetric.[19] Advances in HgCdTe technology have recently resulted in HgCdTe diodes with risetimes of ~ 20 ns and avalanche gain.[2] However, these devices were not available for evaluation on this program.

REFERENCES

1. E.P. Chicklis, "Development of Multiply Sensitized Ho:YLF as a Laser Material", Tech. Report ECOM-0013-F (Jan. 1973)

2. E.J. Schiel, V. Rosati, R.G. Buser, E.P. Chicklis, C.S. Naiman and R.C. Folweiler, "Two Micron Laser Rangefinder and Target Designator"(U), Sixth DOD Conf. in Laser Technology, U.S. Air Force Academy (March 1974), (Confidential)

3. E.P. Chicklis, R.C. Folweiler, C.S. Naiman, et al., "0.85 Micron Solid State Laser Material Evaluation", Tech. Report AFAL-TR-73-94 (April 1973)

4. E.P. Chicklis, C.S. Naiman, R.C. Folweiler, D.R. Gabbe, H.P. Jenssen and A. Linz, Appl. Phys. Let. 19, 4, pp. 119-121 (1971)

5. H.P. Jenssen, D. Castleberry, D. Gabbe and A. Linz, "Stimulated Emission at 5445 Å in Tb^{+3}:YLF", Paper 8.4 presented at the 1973 IEEE/OSA Conference on Laser Engineering and Applications, Washington, D.C., 20 May-1 June 1973

6. Reactor Chemistry Division Annual Progress Report for period ending Jan. 31, 1965, AEC Report No. ORNL-3789

7. R.E. Thoma, C.F. Weaver, H.A. Friedman, H. Insley, L.A. Harris and H.A. Yakel, Jr., J. Phys. Chem. 65, 1096 (1961)

8. D.C. Henderson, "The Preparation and Some High Temperature Properties of the Rare Earth Trifluorides", PhD. Thesis, Iowa State University (1970)

9. T.G. Stoebe, J. Phys. Chem. Solids 31, 12, 1291 (1970)

10. T.G. Stoebe, J. Phys. Chem. Solids 28, 1375 (1967)

11. R.N. Kniseley, Inst. for Atomic Research, Ames, Iowa (private communication)

12. G.D. Baldwin, "Q-Switched Evaluation of CaLaSOAP:Nd", Tech. Report AFAL-TR-72-334 (September 1972)

13. Sanders Associates IR&D Task NTF, "Medium Repetition Rate 2 μm Laser", (September 1973), (unpublished)

14. L.A. Riseberg, H.W. Moos and W.D. Partlow, IEEE J. Quantum Electronics QE-4, No. 10, 609 (1968)

15. H.P. Jenssen, "Phonon Assisted Laser Transitions and Energy Transfer in Rare Earth Laser Crystals", Crystal Physics Laboratory Tech. Report No. 16, Center for Material Sciences and Engineering, Massachusetts Institute of Technology (September 1971)

16. J.R. Oliver and F.S. Barnes, IEEE J. Quantum Electronics QE-5, No. 5, 232 (1969)

17. L. Nobel, ILC Corporation (private communication)

18. L. Noble, "Optical Pumps for Holmium Lasers", Triannual Report No. 2, ECOM-0274-2 (1974)

19. Sanders Associates IR&D Task NWC (unpublished results)

20. L.F. Johnson, J.E. Gensic, and L.G. Van Vitert, Appl. Phys. Let. 8, 200 (1966)

21. R.P. Hilberg and W.R. Hook, Applied Optics 9, No. 8, 1939 (1970)

22. M.K. Chun and J.T. Bischoff, IEEE J. Quantum Electronics QE-8, No. 8, 715 (1972)

23. M. Bass, et al, "Experimental Investigation of Optical-Irradiation-Induced Surface Damage in Optically Non-Linear Materials", AFCRL-71-0573 (Feb. 1972)

APPENDIX I

COMPARISON OF Ho:YLF and Ho:YAG

Although 2 μm laser operation has been reported in a number of different materials,[1-3]* efficient room temperature operation has only been observed in sensitized YLF. The superiority of YLF for this application results from fundamental properties of this host which are discussed below. Let us consider the case of identically doped αβYLF and αβYAG. Ho laser operation in YLF was found to be considerably more efficient than in YAG in room temperature pulsed operation.[4] This can only be the result of differences in the following laser parameters:

(a) Energy transfer efficiency

(b) Ground and upper state splittings of the Ho^{3+} ion

(c) Specific gain of the laser transition

(d) Optical quality of the host.

In the comparative experiments the YAG rods exhibited considerably higher optical quality than the YLF rods available at the time; the specific gain of the laser transition is probably somewhat higher in YAG as the lines are somewhat narrower.[4] Furthermore, the level splittings of Ho^{3+} are somewhat higher in YAG. From reference 5 and 6 we compute the occupation factors of the pertinent levels of the laser transition tabulated below.

* See references at end of this Appendix.

TABLE AI-1

RELEVANT LEVEL SPLITTING OF Ho:YLF and Ho:YAG

	Ho:YLF	Ho:YAG
ΔE^8: Ground State Splitting	306 cm^{-1}	540 cm^{-1}
B^8: Occupation factor of lower laser level (room temperature)	2.8×10^{-2}	1.3×10^{-2}
ΔE^7: Upper Manifold Splitting	191.5 cm^{-1}	225 cm^{-1}
B^7: Occupation factor of upper laser level (room temperature)	0.13	0.2

As the Ho^{3+} concentration was high (1.7%) in the rods we can neglect resonator and scattering losses. The upper manifold population at threshold, N_7, for both materials is given by[7]

$$N_7 = \frac{B^8}{B^7+B^8} N_o,$$

where N_o is the active ion concentration. Using the values in Table A-I we have

$$N_7 \text{ (Ho:YLF)} = (0.14)\ N_o$$

and

$$N_7 \text{ (Ho:YAG)} = (0.06)\ N_o$$

Now N_7 is proportional to the input energy to a flashlamp at threshold. For the same active ion density this analysis predicts a considerably lower threshold in YAG - contrary to what is observed[4].

The remaining identifiable host related property is the energy transfer efficiency. While detailed studies of the transfer mechanisms in YAG are not available, Johnson[1],[8] has proposed the following transfer mechanism in Er-Tm sensitized Ho:YAG and $CaMoO_4$:

- Er^{3+} absorption with rapid non-radiative decay to $^4I_{13/2}$ with the energy decrement taken up by lattice phonons
- Rapid $^4I_{13/2}$ (Er) → $^3H_4$ (Tm) → $^5I_7$ (Ho) transfer.

In YLF, on the other hand, non-radiative, phonon assisted decay of the higher excited Er^{3+} levels to $^4I_{13/2}$ positively does not occur.(4) Instead the higher lying Er^{3+} pump bands of each ion are de-excited by resonant transfer with simultaneous excitation of other Er^{3+} and Tm^{3+} ions to $^4I_{13/2}$ and $^3H_4$ respectively.(7) Subsequent rapid transfer from $^4I_{13/2}$ → $^3H_4$ → $^5I_7$ completes the transfer sequence. These steps are discussed in great detail in this report (Section 4.0) and in reference 7.

In YLF, for each photon absorbed at 0.55 μm, three Ho ions are excited and 3600 cm^{-1} of heat is deposited in the crystal. In the proposed transfer scheme in YAG for each 0.55 μm absorption one Ho ion is excited and 13330 cm^{-1} of heat is taken up by the lattice. Note that although the resonances between the Er^{3+}, Tm^{3+}, and Ho^{3+} levels are fortuitous, the dominance of resonant transfer over phonon-assisted non-radiative decay in YLF is not.

An excited ion may decay via emission, non-radiative decay with emission of phonons to the lattice (multiphonon relaxation), or ion-ion interactions (resonant transfer). Phonon assisted transfer also can occur although the rates for this process are generally small.(6) In general for 4f-4f transitions spontaneous emission rates are the order of 10^3 sec^{-1} for transitions in the visible. The spontaneous rates depend on ν^3 where ν is the frequency of the transition above the ground state and are relatively insensitive to the host lattice. In

most "αβ" materials nearly all the levels are quenched indicating that spontaneous rates are not important (except, of course, for the laser transition).

Multiphonon rates are, however, strongly dependent on the host lattice.[9] Figure AI-1 shows the measured multiphonon relaxation rates for YLF,[6] Y_2O_3[9] and $LaBr_3$;[9] the rates for Y_2O_3 are representative of those of YAG. The multiphonon relaxation rates of YAG are seen to be approximately a factor of five greater than those of YLF. Simply stated, oxide hosts exhibit higher rates of phonon assisted non-radiative decay than fluoride hosts. While in some systems (Nd:YAG) a high rate of phonon assisted decay is advantageous,[9] in sensitized systems such as the Ho laser this non-radiative rate is competitive with rates for transfer.

From Figure AI-1 it appears that improved transfer efficiency from a host like $LaBr_3$ (or in fact $LaCl_3$) might be significantly better than in YLF. However, the physical properties of these materials prohibit their use for laser applications.

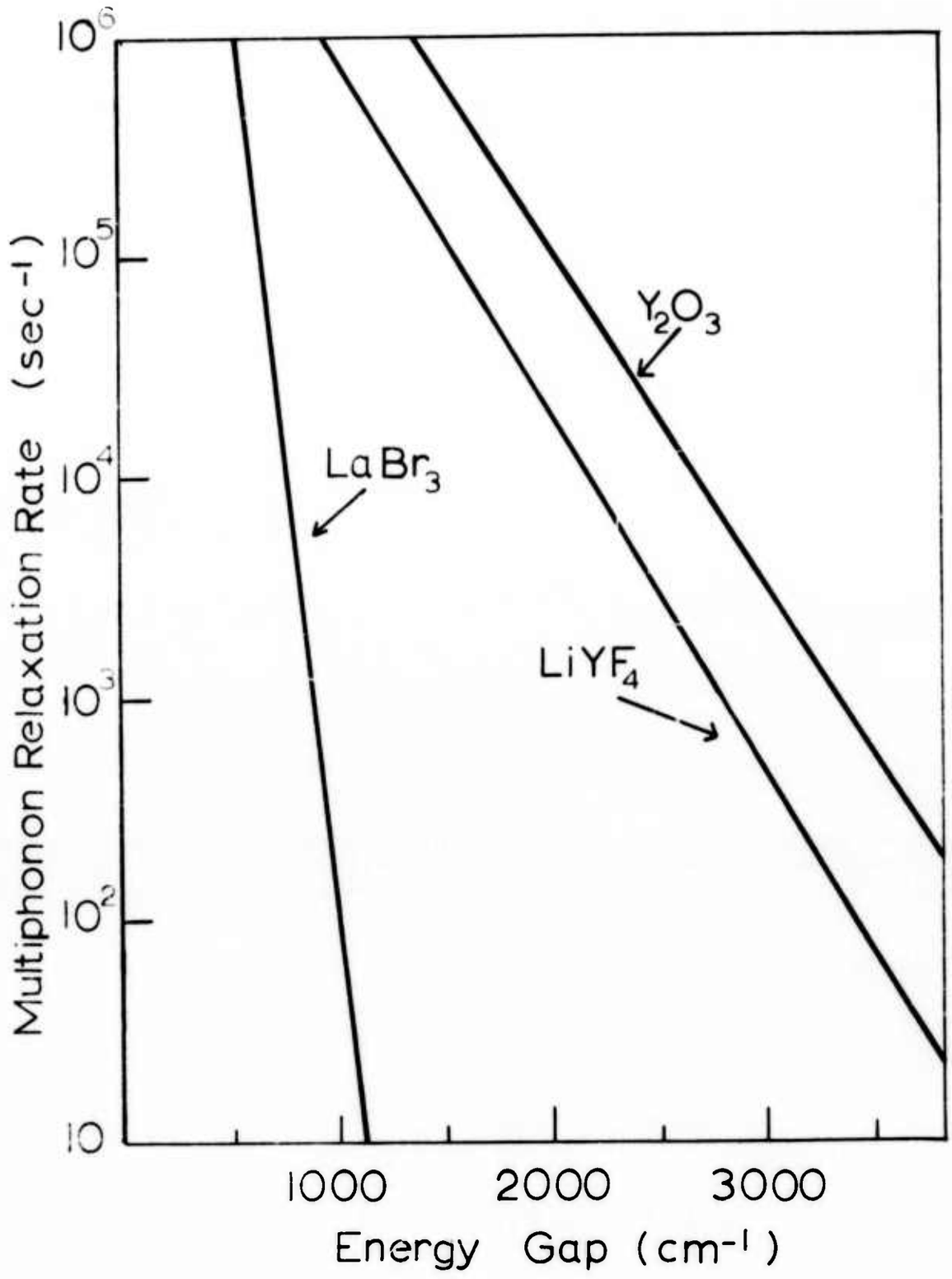

Figure AI-1 Multiphonon Relaxation Rates vs Energy Gap for $LaBr_3$, $LiYF_4$ and Y_2O_3

REFERENCES (A-I)

1. L.F. Johnson, et al, Appl. Phys. Let. 8, No. 8, 200 (1966)

2. M.J. Weber, et al, IEEE J. Quant. Electronics QE-9, No. 11, 1079 (1973)

3. R.H. Hopkins, et al, "Rare Earth Doped Apatite Laser Materials," Tech. Report AFAL-TR-70-249, Dec. 1970

4. E.P. Chicklis, et al, IEEE J. Quant. Electronics QE-8, No. 2, 225 (1972

5. J.T. Karpick and B. DiBartolo, "Thermal Dependence of Energy Transfer Processes Between Rare Earth Ions in Crystals," Tech. Report AFAL-TR-71-114, May 1971

6. H.P. Jenssen, "Phonon Assisted Laser Transitions and Energy Transfer in Rare Earth Laser Crystals", Dept. of Electrical Engineering, MIT, Cambridge, Massachusetts (1971)

7. E.P. Chicklis, et al, "Development of Multiply Sensitized Ho:YLF as a Laser Material," R & D Tech. Report TRECOM-0013-F, Jan. 1973

8. L.F. Johnson, et al, Phys. Rev. 133, No. 2A, A494 (1964)

9. L.A. Riseberg, et al, IEEE J. Quant. Electronics QE-4, No. 10, 609 (1968)

APPENDIX II

SCANNING ELECTRON MICROSCOPE STUDY OF INCLUSIONS

The scanning electron microscope (SEM) is a tool very well suited for the study of inclusions in crystals, provided that the defect can be made to intersect the sample surface. Detailed visualization of the specimen surface can be realized with significantly better contrast, depth of field and resolution than is obtainable by optical microscopy. X-rays from any area of interest can be analyzed, using a Li drifted Si detector and associated multichannel analyzer. Counts can be accumulated for selected intervals ranging from 100 to 8×10^4 seconds. Under normal laboratory conditions only elements heavier than neon can be detected.

X-ray data from the SEM is printed out in counts/channel over the energy range selected. For low resolution spectra the whole 20 keV range covered by the SEM is divided into 200 equally spaced channels. High resolution spectra record the same energy range in 1000 channels, but the data must be measured in five 200 channel blocks spanning 4 keV each. Interpretation of the data must be computer assisted. The available instrumentation allows only off-line data processing. An HP 9820A desk-top computer with a digital plotter and magnetic tape cassette memory was used for reduction of the data reported here.

Over the 0-20 keV region both K and L spectra are observed. In addition M spectra are observed up to about 3.2 keV. The exciting

electron beam has an energy of 20 keV; therefore the excitation cross section and the observed line intensity per unit concentration decreases with increasing energy.

Line assignment and element identification is made with the aid of translucent standard overlays. For positive identification of a given element at least two lines must be assigned. The first criterion to be met is line energy and if there are still doubts, the intensity ratios are considered. Not all local maxima in a given spectrum are peaks. Even if the above two conditions are seemingly met, one must also take into account height above background, peak width, and the synergistic contribution of minor lines of the major elements. Thus in Figure AII-1, which is a 100 second low resolution spectrum of an αβYLF sample, numerous "peaks" have not been assigned because they could not be uniquely attributed to one element.

Figure AII-2 is a smoothed high resolution x-ray spectrum counted for 400 seconds per 200-channel block. An improvement in line shape is apparent when low and high resolution spectra are compared. Additional line assignments over the 3 to 6.5 keV region have been made, but their validity is in doubt. Further exploration of this portion of the x-ray spectrum would require counting several thousand seconds or longer to accumulate data amenable to line shape analysis.

Samples for the SEM were prepared by mechanical polishing with Syton, followed by argon ion milling to expose a clean, damage-free surface.

A sample of αβYLF with well defined bubble inclusions was investigated first in order to characterize the formations and to determine if the bubbles were associated with local concentrations of

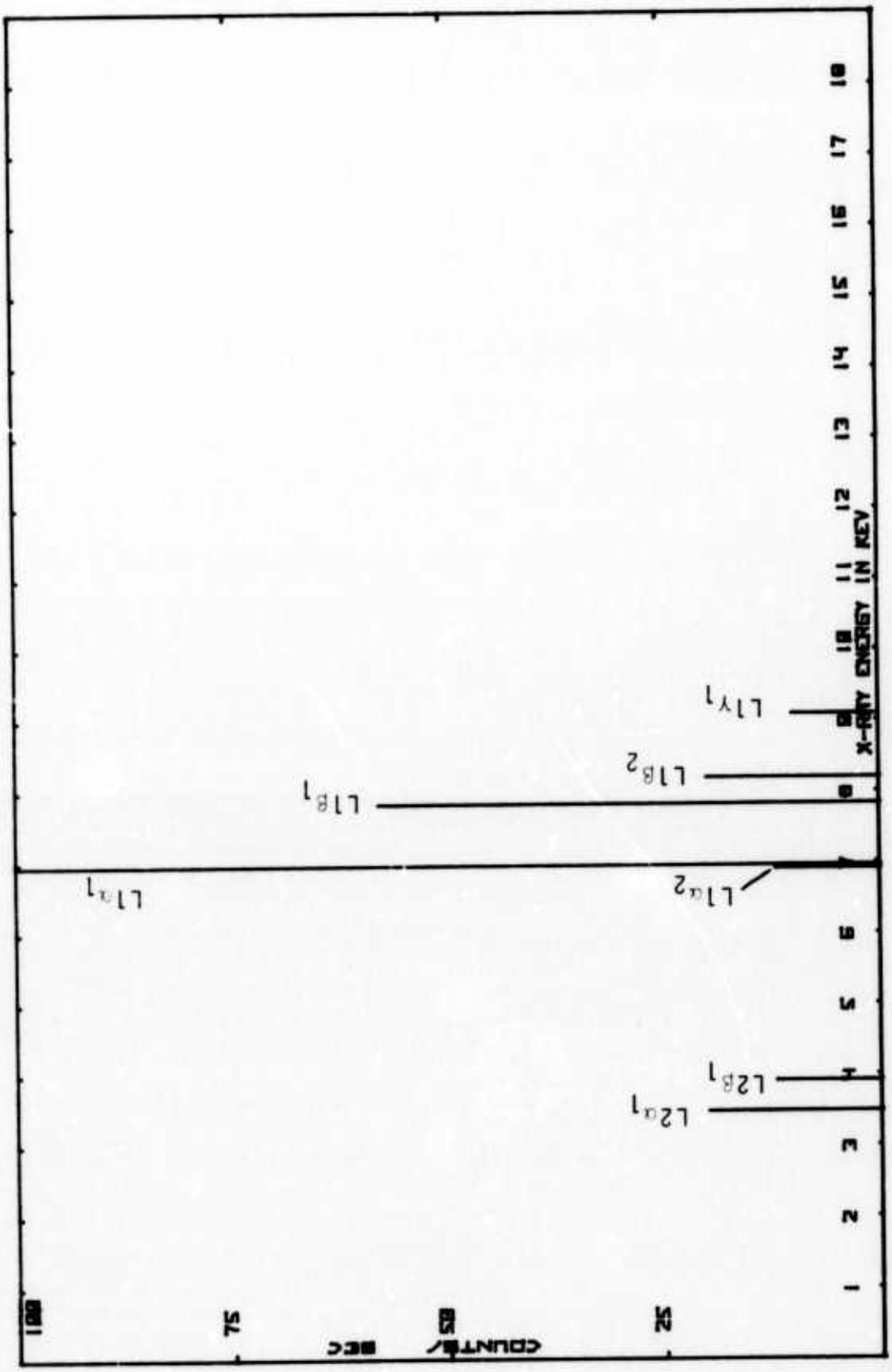

Figure AII-1 Standard Er L Spectrum
Only Lines with Relative Intensity Greater Than 10 Are Included

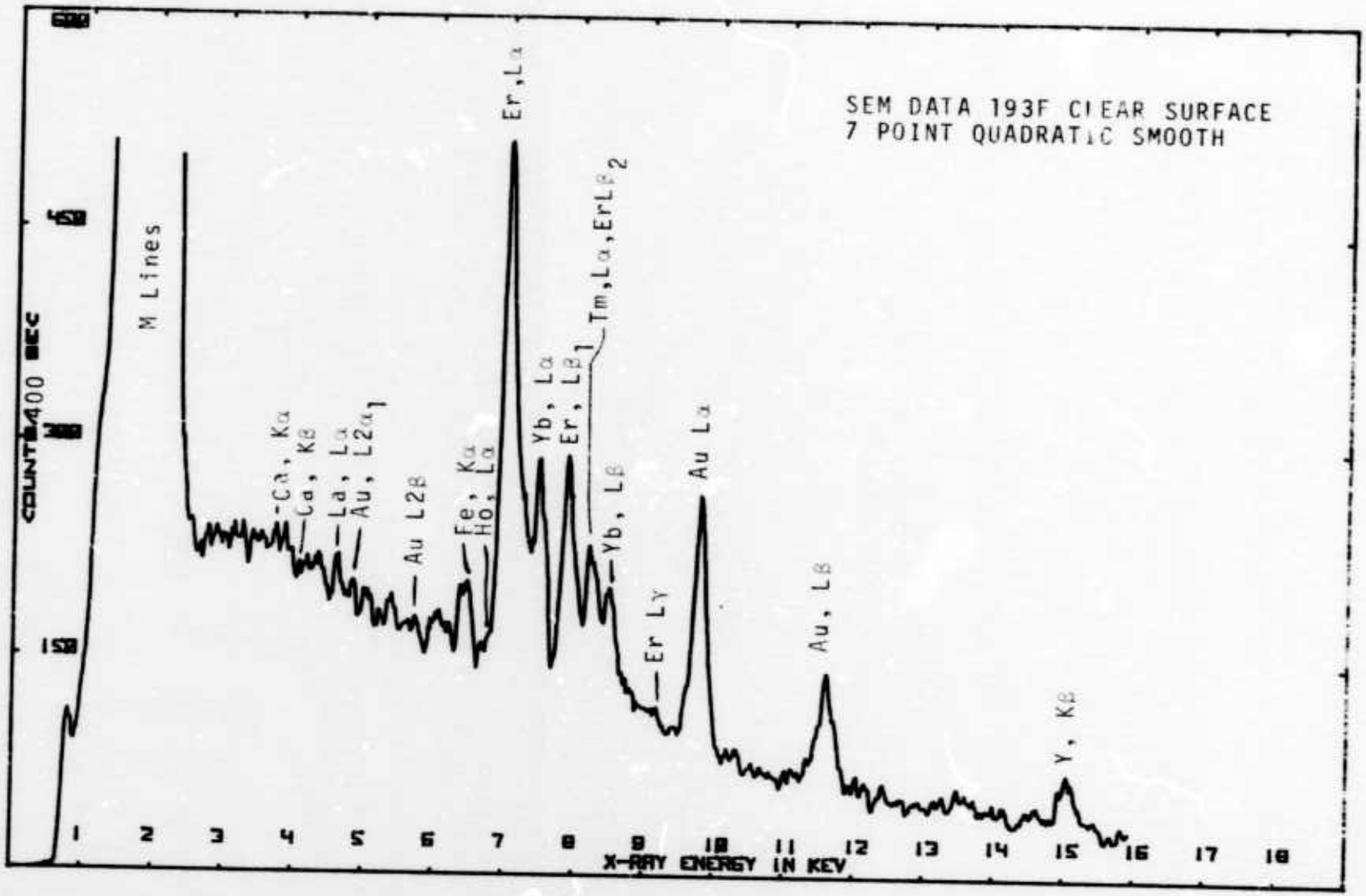

Figure AII-2 X-ray Spectrum from Boule 193f

impurity elements. Several cycles of ion milling - scanning electron microscopy were done in order to expose and examine successively deeper layers of the sample. Figure AII-3 shows a typical bubble in αβ193F. One observes a central hole, a lining and a sharp boundary with the matrix material. Low resolution x-ray spectra were obtained for spots located both on the matrix and at various locations on the bubble lining. The x-rays were counted for 100 seconds. A typical spectrum is shown in Figure AII-4. At the resolution and counting time used, the spectra do not indicate the presence in the bubble region of local concentrations of impurity elements. Low resolution spectra measured over short counting times are too noisy to be made to reveal minor differences in composition by subtraction. The appearance of the bubble core may be due to the effect of poor melt circulation coupled with rapid solidification near its surface.

However, since the use of Ar as the furnace gas has been introduced, the occurrence of such bubbles in YLF has been almost completely eliminated. Therefore, attention has been directed at analysis of the other light scattering centers.

Careful examination at magnifications up to 10^4 of ion-milled and freshly fractured surfaces of various YLF samples has indicated complete agreement between optical and scanning electron microscopy in characterizing an inclusion as a bubble. What optical microscopy does not always reveal is the nature of the bubble's interior. The remaining light scattering centers could not be characterized as bubbles by either technique. Extensive SEM observations on ion-milled samples have not indicated the presence of a well defined crystalline inclusion phase. One might expect to find differences in ion milling rates

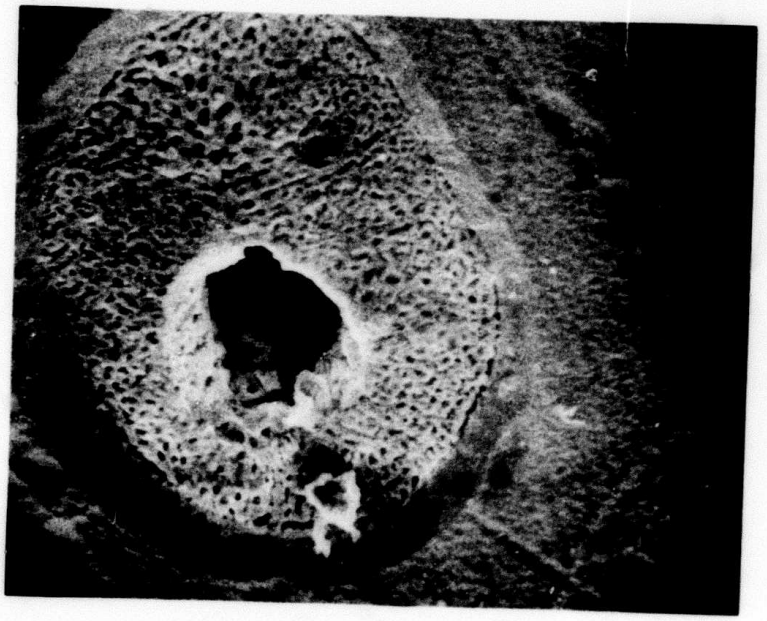

Figure AI1-3 SEM Photo #193f

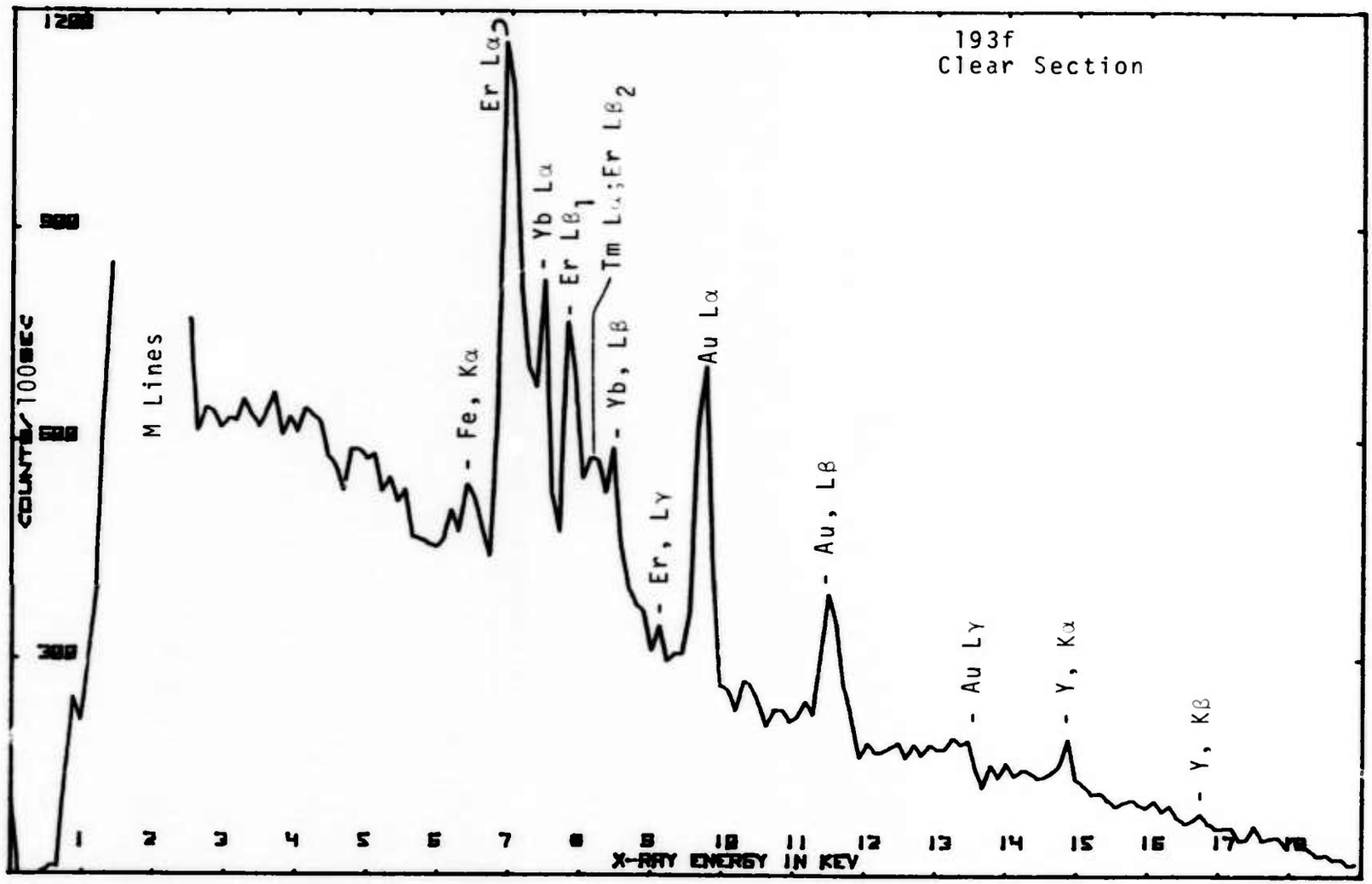

Figure AII-4 X-ray Spectrum from Boule 193f

among various phases. Various surface features have been seen and x-ray analysis indicates absence of high local concentrations of impurity elements. The freshly fractured surface also gave no indication of the presence of inclusions. To continue this work, one should accentuate phase differences by ion milling in various crystallographic directions and at varying Ar ion energies. High resolution x-ray spectra should be measured over long counting times to enable identification of elements present at levels below 1%.

APPENDIX III

TRANSMISSION AND SWITCHING TIME OF $LiNbO_3$

Difficulties encountered in the operation of $LiNbO_3$ as a Q-switch for Ho:YLF led to an investigation of the dynamic characteristics of this material. Figure AIII-1 shows the experimental setup utilized to measure the risetime and transmission of the $LiNbO_3$ Q-switch. The $LiNbO_3$ was placed between crossed calcite polarizers; a He-Ne probe beam was detected by a RCA S-20 photomultiplier tube terminated with 50 ohms whose output was photographed using a Tektronix 585 oscilloscope with a Type 82 preamplifier. Figure AIII-2 shows the results: the A trace corresponds to the output of the tube with the Q-switch shorted; the B trace to the tube output with 1/2 wave voltage on the Q-switch (not switched); and the C trace to the tube output when the 1/2 wave voltage to the $LiNbO_3$ is switched. The rise occurs within 20 ns. However, the peak transmission is not as high as in the steady state case (voltage off), differing by approximately 15-25%.

This effect would be expected to be more severe at 2 μm as the initial voltage is higher. That is the <u>half</u> wave voltage at .63 is 1.2KV and the quarter wave voltage at 2 μm is 1.9KV.

These results indicate that, although the voltage switches to zero, the retardation in the polarizer apparently does not completely extinguish. The minimum in transmission occurs some 400 ns after the

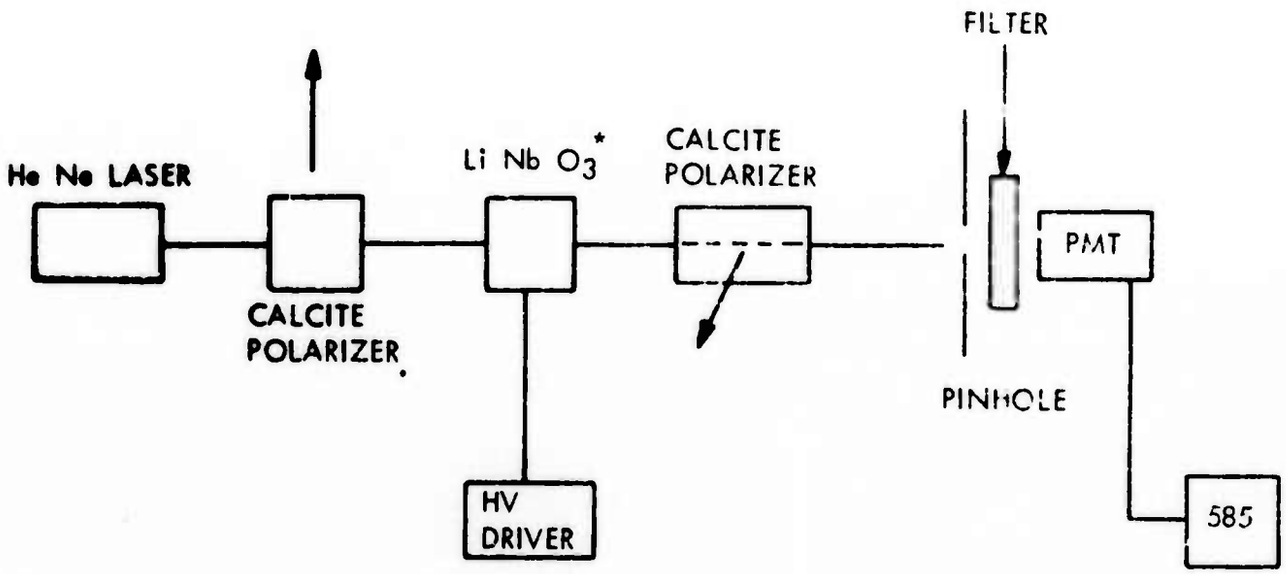

D-117

*LASERMETRICS EOM-902

Figure AIII-1 Q-Switch Risetime Experiment

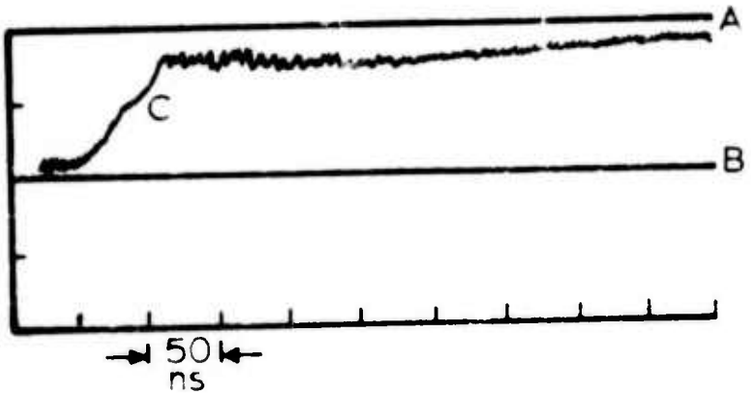

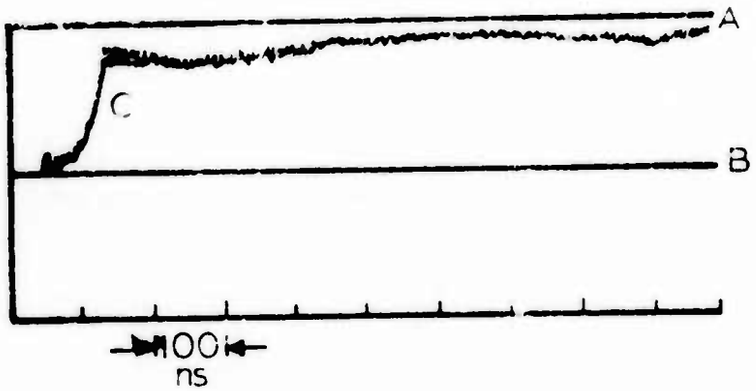

A : Half Wave Voltage off

B : Half Wave Voltage on - not Switched

C : Half Wave Voltage Switched

D-118

Figure AIII-2 $LiNbO_3$ Rise Time

initial rise; somewhat later (~ 10 μs) large oscillations in retardation similar to results reported by Hilberg and Hook(AIII-1) were observed. This effect discussed in references (AIII-1, 2) is attributed to piezo-optic oscillations in the $LiNbO_3$ which may be a substantial fraction (>20%) of the electro-optic effect. The piezo-optic effect was found to depend on the initial stress in the crystal (hence the voltage) and could be overcome by applying an electrical bias to the crystal to null the mechanically generated retardation.

Laser measurements using a back biased crystal confirm the above observations. However, transmission measurements were not made under these conditions.

REFERENCES (A-III)

A-1 R.P. Hilberg and W.R. Hook, Applied Optics 9, No. 8, 1939 (1970)

A-2 M.K. Chun and J.T. Bischoff, IEEE J. Quantum Electronics QE-8, No. 8, 715 (1972)